

**UNCLASSIFIED**

**AD 419306**

**DEFENSE DOCUMENTATION CENTER**

**FOR**

**SCIENTIFIC AND TECHNICAL INFORMATION**

**CAMERON STATION, ALEXANDRIA, VIRGINIA**



**UNCLASSIFIED**

## **DISCLAIMER NOTICE**

**THIS DOCUMENT IS BEST QUALITY  
PRACTICABLE. THE COPY FURNISHED  
TO DTIC CONTAINED A SIGNIFICANT  
NUMBER OF PAGES WHICH DO NOT  
REPRODUCE LEGIBLY.**

/

NOTICE: When government or other drawings, specifications or other data are used for any purpose other than in connection with a definitely related government procurement operation, the U. S. Government thereby incurs no responsibility, nor any obligation whatsoever; and the fact that the Government may have formulated, furnished, or in any way supplied the said drawings, specifications, or other data is not to be regarded by implication or otherwise as in any manner licensing the holder or any other person or corporation, or conveying any rights or permission to manufacture, use or sell any patented invention that may in any way be related thereto.

41 9306

AFSWC-TDR-63-50

SWC  
TDR  
63-50

CALCULATION OF HIGH-ENERGY  
SECONDARY ELECTRON EMISSION

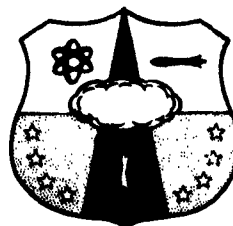
by

Jerry A. Sawyer  
Lt USAF

64-5-

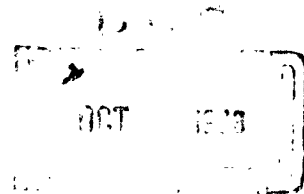
August 1963

TECHNICAL DOCUMENTARY REPORT NUMBER AFSWC-TDR-63-50



Research Directorate  
AIR FORCE SPECIAL WEAPONS CENTER  
Air Force Systems Command  
Kirtland Air Force Base  
New Mexico

Project No. 8812



419306

CATALOGED BY DUL  
AS AD NO. \_\_\_\_\_

**HEADQUARTERS  
AIR FORCE SPECIAL WEAPONS CENTER  
Air Force Systems Command  
Kirtland Air Force Base  
New Mexico**

**When Government drawings, specifications, or other data are used for any purpose other than in connection with a definitely related Government procurement operation, the United States Government thereby incurs no responsibility nor any obligation whatsoever; and the fact that the Government may have formulated, furnished, or in any way supplied the said drawings, specifications, or other data, is not to be regarded by implication or otherwise as in any manner licensing the holder or any other person or corporation, or conveying any rights or permission to manufacture, use, or sell any patented invention that may in any way be related thereto.**

**This report is made available for study upon the understanding that the Government's proprietary interests in and relating thereto shall not be impaired. In case of apparent conflict between the Government's proprietary interests and those of others, notify the Staff Judge Advocate, Air Force Systems Command, Andrews AF Base, Washington 25, DC.**

**This report is published for the exchange and stimulation of ideas; it does not necessarily express the intent or policy of any higher headquarters.**

**Qualified requesters may obtain copies of this report from DDC. Orders will be expedited if placed through the librarian or other staff member designated to request and receive documents from DDC.**

TDR-63-50

## FOREWORD

The author takes this opportunity to acknowledge the aid and support given by James W. Garner of the mathematics group at AFWL. He is responsible for writing and executing all three programs on the CDC 1604 computer, and for other valuable suggestions made during this work. Also appreciated are the helpful remarks by Dr. Victor A. J. van Lint, General Atomic, San Diego, California. It is hereby acknowledged that the original concept for this study came from him through AFSWC TDR-62-63.


TDR-63-50

# ABSTRACT

Thin targets of low atomic number were assumed to be bombarded with 25-Mev electrons, 600-kv X rays and prompt fission gamma radiation. The resulting high-energy secondary electrons were calculated theoretically on a high-speed digital computer with respect to their intensity, energy losses, energy spectra and angle of emission spectra. The results show that 25-Mev electrons, 600-kv X rays and prompt fission gamma radiation produce a maximum efficiency of high-energy secondary-electron emission of 8.0, 0.05, and 0.3 percent, respectively. Experimental results from 25-Mev electron irradiations agree very closely with these theoretical numbers. An experiment is planned for the 600-kv X-ray radiation source.

## PUBLICATION REVIEW

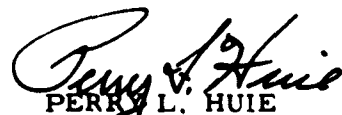
This report has been reviewed and is approved.



Jerry A. Sawyer  
Lt USAF  
Project Officer



DAVID R. JONES  
Colonel USAF  
Chief, Physics Branch



PERRY L. HUIE  
Colonel USAF  
Chief, Research Division

## CONTENTS

	<u>Page</u>
Introduction . . . . .	1
Secondary Electron Emission by Prompt Fission Gamma Radiation . . . . .	1
Secondary Electron Emission by 25-Mev Electrons . . . . .	60
Secondary Electron Emission by a 600-kv Pulsed X-ray Source . . . . .	96
Assumptions and Percent Errors . . . . .	110
Results . . . . .	111
Conclusions and Recommendations . . . . .	113
Appendix A -- Prompt Fission Gamma Program . . . . .	115
B -- 25-Mev Electron Program . . . . .	129
C -- 600-kv X-ray Program . . . . .	149
Bibliography . . . . .	159
Distribution . . . . .	161



## ILLUSTRATIONS

<u>Figure</u>		<u>Page</u>
2.1	Relative importance of the three major types of gamma-ray interactions. The lines show the values of $Z$ and $h\nu$ for which the two neighboring effects are just equal.	33
2.2	Trajectories in the scattering plane for the incident photon $h\nu_0$ , the scattered photon $h\nu$ , and the scattered electron which acquires momentum $p$ and kinetic energy $T$ .	34
2.3	A thin absorbing sample	35
2.4	The number-distance curve for an electron with energy $E$ , i. e., monoenergetic particles.	36
2.5	Empirical range-energy relationship for electrons absorbed in aluminum with data points shown.	37
2.6	Experimentally measured absorption curves for monochromatic electrons in aluminum.	38
2.7	Gamma flux to give 1 roentgen/hour.	39
2.8	Energy spectrum of prompt fission gamma rays from $U^{235}$ fission for times less than $5 \times 10^{-8}$ seconds.	40
2.9	A typical sample division.	41
2.10	Diagram of the probability of escape $P_e$ .	42
2.11	Diagram for the calculation of the energy of escape $E_e$ .	43
2.12	The number of secondaries escaping $S_e$ as a function of thickness for prompt fission gamma radiation.	44
2.13	The number of secondaries deposited $S_d$ as a function of thickness for prompt fission gamma radiation.	45
2.14	The energy of escape per unit path length as a function of thickness for prompt fission gamma radiation.	46

## ILLUSTRATIONS (cont'd)

<u>Figure</u>		<u>Page</u>
2. 15	The energy deposited per unit path length as a function of thickness for prompt fission gamma radiation.	47
2. 16	Energy and angle of emission spectra for prompt fission gamma radiation incident on a sample of thickness $0.01 \text{ gm/cm}^2$ ( $\Delta E = 0.1 \text{ Mev}$ ; $\Delta \theta = 2^\circ$ ).	48
2. 17	Energy and angle of emission spectra for prompt fission gamma radiation incident on a sample of thickness $0.025 \text{ gm/cm}^2$ .	49
2. 18	Energy and angle of emission spectra for prompt fission gamma radiation incident on a sample of thickness $0.05 \text{ gm/cm}^2$ .	50
2. 19	Energy and angle of emission spectra for prompt fission gamma radiation incident on a sample of thickness $0.10 \text{ gm/cm}^2$ .	51
2. 20	Energy and angle of emission spectra for prompt fission gamma radiation incident on a sample of thickness of $0.25 \text{ gm/cm}^2$ .	52
2. 21	Energy and angle of emission spectra for prompt fission gamma radiation incident on a sample of thickness $0.50 \text{ gm/cm}^2$ .	53
2. 22	Energy and angle of emission spectra for prompt fission gamma radiation incident on a sample of thickness $0.75 \text{ gm/cm}^2$ .	54
2. 23	Energy and angle of emission spectra for prompt fission gamma radiation incident on a sample of thickness $1.0 \text{ gm/cm}^2$ .	55
2. 24	Energy and angle of emission spectra for prompt fission gamma radiation incident on a sample of thickness $2.5 \text{ gm/cm}^2$ .	56
2. 25	Energy and angle of emission spectra for prompt fission gamma radiation incident on a sample of thickness $5.0 \text{ gm/cm}^2$ .	57
2. 26	Energy and angle of emission spectra for prompt fission gamma radiation incident on a sample of thickness $10 \text{ gm/cm}^2$ .	58

## ILLUSTRATIONS (cont'd)

<b>Figure</b>		<b>Page</b>
2.27	Energy spectra for prompt fission gamma radiation for thicknesses in the range from 0.01 to 10 gm/cm <sup>2</sup> .	59
3.1	Trajectories in the scattering plane for the incident electron $E_0$ , the scattered electron $E'$ , and the secondary electron $E$ . The momentum is represented by $p$ .	78
3.2	Energy groups for the 25-Mev electron program.	79
3.3	The number of secondaries escaping $S_e$ as a function of thickness for 25-Mev electrons.	80
3.4	The number of secondaries deposited $S_d$ as a function of thickness for 25-Mev electrons.	81
3.5	The energy of escape per unit path length as a function of thickness for 25-Mev electrons.	82
3.6	The energy deposited per unit path length as a function of thickness for 25-Mev electrons.	83
3.7	Energy and angle of emission spectra for 25-Mev electrons incident on a sample of thickness 0.01 gm/cm <sup>2</sup> .	84
3.8	Energy and angle of emission spectra for 25-Mev electrons incident on a sample of thickness 0.025 gm/cm <sup>2</sup> .	85
3.9	Energy and angle of emission spectra for 25-Mev electrons incident on a sample of thickness 0.05 gm/cm <sup>2</sup> .	86
3.10	Energy and angle of emission spectra for 25-Mev electrons incident on a sample of thickness 0.10 gm/cm <sup>2</sup> .	87
3.11	Energy and angle of emission spectra for 25-Mev electrons incident on a sample of thickness 0.25 gm/cm <sup>2</sup> .	88
3.12	Energy and angle of emission spectra for 25-Mev electrons incident on a sample of thickness 0.50 gm/cm <sup>2</sup> .	89

## ILLUSTRATIONS (cont'd)

<u>Figure</u>		<u>Page</u>
3.13	Energy and angle of emission spectra for 25-Mev electrons incident on a sample of thickness $0.75 \text{ gm/cm}^2$ .	90
3.14	Energy and angle of emission spectra for 25-Mev electrons incident on a sample of thickness $1.0 \text{ gm/cm}^2$ .	91
3.15	Energy and angle of emission spectra for 25-Mev electrons incident on a sample of thickness $2.5 \text{ gm/cm}^2$ .	92
3.16	Energy and angle of emission spectra for 25-Mev electrons incident on a sample of thickness $5.0 \text{ gm/cm}^2$ .	93
3.17	Energy and angle of emission spectra for 25-Mev electrons incident on a sample of thickness $10 \text{ gm/cm}^2$ .	94
3.18	Energy spectra for 25-Mev electrons for thicknesses in the range from $0.01$ to $10 \text{ gm/cm}^2$ .	95
4.1	Energy spectrum from 600-kv flash X-ray machine as a function of photon energy.	103
4.2	The number of secondaries escaping $S_e$ as a function of thickness for 600-kv X rays.	104
4.3	The number of secondaries deposited $S_d$ as a function of thickness for 600-kv X rays.	105
4.4	The energy of escape per unit path length as a function of thickness for 600-kv X rays.	106
4.5	The energy deposited per unit path length as a function of thickness for 600-kv X rays.	107
4.6	Energy spectra for 600-kv X rays for thicknesses in the range from $0.01$ to $10 \text{ gm/cm}^2$ .	108
4.7	Angle of emission spectrum for 600-kv X rays. The numbers $10, 5, 2.5 \dots$ etc., are thicknesses in $\text{gm/cm}^2$ .	109

## TABLES

<u>No.</u>		<u>Page No.</u>
2.1	Number of Gamma Rays per Fission as a Function of Incident Gamma Energy	25
2.2	Parameters for Sample Problem	26
2.3	Energy Losses and Secondary Electron Emission Efficiencies as a Function of Thickness for Prompt Fission Gamma Radiation	27
2.4	Number of Secondaries which Escape as a Function of Energy, Average Angle of Emission and Thickness for Prompt Fission Gamma Radiation	28
2.5	Number of Secondaries which Escape as a Function of Angle and Thickness for Prompt Fission Gamma Radiation	31
3.1	Critical Energy $E_C$ and the Ratio of the Radiative Loss to the Ionization Loss for Various Materials	71
3.2	Energy Losses and Secondary Electron Emission Efficiencies as a Function of Thickness for 25-Mev Electron	72
3.3	Number of Secondaries which Escape as a Function of Energy, Average Angle of Emission and Thickness for 25-Mev Electrons	73
3.4	Number of Secondaries which Escape as a Function of Angle and Thickness for 25-Mev Electrons	76
4.1	Energy Groups and Weighting Factors for 600-kv X-rays	98
4.2	Energy Losses and Secondary Electron Emission Efficiencies as a Function of Thickness for 600-kv X-rays	99
4.3	Number of Secondaries which Escape as a Function of Energy, Average Angle of Emission and Thickness for 600-kv X-rays	100
4.4	Number of Secondaries which Escape as a Function of Angle and Thickness for 600-kv X-rays	101
6.1	Summary	112

## SYMBOLS

<u>Symbol</u>	<u>Definition</u>
$h$	Planck's constant ( $6.6252 \times 10^{-27}$ erg · sec).
$\nu_0$	Frequency of the incident prompt fission gamma ray.
$c$	Speed of light ( $2.998 \times 10^{10}$ cm/sec).
$\nu$	Frequency of the scattered photon.
$\varphi$	Angle between the direction of the incident photon and the direction of the scattered photon.
$\theta$	Angle between the direction of the incident photon and the direction of the Compton electron.
$p$	Momentum of the Compton electron.
$T$	Kinetic energy of the Compton electron.
$m_0$	Rest mass of an electron ( $9.11 \times 10^{-28}$ gm).
$m_0 c^2$	Rest mass energy of an electron (0.51098 Mev).
$\alpha$	The incident photon energy over the rest mass energy of the electron ( $h\nu_0/m_0 c^2$ ).
$\sigma$	Average collision cross section for a Compton interaction in $\text{cm}^2/\text{e}$ .
$r_0$	Classical radius of an electron ( $2.818 \times 10^{-13}$ cm).
$\sigma_s$	Average scattered cross section for a Compton interaction in $\text{cm}^2/\text{e}$ .
$\sigma_a$	Average absorption cross section for a Compton interaction in $\text{cm}^2/\text{e}$ .
$T_{AV}$	Average energy of the recoil Compton electron.
$\theta_{AV}$	Average angle the recoil electron scatters with respect to the direction of incident photon.
$N_a$	Avogadro's number ( $6.025 \times 10^{23}$ $\frac{\text{atom}}{\text{mole}}$ ).
$A$	Atomic weight (gm/mole).
$Z$	Atomic number (number of electrons per atom).

## SYMBOLS (cont'd)

<u>Symbol</u>	<u>Definition</u>
$\Delta R$	A differential scattering element within a sample in $\text{gm/cm}^2$ .
$n_0$	Initial number of particles passing through a sample.
$n$	Number of particles escaping from the sample which did not have an interaction producing secondaries.
$dn$	Number of secondaries produced ( $n_0 - n$ ).
$E_0$	Initial energy of the incident particle (Mev).
$T$	Thickness of the sample in $\text{gm/cm}^2$ .
$P_e(E)$	Intensity or probability of escape for an electron of energy $E$ .
$P_d(E)$	Probability of deposition for an electron of energy $E$ .
$R$	The distance an electron traverses in $\text{gm/cm}^2$ .
$\bar{R}$	The average range of an electron with energy $E$ in $\text{gm/cm}^2$ .
$\alpha$	Range-straggling parameter. (The half-width of the Gaussian curve at $1/e$ of the maximum).
$\sigma$	The standard deviation.
$R_p$	Practical range in $\text{gm/cm}^2$ .
$S(E)$	The total number of secondaries born in some $\Delta R$ with energy $E$ per incident particle.
$S_e(E)$	The total number of secondaries born in some $\Delta R$ with energy $E$ which escape with energy $E_e$ per incident particle.
$S_d(E)$	The total number of secondaries born in some $\Delta R$ with energy $E$ which are deposited per incident particle.
$S_d$	Total number of secondaries per incident particle summed on $R$ and $E$ .
$E$	Energy the secondary is born with in Mev.
$E_e$	Energy the secondary escapes with in Mev.
$E_s$	Energy lost from the sample in Mev.
$E_d$	Energy deposited in the sample in Mev.

## SYMBOLS (cont'd)

<u>Symbol</u>	<u>Definition</u>
$N_m$	Number of gamma rays per fission in energy group $m$ .
$I$	Intensity of the gamma beam as a function of distance.
$I_0$	The initial intensity of the gamma beam.
$\frac{\mu}{\rho}$	Mass absorption in $\frac{\text{cm}^2}{\text{gm}}$
$A$	Attenuation factor.
$n$	Subscript.
$m$	Subscript.
$R_e$	Distance in $\text{gm}/\text{cm}^2$ to one-half the probability of escape.
$\Delta R_e$	The range left over after the electron escapes.
$E'$	The energy of an incident electron after a collision.
$\theta$	Angle between the incident electron and the secondary electron.
$\phi$	Angle between the incident electron and the scattered incident electron.
$d\sigma(E_0, E)$	Differential cross section which represents the probability at least one particle will have energy $E$ after a collision with an electron of energy $E_0$ .
$\sigma(E_0, E)$	Total cross section and represents the probability that one of the electrons will have energy between $E$ and $E_0/2$ when colliding with an electron of energy $E_0$ .



1. INTRODUCTION.

a. Objectives

(1) To aid in the simulation of the prompt fission gamma radiation field associated with a nuclear detonation by comparing the efficiencies of secondary-electron emission, energy spectra, angle-of-emission spectra, and energy losses for various laboratory radiation sources. Interest will be concentrated on 25-Mev electrons from a linear accelerator and a 600-kv pulsed X-ray source.

(2) To establish computer programs which can be used in transient radiation effects (TREE) studies to simulate any desired radiation energy source.

b. Background

The basic parameters for work in transient radiation effects have not been determined satisfactorily. This study was necessary because in weapon effects work instrumentation may be exposed to radiation fields as high as  $10^{12}$  r/sec. This extreme flux will cause electronic components to fail; therefore, the components must be tested beforehand in the laboratory to establish and possibly eliminate the effects expected in the nuclear environment. This work will permit the laboratory work to be done much more accurately.

2. SECONDARY ELECTRON EMISSION BY PROMPT FISSION GAMMA RADIATION.

a. General remarks

In this section a theoretical calculation is made of the energy spectra, the angle-of-emission spectra, the energy losses, and the efficiencies for secondary electrons emitted because of prompt fission gamma radiation. The calculation was done for low-Z materials with thicknesses

in the range from 0.01 to 10 gm/cm<sup>2</sup>. The Maienschein (1958) prompt fission gamma ray spectrum for U<sup>235</sup> fissions was used during the time interval less than  $5 \times 10^{-8}$  second. The Klein-Nishina cross sections were used to evaluate the above parameters.

There are three ways in which a photon can interact with matter to lose its energy: interaction with an atom as a whole, interaction with a free electron, and interaction with the Coulomb field of the nucleus.

The interaction of a photon with an atom as a whole leads to the photoelectric effect. The importance of this effect in the field of high energies and low-Z materials is negligible, so that it need not be considered in detail. The interaction of a photon with a free electron leads to the Compton effect. In this phenomenon the photon transfers part of its energy and momentum to the electron initially at rest. The interaction of a photon with the Coulomb field of the nucleus leads to the phenomenon of pair production, whereby the photon disappears and a positive and a negative electron simultaneously come into existence. For this phenomenon to occur, the energy of the photon must exceed the rest energy of two electrons. The excess energy appears almost completely as kinetic energy of the two electrons, while the recoil of the nucleus accounts for the momentum balance. Pair production predominates in the high-Z, high-energy region, whereas the Compton effect predominates in the low-Z, intermediate-energy group (figure 2.1) which is the region of interest in this report.

Both the Compton effect and pair production are typical quantum phenomena without a classical counterpart. Their description requires the use of quantum electrodynamics along with quantum mechanics.

#### b. Theory.

##### (1) Conservation laws for the Compton effect

As was stated above, the area of interest in this report is the area in figure 2.1 labeled the Compton effect.

In figure 2.2, the incident photon is represented by an energy  $h\nu_0$ . The scattered photon is emitted at an angle  $\phi$  with an energy  $h\nu$ , and

the electron recoils at an angle  $\theta$  with a momentum  $p$  and a kinetic energy  $T$ . The relations for the conservation of momentum for this collision can now be written, remembering that the momentum of a photon is  $\frac{h\nu}{c}$ . Conservation of momentum in the direction of  $h\nu_0$  is expressed by

$$\frac{h\nu_0}{c} = \frac{h\nu}{c} \cos \phi + p \cos \theta \quad (2.1)$$

while conservation of momentum normal to this direction gives

$$0 = \frac{h\nu}{c} \sin \phi - p \sin \theta \quad (2.2)$$

A third relation between these variables is obtained from the conservation of energy,

$$h\nu_0 = h\nu + T. \quad (2.3)$$

Using the relativistic relationship

$$pc = \sqrt{T(T + 2m_0c^2)} \quad (2.4)$$

and some algebra, one can eliminate any two parameters from these three equations. It should be noted that these equations represent only the fundamental conservation laws as applied to a two-body collision. They must, therefore, be obeyed regardless of the details of the interactions at the scene of the collision.

To describe the angular distribution of the Compton electrons

and to take into account the true distance they travel through the sample, it is necessary to derive by the proper combination of the four preceding equations the following equation for the energy of the Compton electron in terms of its scattering angle:

$$T = h\nu_0 \frac{2\alpha \cos^2 \theta}{(1 + \alpha)^2 - \alpha^2 \cos^2 \theta} \quad (2.5)$$

where  $\alpha = h\nu_0/m_0c^2$ . The details of this derivation can be found in the appendix of Semat (1958).

## (2) Klein-Nishina cross sections

Because classical methods cannot cope with the general collision involving high-energy photons, Klein-Nishina successfully applied Dirac's relativistic theory of the electron to this problem and obtained a general solution which is in remarkable agreement with experiments.

The summation of the probabilities of all possible collisions between the incident photon and each free electron is generally the total collision cross section. Because it represents the integrated probability per electron that some scattering event will occur, it is physically clearer to speak of this integral as the average collision cross section  $\sigma$ . The average collision cross section is the same for polarized or unpolarized incident radiation. By integrating the differential cross section over all permissible angles, one finds the following result:

$$\sigma = 2\pi r_0^2 \left\{ \frac{1+\alpha}{\alpha^2} \left[ \frac{2(1+\alpha)}{1+2\alpha} - \frac{1}{\alpha} \ln(1+2\alpha) \right] + \frac{1}{2\alpha} \ln(1+2\alpha) - \frac{1+3\alpha}{(1+2\alpha)^2} \right\} \text{ cm}^2/\text{e} \quad (2.6)$$

where  $r_0$  is the classical electron radius.

Experimental interest often centers on the average properties of the scattered radiation; thus, the average scattered cross section  $\sigma_s$  is

$$\sigma_s = \pi r_o^2 \left[ \frac{1}{3} \ln(1 + 2a) + \frac{2(1+a)(2a^2 - 2a - 1)}{a^2(1+2a)^2} + \frac{8a^2}{3(1+2a)^3} \right] \text{ cm}^2/\text{e}. \quad (2.7)$$

The total cross section or average collision cross section is given by

$$\sigma = \sigma_a + \sigma_s \quad (2.8)$$

where  $\sigma_a$  is the average absorption cross section. Thus,

$$\sigma_a = \sigma - \sigma_s \quad (2.9)$$

or

$$\sigma_a = 2\pi r_o^2 \left[ \frac{2(1+a)^2}{a^2(1+2a)} - \frac{1+3a}{(1+2a)^2} - \frac{(1+a)(2a^2 - 2a - 1)}{a^2(1+2a)^2} - \frac{4a^2}{3(1+2a)^3} - \left( \frac{1+a}{a^3} - \frac{1}{2a} + \frac{1}{2a^3} \right) \ln(1+2a) \right] \text{ cm}^2/\text{e} \quad (2.10)$$

From the conservation of energy, equation (2.3), each scattered photon  $h\nu$  has associated with it a recoil electron whose energy is

$$T = h\nu_o - h\nu. \quad (2.11)$$

Therefore, the average kinetic energy  $T_{AV}$  of all recoil electrons from Compton interactions will be

$$T_{AV} = h\nu_o - h\nu_{AV} \quad (2.12)$$

Hence

$$\frac{T_{AV}}{h\nu_o} = 1 - \frac{h\nu_{AV}}{h\nu_o} = 1 - \frac{\sigma_s}{\sigma} = \frac{\sigma_a}{\sigma} \quad (2.13)$$

(Evans, 1955, p. 688).

An electron born with an average energy  $T_{AV}$ , scattered at an average angle  $\theta_{AV}$ , and at a given distance  $R_n$  in the sample with respect to the escaping interface, has a true distance of  $R_n/\cos \theta_{AV}$  to traverse before escaping from the sample. Therefore, to account for the angular distribution it is necessary to derive an expression for the  $\cos \theta_{AV}$ . By solving equation (2.5) explicitly for  $\cos \theta$  and taking an average value for  $\theta$  and  $T$ , one gets

$$\cos \theta_{AV} = \sqrt{\frac{T_{AV} (1 + a)^2}{T_{AV} a^2 + 2a h\nu_o}} \quad (2.14)$$

All the pertinent parameters needed to describe the interaction between an incident photon and an atomic electron have now been derived. Now, the theory necessary for calculating the number of secondary electrons produced per incident particle will be developed.

### (3) Secondary electron production

In a thin absorbing sample, having  $\frac{N}{A}$  atoms/gm, each with  $Z$  electrons/atom, and of a thickness  $\Delta R$  in gm/cm<sup>2</sup>, there are  $\frac{N Z}{A} \Delta R$

electrons/gm and  $\frac{N Z \Delta R}{A}$  electrons/cm<sup>2</sup>. Let a collimated beam of  $n_0$  particles, each with energy  $E_0$ , pass normally through the sample (figure (2.3)).

The number  $dn = n_0 - n$  is the number of primary particles giving up some of its energy to produce secondary electrons. Therefore, the number of secondary electrons per incident particle produced in  $\Delta R$  is

$$-\frac{dn}{n_0} = \frac{N Z \Delta R}{A} \sigma \quad (2.16)$$

$-\frac{dn}{n_0}$  will be redefined to equal  $S$ : therefore, equation (2.16) becomes

$$S(E) = \frac{N Z \Delta R}{A} \sigma(E) \quad (2.17)$$

with its energy functional dependence included. The constant in equation (2.17) can be evaluated by assuming  $A = 2Z$  (low  $Z$  materials) and its value is  $0.30125 \times 10^{24}$  electrons/gm or  $0.30125 \frac{\text{cm}^2 \cdot e}{\text{gm} \cdot \text{barns}}$ . Therefore, equation (2.17) becomes

$$S(E) = 0.30125 \Delta R \sigma(E) \quad (2.18)$$

where  $S(E)$  is in secondary electrons per incident particle,  $\Delta R$  is in gm/cm<sup>2</sup>, and  $\sigma(E)$  is in barns/electron. This is a general derivation since the incident particle can be a gamma ray, an electron, or an X ray if the appropriate cross sections are taken into account.

Now that the number of secondaries produced per incident particle in a differential element  $\Delta R$  have been determined, it is appropriate to evaluate the number of those produced which escape and the number which are deposited.

## (4) Probability of escape and deposition

Since the range of any one of a group of initially monoenergetic particles can be regarded as the sum of a very large number of statistically independent displacements corresponding to a succession of small energy losses, it should be expected that the probability distribution of the ranges about the average value,  $\bar{R}$ , is given by the Gaussian function. The width of the Gaussian curve will be proportional to the mean squared fluctuation  $(R - \bar{R})^2_{AV}$ . Thus the probability of finding a particle with range between  $R$  and  $R + dR$  is (Segre, 1953, p. 245)

$$P_e(R) dR = \frac{1}{a\sqrt{\pi}} \exp \left[ - \frac{(R - \bar{R})^2}{a^2} \right] dR \quad (2.19)$$

where

$$(R - \bar{R})^2_{AV} = \int_{-\infty}^{\infty} P_e(R) (R - \bar{R})^2 dR = \frac{1}{2} a^2. \quad (2.20)$$

Experimentally, it is not very convenient to make direct measurement of the number of particles whose ranges end in the interval from  $R$  to  $R + dR$ . Instead, the number of particles which reach a certain distance  $R$  from the source, that is, particles whose range is greater than  $R$ , are usually measured.

Equation (2.19) can be integrated from  $R$  to infinity to give

$$P_e(R) = \frac{1}{2} (1 - \operatorname{erf} \frac{R - \bar{R}}{a}) \quad (2.21)$$

where  $P_e(R)$  is the probability of escape or the intensity of the electrons as a function of distance (the ordinate of the number-distance curve in figure



2.4),  $\text{erf } x = \frac{2}{\sqrt{\pi}} \int_0^x e^{-t^2} dt$  is the error function or the probability integral, and  $\alpha$  is the range-straggling parameter (the half-width of the Gaussian distribution at  $1/e$  of the maximum). The quantity  $\alpha$  is also equal to  $\sqrt{2}$  times the standard deviation,  $\sigma$ . The slope of the curve in figure 2.4 is equal to  $1/\alpha\sqrt{\pi}$ . Therefore, the relationship between the practical  $R_p$  and average ranges  $\bar{R}$  is

$$\frac{.5}{R_p - \bar{R}} = \frac{1}{\alpha\sqrt{\pi}} \quad (2.22)$$

Solving explicitly for the range straggling parameter  $\alpha$ , one finds the following relationship

$$\alpha = \frac{2}{\sqrt{\pi}} (R_p - \bar{R}). \quad (2.23)$$

To evaluate the probability of escape or the probability of being deposited  $P_d(E)$  which is by definition  $[1 - P_e(R)]$ , it is only needed to determine the practical and average ranges.

#### (5) Range of electrons.

Empirical relationships between the practical range  $R_p$  and the energy  $E$  have been proposed by many workers. An excellent review of all electron range-energy work up to 1951 has been given by Katz and Penfold (1952). Based on a compilation of all available data, these authors propose the following empirical relationships, where  $E$  is in Mev and  $R_p$  is in  $\text{gm/cm}^2$ . For energies from 0.01 to ~3 Mev

$$R_p = 0.412 E^n$$

$$n = 1.265 - 0.0954 \ln E \quad (2.24)$$

and for energies from ~1 to ~20 Mev

$$R_p = 0.530 E - 0.106. \quad (2.25)$$

The agreement between the above empirical analytical forms and experimental range-energy curves is excellent. This fact can be observed in figure 2.5.

By comparing the average range  $\bar{R}$  and the practical range  $R_p$  of the experimental absorption curves given in figure 2.6, the relationship relating then, averaged, gives

$$\bar{R} = 0.662 R_p. \quad (2.26)$$

The three preceding equations will be used for determining the average range of an electron as a function of energy.

Now, it is possible to evaluate equation (2.23) in terms of the average range  $\bar{R}$ . The result is

$$a = 0.5762 \bar{R}. \quad (2.27)$$

#### (6) Number and energy losses.

The total number of secondary electrons born per incident particle in  $\Delta R$  is  $S(E)$  given by equation (2.18). The probability of these electrons escaping from  $\Delta R$  is  $P_e(E)$ . Therefore, the fraction of secondaries which escapes per incident particle  $S_e(E)$  is

$$S_e(E) = S(E) P_e(R) \quad (2.28)$$

TDR-63-50

or

$$S_e(E) = 0.30125 \Delta R \sigma(E) P_e(R) \quad (2.29)$$

By the same argument, the number of secondaries deposited per incident particle  $S_d(E)$  is

$$S_d(E) = S(E) P_d(R). \quad (2.30)$$

Since,

$$P_d(E) = 1 - P_e(R) \quad (2.31)$$

Equation (2.30) can be written in the form

$$S_d(E) = S(E) [1 - P_e(R)] \quad (2.32)$$

or

$$S_d(E) = 0.30125 \Delta R \sigma(E) [1 - P_e(R)] \quad (2.33)$$

The total number of secondaries produced per incident particle is also equal to

$$S(E) = S_e(E) + S_d(E). \quad (2.34)$$

The energy which is lost from the sample would be equal to the number which escape  $S_e(E)$  times the electron energy of escape  $E_e$ .

$$E_L = E_e S_e(E). \quad (2.35)$$

Conversely, the energy deposited is the sum of the energy deposited by the electrons which escape and the energy deposited by the electrons that did not escape.

$$E_d = (E - E_e) S_e(E) + E S_d(E) . \quad (2.36)$$

Equation (2.36) can also be written in the following form:

$$E_d = E S(E) - E_e S_e(E) \quad (2.37)$$

by combining and substituting equation (2.34). The energy lost  $E_e$  and the energy deposited  $E_d$  are in units of Mev. To change units to Mev/gm/cm<sup>2</sup>, it is only necessary to divide by the sample thickness  $T$ .

#### (7) Energy losses by gamma rays

The energy losses by gamma rays can be determined by use of figure 2.7. By a weighted average of the prompt fission spectrum, figure 2.8, it was found from figure 2.7 that

$$1 \frac{r}{hr} = 5.3 \times 10^5 \text{ Mev/cm}^2 \cdot \text{sec.}$$

By eliminating time, 1 r is  $1.91 \times 10^9$  Mev per cm<sup>2</sup> and deposits 100 ergs/gm of material or

$$1 \frac{\text{Mev}}{\text{cm}^2} = 5.24 \times 10^{-8} \text{ ergs/gm.}$$

Approximately 7.7 Mev/fis are liberated when an atom of U<sup>235</sup> fissions. Therefore the energy deposited per unit thickness per fission in a sample material is

$$1 \text{ fission} = 0.252 \text{ Mev/gm/cm}^2.$$

However, the soft collisions (low-energy secondary electrons) cause approximately half of this energy deposition. Therefore since the interest is in the hard collisions (high energy secondary electrons), the above number will be divided by two with the result

$$1 \text{ fission} = 0.126 \text{ Mev/gm/cm}^2.$$

### c. Procedure

The calculations in this report were made on a CDC 1604 high-speed digital computer. The programs and sample outputs are contained in the appendixes. To simplify the explanation of the calculational procedure, a slide-rule accuracy example will be presented. The calculations were done for sample thicknesses in the range from 0.01 to 10 gm/cm<sup>2</sup>.

#### (1) Energy groups

The Maienschein (1958) energy spectrum, figure 2.8, for prompt fission gamma radiation from U<sup>235</sup> fission for times less than  $5 \times 10^{-8}$  seconds, was used in the gamma-ray program. This spectrum was considered to be the best available for this type of calculation by several of the prominent people in the field. The average gamma ray energy from this spectrum was determined and found to be approximately 0.85 Mev. The number of gamma rays per fission was found to be 9.1 with energy being emitted at a rate of 7.7 Mev/fission. All this information was evaluated by choosing a  $\Delta E$  of 0.2 Mev on the abscissa and reading the average ordinate. Table 2.1 contains the results of the average ordinate multiplied by  $\Delta E$  as a function of the appropriate energies. The number of gamma rays per fission  $N_m$  was used as a weighting factor in determining the following parameters.

The energies of the incident photons were divided up into 39 groups as shown in table 2.1. The average energy of the group was chosen as the representative photon; for example, the first group with energies between 0.0 and 0.2 Mev has an average photon energy of 0.1 Mev.

#### (2) Sample division

The sample was divided into  $\Delta R$ s with thicknesses decreasing by one-half each time, figure 2.9. The numbers  $n$  represent the center lines of each  $\Delta R$ . The quantity  $R_n$  represents the shortest distance a secondary electron would have to travel before escaping. These quantities are related mathematically by the following relationships:

$$\begin{array}{ll}
 R_1 = \frac{3}{4} T & \Delta R_1 = \frac{1}{2} T \\
 R_2 = \frac{1}{2} R_1 & \Delta R_2 = \frac{1}{2} \Delta R_1 \\
 \vdots & \vdots \\
 R_n = \frac{1}{2} R_{n-1} & \Delta R_n = \frac{1}{2} \Delta R_{n-1} \\
 \vdots & \vdots \\
 R_f = \frac{2}{3} R_{f-1} & \Delta R_f = 2 R_f
 \end{array} \quad (2.38)$$

The final  $R_n$  was chosen to be greater than  $5 \times 10^{-4} \text{ gm/cm}^2$ . Therefore, the final  $R$  must be equal to or less than  $3 \frac{1}{3} \times 10^{-4} \text{ gm/cm}^2$ , or  $\Delta R$  must be equal to or less than  $6 \frac{2}{3} \times 10^{-4} \text{ gm/cm}^2$ . There were 5 divisions or  $\Delta R$ s for a sample thickness of  $0.01 \text{ gm/cm}^2$  ranging to 15 divisions for a thickness of  $10 \text{ gm/cm}^2$ .

### (3) Attenuation

In the passage of gamma-ray photons through matter, they are absorbed so that the intensity falls off exponentially. This arises from the fact that the extent of absorption in a small thickness  $dR$  in  $\text{gm/cm}^2$  of matter, at any point in the medium, is proportional to the radiation intensity at that point and to the thickness traversed; that is,

$$\frac{dI}{I} = - \frac{\mu}{\rho} dR \quad (2.39)$$

Integrating this equation gives

$$I = I_0 e^{-\frac{\mu}{\rho} R} \quad (2.40)$$

where  $\mu$  is the linear absorption coefficient of the absorber for the given radiation. If  $A = 2Z$ , then  $\mu/\rho = 0.30125 \sigma$ , where  $\sigma$  is the total cross section in barns. Therefore, equation (2.40) becomes

$$I = I_0 e^{-0.30125 \circ (T - R_n)} \quad (2.41)$$

where  $T$  and  $R_n$  are the same quantities as defined in figure 2.9. The attenuation factor  $A$  is

$$A = \frac{I}{I_0} = e^{-0.30125 \circ (T - R_n)} \quad (2.42)$$

This factor was multiplied by the secondary electron emission efficiencies, equations (2.29) and (2.33), to take into account the attenuation of the incident gamma rays.

#### (4) Sample problem

The parameters in table 2.2 will be used in the following sample calculation.

In the beginning, equation (2.21), the probability of escape  $P_e$ , was investigated:

$$P_e(R) = \frac{1}{2} (1 - \operatorname{erf} \frac{R - \bar{R}}{\alpha}) \quad (2.21)$$

Notice, if  $R = \bar{R}$  the argument of the error function is zero; hence, the error function is zero making  $P_e(\bar{R}) = 0.5$ , which is the correct value. As  $R$  approaches infinity the error function approaches 1, thus,  $P_e(\infty) = 0$ , which is a correct value. However, on the other end where  $R = 0$ , the argument of the error function becomes, by employing equation (2.27), a negative  $1/0.5762$ . This makes the error function take on a value of negative 0.98588; hence, the  $P_e(0) = 0.99294$ . This value should be exactly 1, since the electron does not have to travel any distance ( $R = 0$ ); thus, the  $P_e(0)$  must equal 1. Therefore, 0.99294 was used as a scaling factor for the probability of escape  $P_e$ .

The next step was to evaluate the cross sections for the energy group of incident photons chosen. In this case the group lies between 1.0 and 1.2 Mev of table 2.1 with an average photon energy of 1.1 Mev. The

quantity,  $\alpha = \frac{\langle h\nu_o \rangle_{AV}}{m_o c^2}$ , is evaluated and in this case equals 2.155.

Substituting this value in equations (2.6) and (2.10), then evaluating, one finds

$$\sigma = 0.2015 \text{ barns}$$

and

$$\sigma_a = 0.0913 \text{ barns.}$$

From equation (2.13), the average kinetic energy  $T_{AV}$  of the recoil Compton electron is

$$T_{AV} = \langle h\nu_o \rangle_{AV} \frac{\sigma_a}{\sigma} = 0.499 \text{ Mev.}$$

By a careful investigation of equations (2.24) and (2.25), it was determined that an energy of 2.4 Mev would be the best cutoff point between the two equations. Therefore, since the above energy is less than 2.4 Mev, equation (2.24) was used in combination with equation (2.26), giving

$$\begin{aligned} \bar{R} &= 0.273 E^n \\ n &= 1.265 - 0.0954 \ln E \end{aligned} \tag{2.43}$$

In this case  $E$  is  $T_{AV}$  and evaluating equation (2.43) for the above  $T_{AV}$  gives

$$\bar{R}(0.499) = 0.1081 \text{ gm/cm}^2.$$

The average kinetic energy  $T_{AV}$  and range  $\bar{R}$  for the Compton electron have been determined. The next most important thing to calculate is the cosine of the angle of emission. As given by equation (2.15), this



quantity can be evaluated immediately.

$$\cos \theta_{AV} = 0.839.$$

The probability of escape was determined by equation (2.21) to be

$$P_{en}(R) = \frac{1}{2} (1 - \operatorname{erf} \frac{R - \bar{R}}{a}).$$

To get a physical meaning of this quantity, figure 2.10 is presented. Notice that  $R$  is the actual distance the electron travels and  $R_n$  is the distance from the center line of the appropriate  $\Delta R$  to the interface (shortest distance). The quantities  $R$  and  $R_n$  are related by the following equation:

$$R = R_n / \cos \theta_{AV} \quad (2.44)$$

In this problem,  $R = 0.223$ . The probability of escape, using the above parameters, is

$$P_{e2}(R) = 0.0047.$$

The attenuation  $A$  of the incident beam will be determined by employing equation (2.42). The result is

$$A = 0.98121.$$

Finally, the secondary electron emission efficiencies may be calculated. Equation (2.29) gives the fraction of secondary electrons which escape per incident particle and takes the following form when the attenuation is included:

$$S_{en}(E) = 0.30125 \Delta R_n \sigma(E) P_{en}(R) A_n \quad (2.45)$$

Substituting and evaluating equation (2.45) for this sample problem gives

$$S_{e2}(1.1) = 3.486 \times 10^{-5} \text{ se/i}\gamma .$$

To properly weight this number for the entire prompt fission spectrum (figure 2.8), the number of gammas per fission  $N_m$  from table 2.1 for the energy group from 1.0 to 1.2 Mev was multiplied by the above number. This gives

$$S_{e2}(1.1) = 1.743 \times 10^{-5} \text{ se/fis} .$$

To determine the number given in column 7 of appendix A for this energy group, the above number must be added to the contribution for all the other  $\Delta R$ s; i. e., column 7 is a sum on  $R$ .

$$S_e(E) = N(E) \sum_{n=1}^R S_{en}(E) \quad (2.46)$$

Notice that this number is very small compared with the number given ( $2.614 \times 10^{-3}$ ). Thus, this indicates that most of the electrons which escape come from the final  $\Delta R$ s. Column 8 is a double sum on  $R$  and  $E$ . It is also weighted by the numbers given in table 2.1 in the following way:

$$S_e = \frac{\sum_{m=1}^E S_{em}(E)}{\sum_{m=1}^E N_m} \quad (2.47)$$

or by substituting equation (2.46)

$$S_e = \frac{\sum_{m=1}^E \left[ N_m \sum_{n=1}^R S_{en}(E) \right]}{\sum_{m=1}^E N_m} \quad (2.48)$$

The final number  $S_e$  in column 8 is the total number of secondaries per incident photon with the proper weighting. In this case, for a thickness of  $0.5 \text{ gm/cm}^2$ ,  $S_e$  is  $2.952 \times 10^{-3}$ .

The number of secondaries per incident particle which are deposited is determined in a similar manner. Equation (2.33) becomes

$$S_{dn}(E) = 0.30125 \Delta R_n \phi(E) [1 - P_{en}(R)] A_n \quad (2.49)$$

after taking the  $R$  dependence and the attenuation into account. Substituting and evaluating equation (2.49) gives

$$S_{d2}(1.1) = 7.410 \times 10^{-3} \text{ se/i}\gamma$$

However, the number in column 9 is given as a sum on  $R$  and is weighted by the numbers in table 2.1; for example,

$$S_{d2}(1.1) = 3.705 \times 10^{-3} \text{ se/fis.}$$

Notice that this number is approximately equal to the one given ( $1.239 \times 10^{-2}$ ), thus indicating that most of the electrons deposited come from the first  $\Delta R$ s. Column 9 is the following sum:

$$S_d(E) = N(E) \sum_{n=1}^R S_{dn}(E) \quad (2.50)$$

in secondaries per fission. Like the preceding discussion, column 10 is

$$S_d = \frac{\sum_{m=1}^E \left[ N_m \sum_{n=1}^R S_{dn}(E) \right]}{\sum_{m=1}^E N_m} \quad (2.51)$$

in secondaries per incident photon.

To calculate the energy of escape, it is necessary to recall the probability function and a diagram for simplification, figure 2.11. The area under the curve to the right of  $P_e(R)$  represents the probability of escape and is equal to the value given for  $P_e(R)$ . Since the curve is Gaussian, the area under the entire curve is unity. Therefore, the remaining area is the probability of being deposited  $[P_d(R) = 1 - P_e(R)]$ . To determine the average energy of escape  $E_e$ , it will be necessary to go to the mid-point of the remaining area, which is the same as taking half of the actual probability of escape  $P_e(R)$ , and work backwards through the probability function. Thus

$$P_e(R_e) = \frac{1}{2} P_e(R). \quad (2.52)$$

The energy of escape is related to the range which remains after escape. Therefore, it is interesting to determine the range which is left over, namely

$$\Delta R_e = R_e - R \quad (2.53)$$

The energy can then be calculated from the semi-empirical range-energy equations given in a previous subdivision. From figure 2.11, the following relationship can be derived by arrangement of parameters:

$$\Delta R_e = \left( \frac{R_e - \bar{R}}{\alpha} \right) \alpha + \bar{R} - R. \quad (2.54)$$

Notice that the argument of the error function from equation (2.52) is the quantity  $\left(\frac{R_e - \bar{R}}{a}\right)$ . Therefore, by solving equation (2.52) for this quantity and substituting it in equation (2.54),  $\Delta R_e$  can be solved since the other quantities are known.

For example, in the sample problem  $P_e(R) = 0.0047$  equation (2.52) give  $P_e(R_e) = 0.00235$ , since

$$P_e(R_e) = \frac{1}{2} (1 - \operatorname{erf} \frac{R_e - \bar{R}}{a})$$

Solving this equation for the argument of the error function gives

$$\left(\frac{R_e - \bar{R}}{a}\right) = 2.007 .$$

Substituting in equation (2.54) and evaluating give

$$\Delta R_e = 9.45 \times 10^{-3} \text{ gm/cm}^2 .$$

By choosing the correct range-energy equation for this  $\Delta R_e$  and solving it explicitly for energy, it is found that

$$E_e = \exp \left[ \frac{1.265 - \sqrt{1.6 - 0.3816 \ln(\Delta R_e/0.273)}}{0.1908} \right] \quad (2.55)$$

Solving equation (2.55) gives

$$E_e = 0.103 \text{ Mev} .$$

The energy lost from the sample was calculated using

equation (2.35).

$$E_{\ell n}(E) = E_{en} S_{en}(E)$$

$$E_{\ell 2}(E) = 1.8 \times 10^{-6} \text{ Mev/fis.}$$

This is not equal to the number  $(8.448 \times 10^{-4})$  given in column 3 for the energy group because column 3 is a sum on  $R$ . Hence, column 3 is

$$E_{\ell}(E) = \sum_{n=1}^R E_{en} S_{en}(E). \quad (2.56)$$

Column 4 is a double sum taking the following form:

$$E_{\ell} = \sum_{m=1}^E \sum_{n=1}^R E_{emn} S_{emn}(E). \quad (2.57)$$

Likewise, columns 5 and 6 take the same form as shown above but they represent the energy deposited. Equation (2.36) gives the energy deposited:

$$E_{dm}(E) = (E - E_e) S_{em}(E) + E S_{dn}(E)$$

$$E_{d2}(E) = 1.89 \times 10^{-3} \text{ Mev/fis.}$$

This is approximately equal to the number given in column 5  $(6.720 \times 10^{-3})$ , indicating that most of the energy which is deposited occurs in the first  $\Delta R$ s. Column 6 is the energy deposited summed on  $R$  and  $E$ .

The second set of data in the appendixes represents the parameters for the energies of escape. Columns 1 and 2 represent the energy bands for the secondary electron energy of escape. Column 3 is

the number of secondaries per incident particle  $S_e$  which escape in that energy band. Column 4 is the average angle of escape in degrees for electrons which escaped in that energy band. Column 5 is the product of the average energy for the group times the number of secondaries per incident particle which escape ( $\bar{E} S_e$ ). The energy spectra to follow were plotted using this data.

The final set of data in the appendixes gives the angular distribution. Columns 1 and 2 are the lower angle limit and upper angle limit, respectively. Notice that the angular interval was chosen to be 2 degrees. Column 3 is the number of secondaries emitted in that angular interval. The angle-of-emission spectra to follow were taken from these data.

#### d. Results

The results are contained in table 2.3 (Energy Losses and Secondary Electron Emission Efficiencies as a Function of Thickness for Prompt Fission Gamma Radiation) and table 2.4 (Number of Secondaries which Escape as a Function of Energy, Average Angle of Emission and Thickness for Prompt Fission Gamma Radiation). The data contained in table 2.3 can be found plotted in figures 2.12 - 2.15, and table 2.4-2.5 data are in figures 2.16 - 2.27.

#### e. Discussion

Figure 2.12 gives the number of secondaries escaping  $S_e$  as a function of thickness. Notice that at a thickness of  $0.01 \text{ gm/cm}^2$ ,  $S_e$  is  $4.7 \times 10^{-4}$  secondary electrons per incident photon (se/i $\gamma$ ) with a constant increase with thickness to approximately  $1 \text{ gm/cm}^2$  where the curve reaches a maximum value of  $3 \times 10^{-3}$  se/i $\gamma$  (0.3%); thereafter it begins to decrease with thickness to a value of  $2 \times 10^{-3}$  se/i $\gamma$  at  $10 \text{ gm/cm}^2$ . The increase is due to more atomic electrons being made available and the decrease is due to the attenuation of the incident beam.

Figure 2.13 is a plot of the number of secondaries deposited  $S_d$  as a function of thickness. It forms a straight line on log-log paper. This function increases with thickness from  $7 \times 10^{-3}$  se/i $\gamma$  at  $0.10 \text{ gm/cm}^2$  to

0.9 se/iy at  $10 \text{ gm/cm}^2$ . This seems reasonable since one would expect more secondary electrons to be deposited as the thickness is increased.

In figure 2.14, the energy of escape per unit path length is given as a function of thickness. It is shown that the energy loss  $E_e$  is greatest for small thicknesses ( $E_e = 1.45 \times 10^{-1} \text{ Mev/gm/cm}^2$ ) and decreases to  $1.25 \times 10^{-3} \text{ Mev/gm/cm}^2$  for large thicknesses ( $10 \text{ gm/cm}^2$ ), which is as expected.

Figure 2.15, the energy deposited as a function of thickness, follows the reverse of figure 2.14; that is, the energy deposited increases with thickness. It should be observed that upon adding the curves in figures 2.14 and 2.15 point for point the total energy removed from the incident beam is  $0.170 \text{ Mev/gm/cm}^2$ . This is in good agreement with the number predicted in section 2b(7) ( $0.126 \text{ Mev/gm/cm}^2$ ).

Figures 2.16 to 2.26 contain the energy and angle-of-emission spectra for prompt fission gamma radiation for thicknesses in the range from  $0.01$  to  $10 \text{ gm/cm}^2$ . The energy spectrum is a plot of the number of secondaries escaping per incident photon per energy interval,  $S_e$  as a function of the energy of escape  $E_e$ .

Figure 2.27 contains all the energy spectra so one can get a relative perspective of their intensities as a function of thickness. Notice that the intensity increases with thickness up to  $0.75 \text{ gm/cm}^2$  and then decreases. The most probable energy of escape  $E_e$  occurs at approximately the same value ( $0.15 \text{ Mev}$ ) for almost all the thicknesses except the larger ones where the peaks are broader, making the most probable energy of escape less pronounced.



Table 2.1

Number of Gamma Rays Per Fission as a Function  
of Incident Gamma Energy

$h\nu_0$ (Mev)	$N_m$ ( $\gamma$ /fis)	$h\nu_0$ (Mev)	$N_m$ ( $\gamma$ /fis)	$h\nu_0$ (Mev)	$N_m$ ( $\gamma$ /fis)
0 - 0.2	2.00	2.6 - 2.8	.068	5.2 - 5.4	.0050
0.2 - 0.4	2.00	2.8 - 3.0	.052	5.4 - 5.6	.0042
0.4 - 0.6	1.46	3.0 - 3.2	.053	5.6 - 5.8	.0034
0.6 - 0.8	0.94	3.2 - 3.4	.034	5.8 - 6.0	.0023
0.8 - 1.0	0.60	3.4 - 3.6	.028	6.0 - 6.2	.0017
1.0 - 1.2	0.50	3.6 - 3.8	.024	6.2 - 6.4	.0010
1.2 - 1.4	0.40	3.8 - 4.0	.014	6.4 - 6.6	.00088
1.4 - 1.6	0.24	4.0 - 4.2	.016	6.6 - 6.8	.00080
1.6 - 1.8	0.20	4.2 - 4.4	.012	6.8 - 7.0	.00090
1.8 - 2.0	0.16	4.4 - 4.6	.010	7.0 - 7.2	.00100
2.0 - 2.2	0.13	4.6 - 4.8	.0064	7.2 - 7.4	.00084
2.2 - 2.4	0.11	4.8 - 5.0	.0044	7.4 - 7.6	.00040
2.4 - 2.6	0.036	5.0 - 5.2	.0043	7.6 - 10.5	.00029

Table 2.2  
Parameters for Sample Problem

Parameter	Value
T (thickness)	0.50 gm/cm <sup>2</sup>
$h\nu_0$	1.0 - 1.2 Mev
$\langle h\nu_0 \rangle_{AV}$	1.1 Mev
$R_2$	0.1875 gm/cm <sup>2</sup>
$\Delta R_2$	0.1250 gm/cm <sup>2</sup>

Table 2.3

Energy Losses and Secondary Electron  
Emission Efficiencies as a Function of  
Thickness for Prompt Fission Gamma Radiation

T (gm/cm <sup>2</sup> )	E <sub>l</sub> (Mev.cm <sup>2</sup> /gm.fis)**	E <sub>d</sub> (Mev.cm <sup>2</sup> /gm.fis)**	S <sub>e</sub> (se/1γ)	S <sub>d</sub> (se/1γ)
10.0	1.20-3*	1.69-1	1.91-3	9.25-1
5.0	2.94-3	1.68-1	2.46-3	4.61-1
2.5	6.51-3	1.64-1	2.81-3	2.29-1
1.0	1.71-2	1.53-1	3.02-3	8.97-2
0.75	2.26-2	1.48-1	3.03-3	6.66-2
0.50	3.24-2	1.38-1	2.95-3	4.35-2
0.25	5.37-2	1.17-1	2.61-3	2.06-2
0.10	8.54-2	8.49-2	1.92-3	7.39-3
0.05	1.08-1	6.29-2	1.36-3	3.29-3
0.025	1.27-1	4.36-2	9.05-4	1.42-3
0.01	1.45-1	2.52-2	4.69-4	4.63-4

\*  $1.2 \times 10^{-3}$

\*\* 9.1 gammas/fis

Table 2.4

Number of Secondaries Which Escape as a Function  
of Energy, Average Angle of Emission and Thickness for  
Prompt Fission Gamma Radiation

$E_e^*$ (Mev)	T = 10 gm/cm <sup>2</sup>		T = 5 gm/cm <sup>2</sup>		T = 2.5 gm/cm <sup>2</sup>		T = 1.0 gm/cm <sup>2</sup>	
	$S_e(10^{-4} \text{ se})$ 1Y	$\theta(\text{deg})$	$S_e(10^{-4} \text{ se})$ 1Y	$\theta(\text{deg})$	$S_e(10^{-4} \text{ se})$ 1Y	$\theta(\text{deg})$	$S_e(10^{-4} \text{ se})$ 1Y	$\theta(\text{deg})$
0.05	7.699	40.43	12.310	40.43	15.580	40.43	15.970	39.45
0.15	17.340	32.93	25.050	32.93	30.130	32.93	29.350	35.36
0.55	13.400	22.45	23.27	23.32	26.190	26.55	20.230	26.44
1.0	7.446	20.57	8.973	20.57	9.837	21.64	4.972	23.08
2.0	1.269	18.76	1.465	18.76	1.574	18.76	1.229	19.33
4.0	0.043	14.62	0.053	14.62	0.056	14.62	0.029	14.70
6.0	0.0007	12.05	0.0008	12.05	0.0008	12.05	0.002	12.05

\*  $\Delta E_e = 0.10 \text{ Mev}$

Table 2.4 (Cont'd)  
 Number of Secondaries Which Escape as a Function  
 of Energy, Average Angle of Emission and Thickness for  
 Prompt Fission Gamma Radiation

$E_e$ (Mev)	$T = 0.75 \text{ gm/cm}^2$		$T = 0.50 \text{ gm/cm}^2$		$T = 0.25 \text{ gm/cm}^2$		$T = 0.10 \text{ gm/cm}^2$	
	$S_e(10^{-4} \text{ se})$	$\theta \text{ (deg)}$	$S_e(10^{-4} \text{ se})$	$\theta \text{ (deg)}$	$S_e(10^{-4} \text{ se})$	$\theta \text{ (deg)}$	$S_e(10^{-4} \text{ se})$	$\theta \text{ (deg)}$
0.05	15.610	40.23	16.730	40.32	17.140	41.08	15.690	42.04
0.15	38.030	35.02	30.540	36.99	31.130	37.73	36.000	38.95
0.55	21.980	27.53	18.200	28.80	14.190	30.04	14.450	31.19
1.0	7.522	23.40	4.214	24.86	4.255	24.86	4.383	25.45
2.0	1.338	19.51	1.090	19.75	0.835	20.06	0.581	20.17
4.0	0.048	14.65	0.029	14.70	0.029	14.70	0.014	14.76
6.0	0.002	12.05	0.002	12.05	0.002	12.05	0.002	12.05

Table 2.4 (Cont'd)  
 Number of Secondaries Which Escape as a Function  
 of Energy, Average Angle of Emission and Thickness for  
 Prompt Fission Gamma Radiation

$E_e$ (Mev)	$T = 0.05 \text{ gm/cm}^2$		$T = 0.025 \text{ gm/cm}^2$		$T = 0.01 \text{ gm/cm}^2$	
	$S_e (10^{-4} \text{ se})$	$\theta$ (deg)	$S_e (10^{-4} \text{ se})$	$\theta$ (deg)	$S_e (10^{-4} \text{ se})$	$\theta$ (deg)
.05	15.640	42.55	15.650	42.86	9.270	43.30
.15	30.430	39.44	22.460	39.72	12.110	40.10
.55	4.113	31.19	4.120	31.19	1.104	31.19
1.0	2.200	25.70	0.736	25.79	0.662	25.79
2.0	0.220	20.24	0.220	20.24	0.038	20.24
4.0	0.005	14.79	0.005	14.79	0.002	14.79
6.0	0.002	12.05	0.001	12.05	---	---

Table 2.5  
Number of Secondaries Which Escape as a Function  
of Angle and Thickness for Prompt  
Fission Gamma Radiation

$\theta$ (deg)	$T = 10 \text{ gm/cm}^2$		$T = 5 \text{ gm/cm}^2$		$T = 2.5 \text{ gm/cm}^2$		$T = 1.0 \text{ gm/cm}^2$		$T = 0.75 \text{ gm/cm}^2$	
	$S_e (10^{-4} \text{ se})$		$S_e (10^{-4} \text{ se})$		$S_e (10^{-4} \text{ se})$		$S_e (10^{-4} \text{ se})$		$S_e (10^{-4} \text{ se})$	
15	3.227	3.607	3.813	3.019	2.386					
21	12.860	15.150	16.450	17.480	17.400					
25	20.220	24.930	27.680	29.930	29.910					
31	15.360	20.300	23.340	25.230	26.080					
35	12.170	17.010	20.110	21.970	22.830					
41	8.483	13.110	16.300	18.700	19.320					
45	0.002	0.004	0.006	0.071	0.278					

\*  $\Delta\theta = 2^\circ$

Table 2.5 (Cont'd)  
 Number of Secondaries Which Escape as a Function  
 of Angle and Thickness for Prompt  
 Fission Gamma Radiation

$\theta$ (deg)	$T = 0.50 \text{ gm/cm}^2$	$T = 0.25 \text{ gm/cm}^2$	$T = 0.10 \text{ gm/cm}^2$	$T = 0.05 \text{ gm/cm}^2$	$T = 0.025 \text{ gm/cm}^2$	$T = 0.01 \text{ gm/cm}^2$
	$S_e(10^{-4} \text{ se})$ $\frac{1}{1\gamma}$	$S_e(10^{-4} \text{ se})$ $\frac{1}{1\gamma}$	$S_e(10^{-4} \text{ se})$ $\frac{1}{1\gamma}$	$S_e(10^{-4} \text{ se})$ $\frac{1}{1\gamma}$	$S_e(10^{-4} \text{ se})$ $\frac{1}{1\gamma}$	$S_e(10^{-4} \text{ se})$ $\frac{1}{1\gamma}$
15	1.643	0.836	0.337	0.169	0.084	0.034
21	14.380	7.960	3.257	1.635	0.819	0.328
25	30.540	23.360	10.210	5.159	2.588	1.038
31	25.940	26.310	20.140	10.840	5.502	2.211
35	22.720	23.110	23.790	18.150	9.811	3.992
41	19.530	19.960	20.500	20.590	2.061	12.110
45	0.077	0.080	0.252	0.254	0.255	0.006



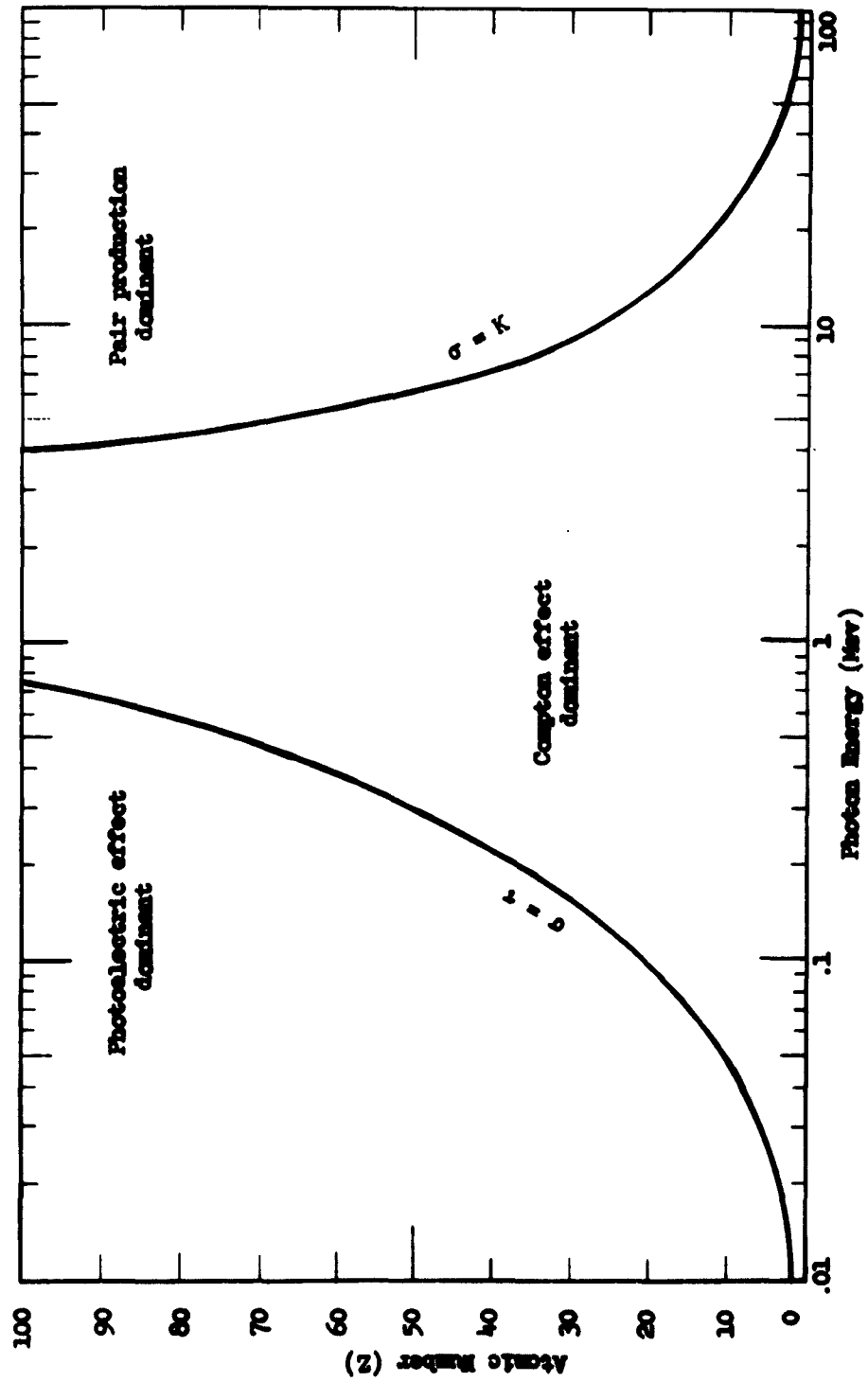


Figure 2.1 Relative importance of the three major types of gamma-ray interactions. The lines show the values of  $Z$  and  $h\nu$  for which the two neighboring effects are just equal (from Evans, 1955, p. 712)

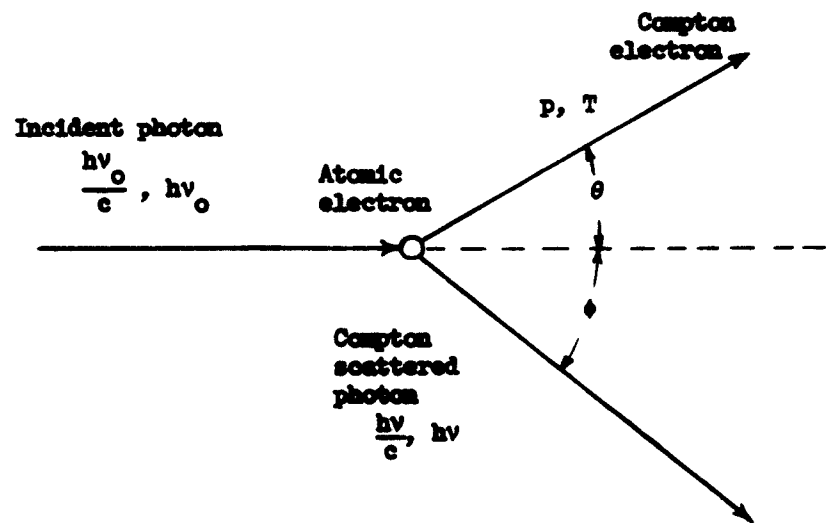


Figure 2.2 Trajectories in the scattering plane for the incident photon  $h\nu_0$ , the scattered photon  $h\nu$ , and the scattered electron which acquires momentum  $p$  and kinetic energy  $T$  (from Evans, 1955, p. 675)

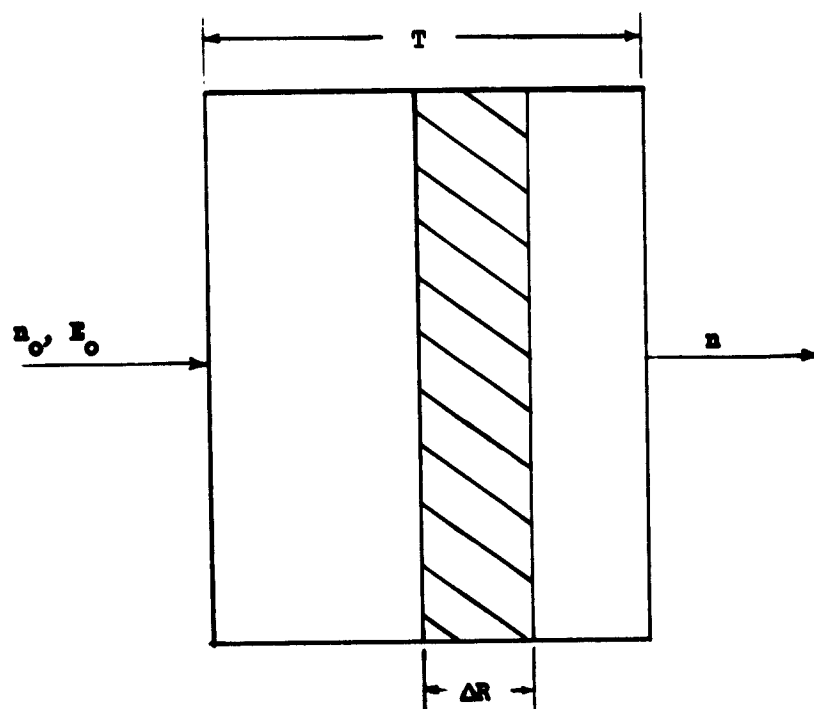


Figure 2.3 A thin absorbing sample

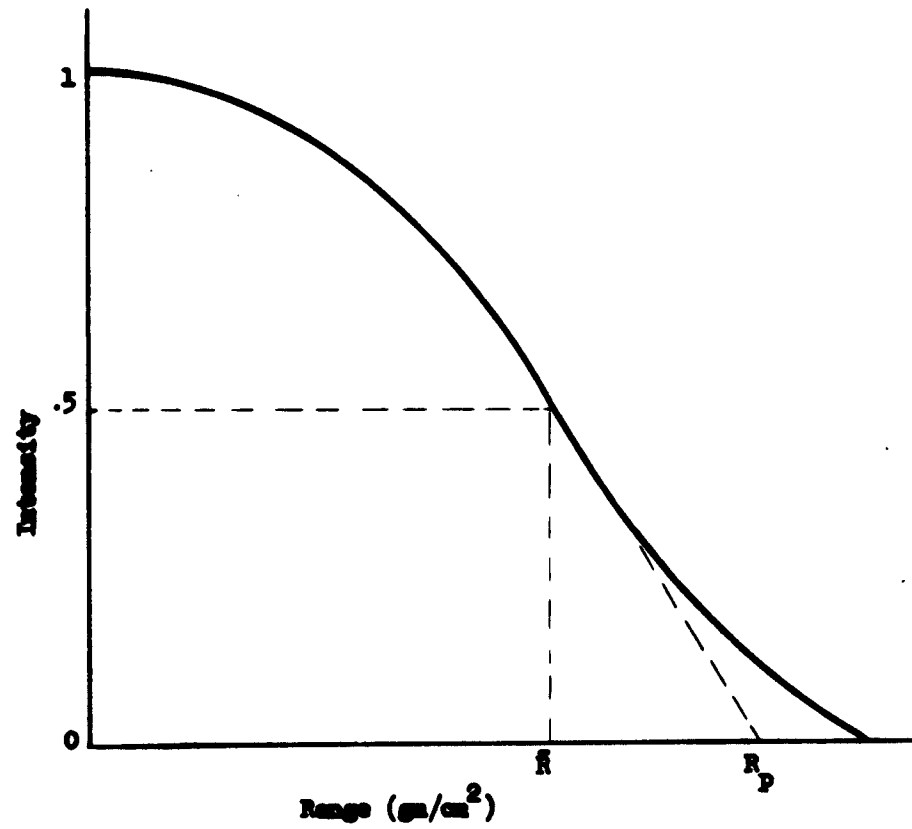


Figure 2.4 The number-distance curve for an electron with energy  $E$ , i. e., monoenergetic particles.

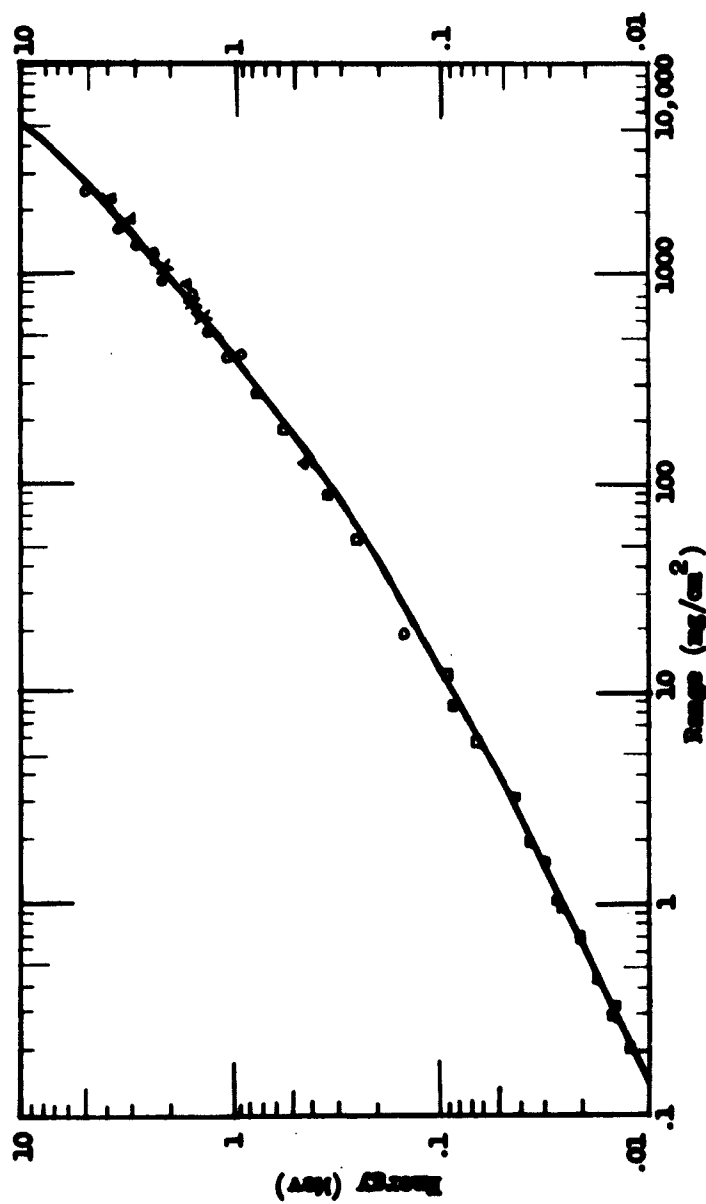


Figure 2.5 Empirical range-energy relationship for electrons absorbed in aluminum with data points shown (Evans, 1955, p. 624)

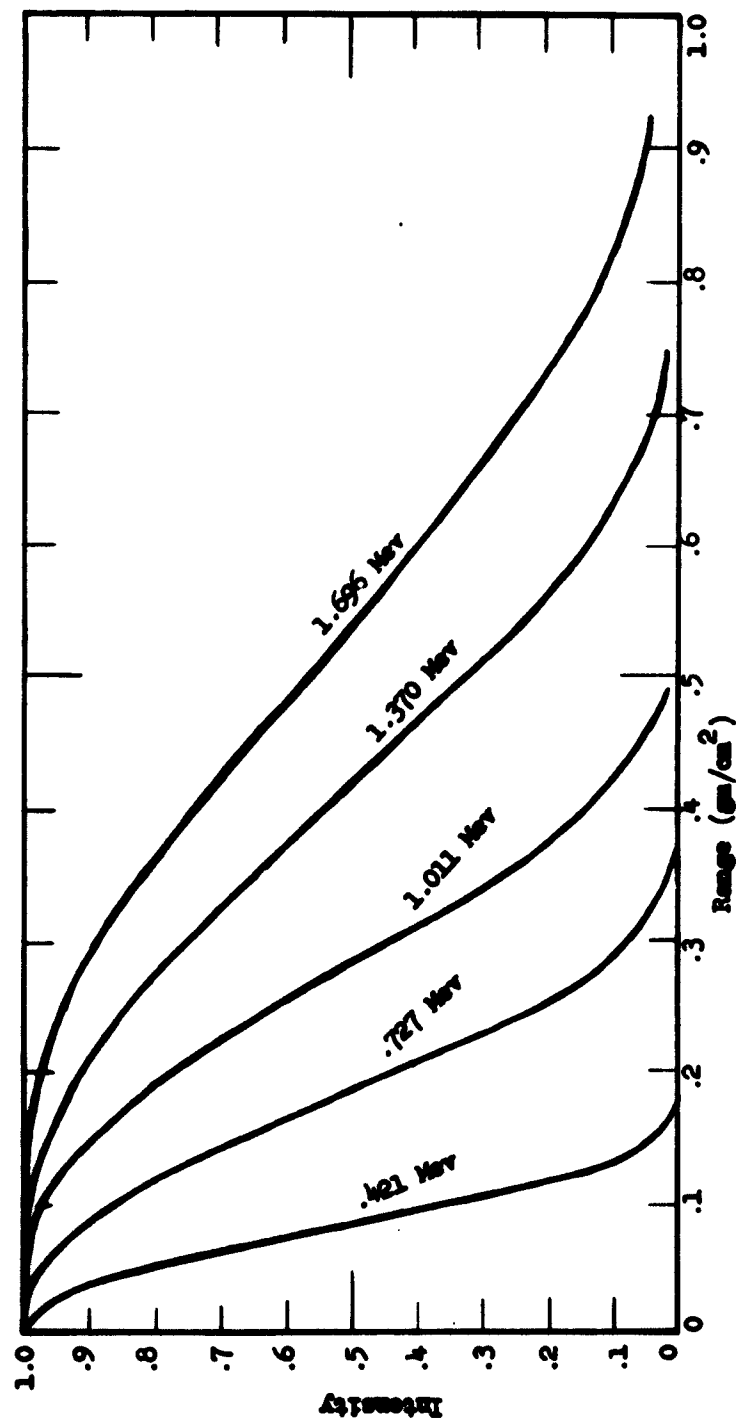


Figure 2.6 Experimentally measured absorption curves for monochromatic electrons in aluminum (from Marshall, J. and Ward, A.G., 1937)

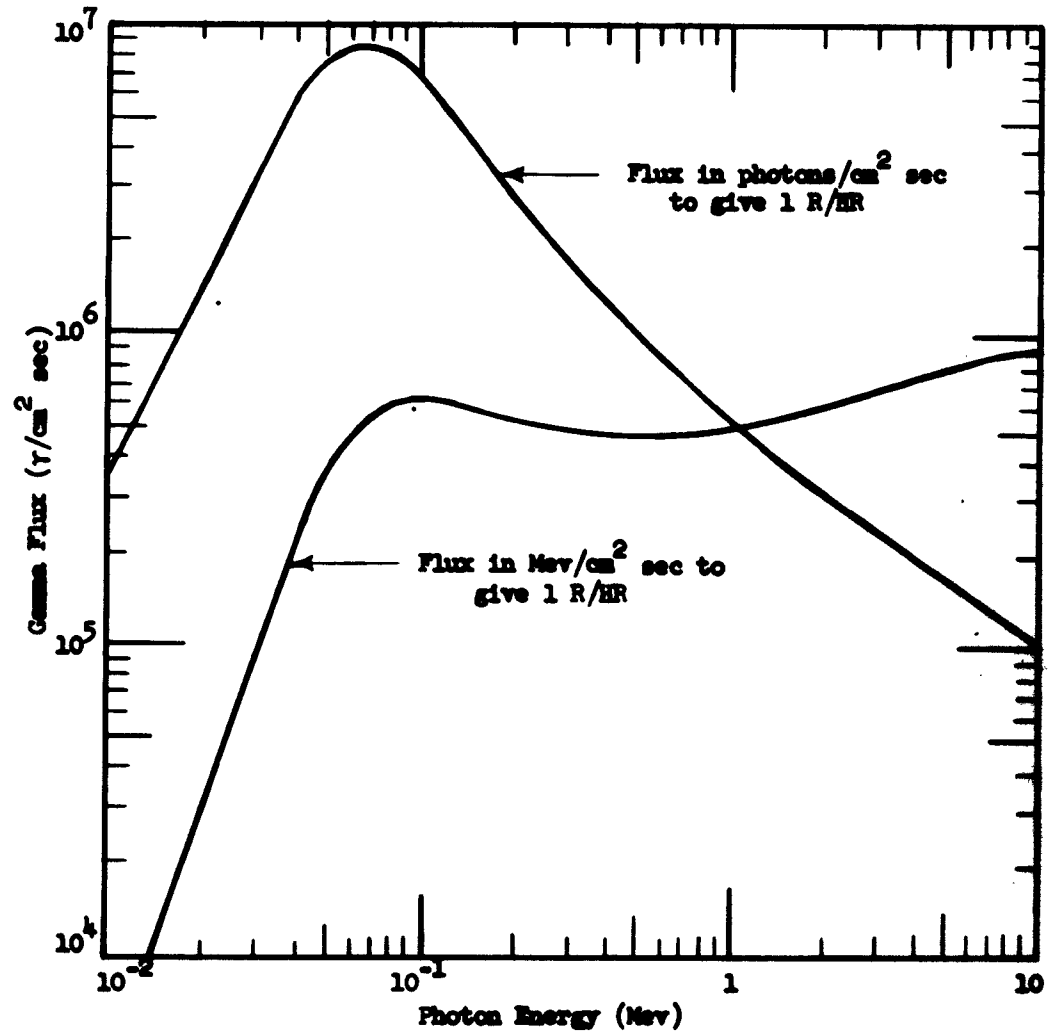


Figure 2.7 Gamma flux to give 1 roentgen/hour  
(from Rockwell, 1956, p. 20)

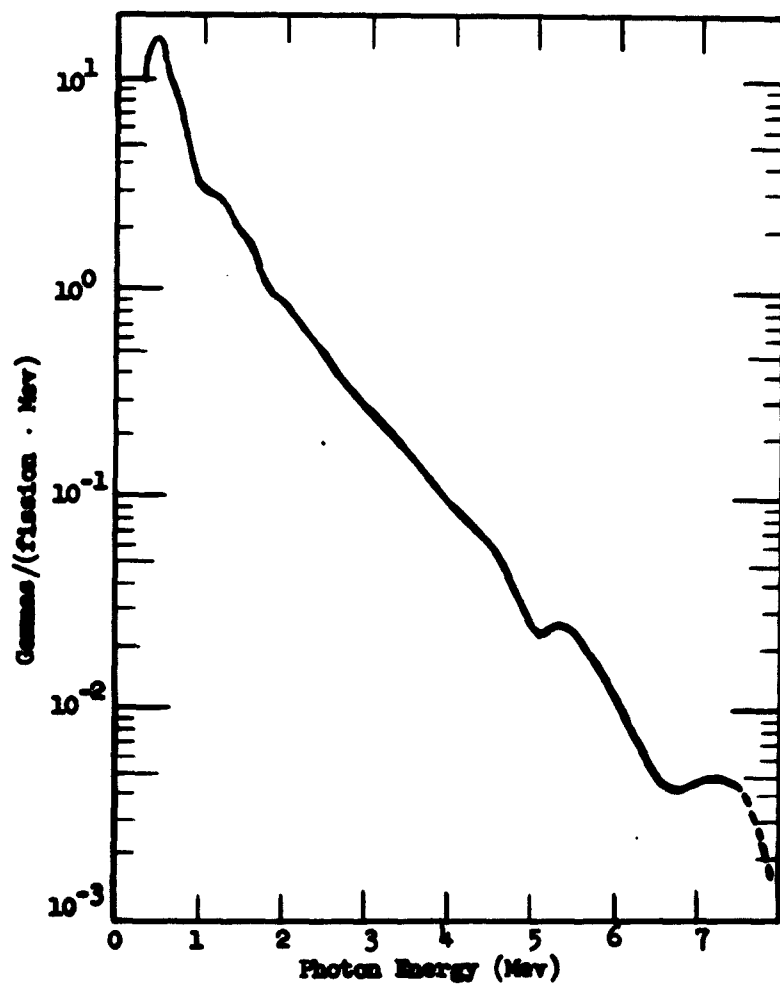


Figure 2.8 Energy spectrum of prompt fission gamma rays from  $U^{235}$  fission for times less than  $5 \times 10^{-8}$  seconds



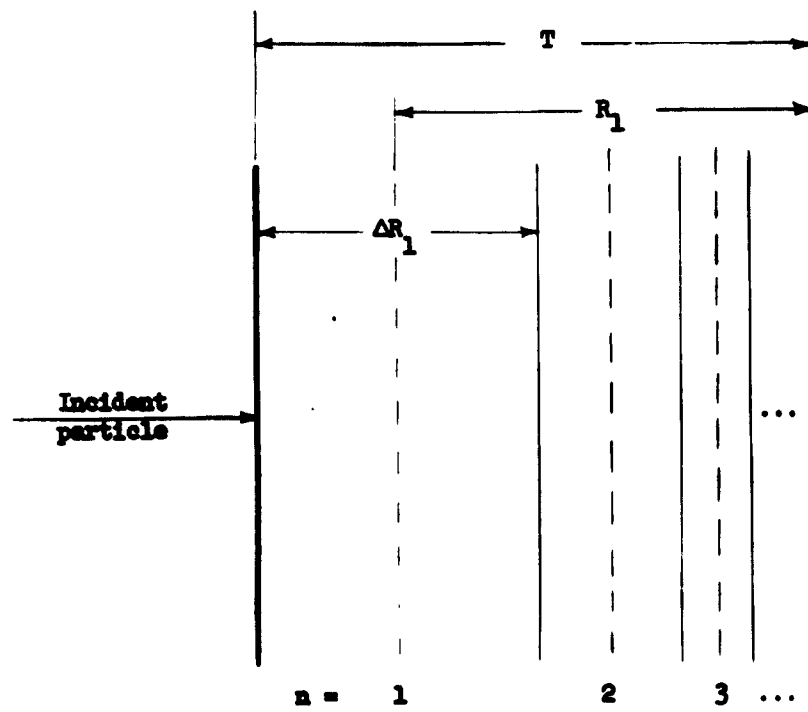


Figure 2.9 A typical sample division

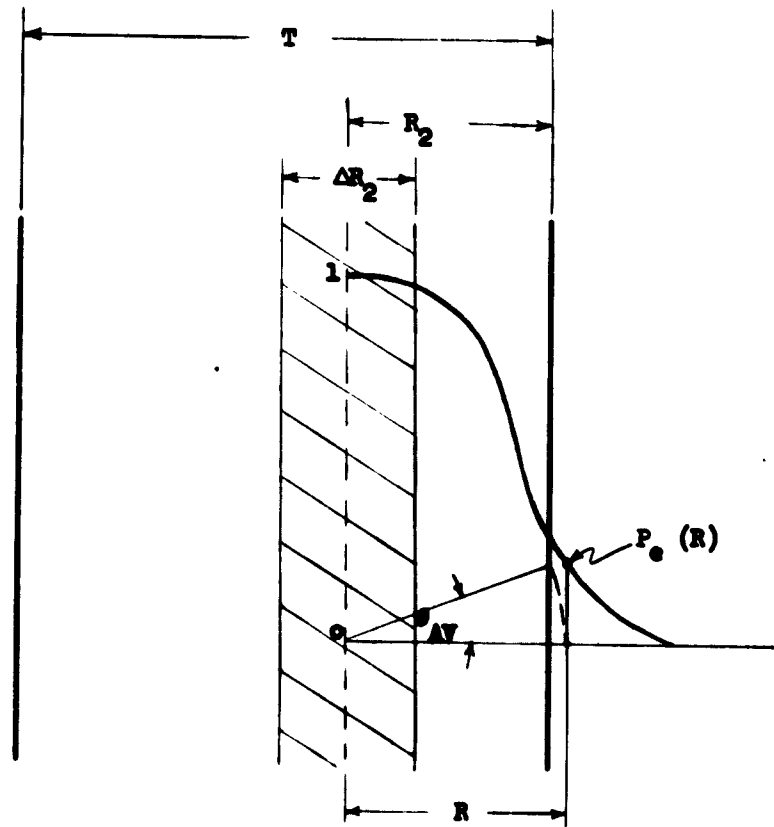


Figure 2.10 Diagram of the probability of escape  $P_e$

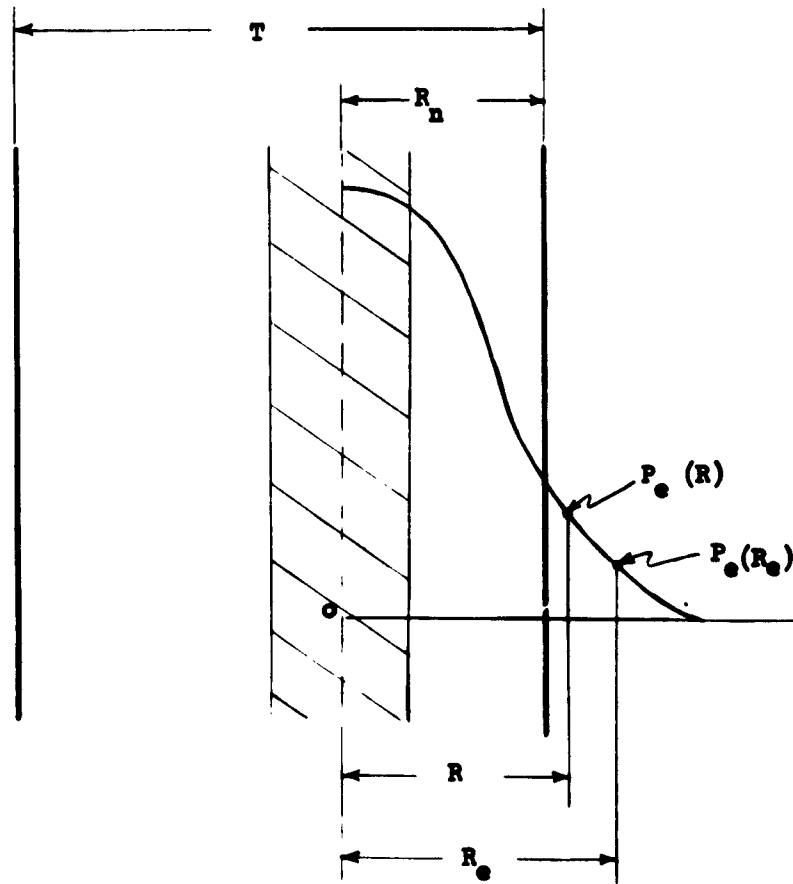


Figure 2.11 Diagram for the calculation of the energy of escape  $E_e$

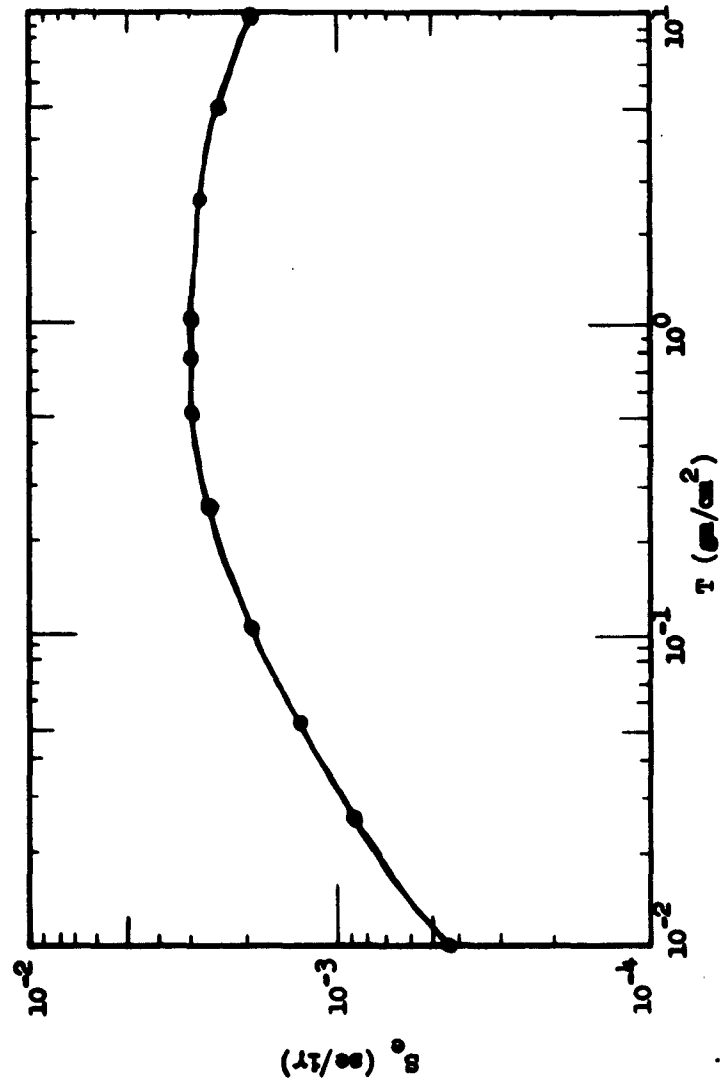


Figure 2.12 The number of secondaries escaping  $S_e$  as a function of thickness for prompt fission gamma radiation

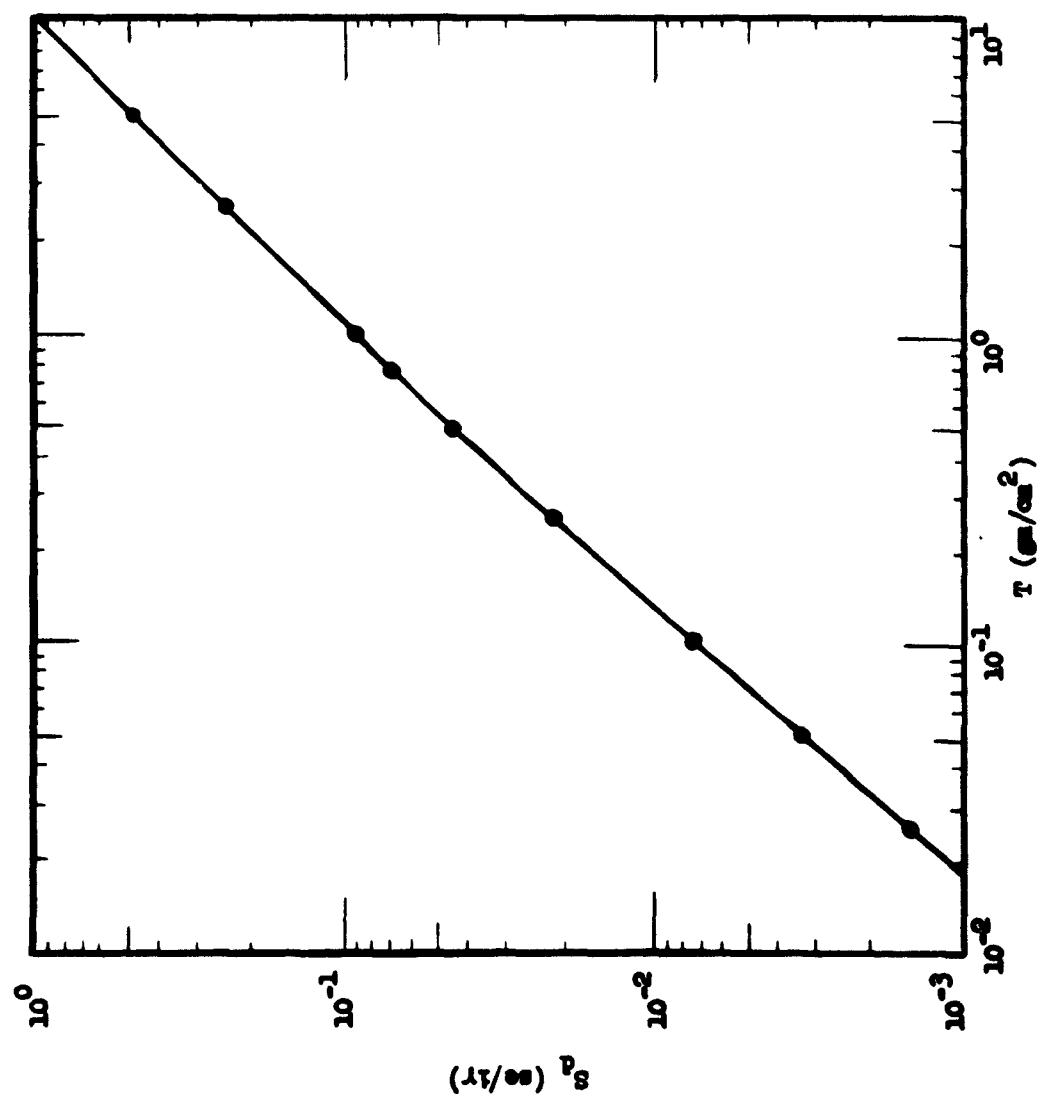


Figure 2.13 The number of secondaries deposited  $S_d$  as a function of thickness for prompt fission gamma radiation

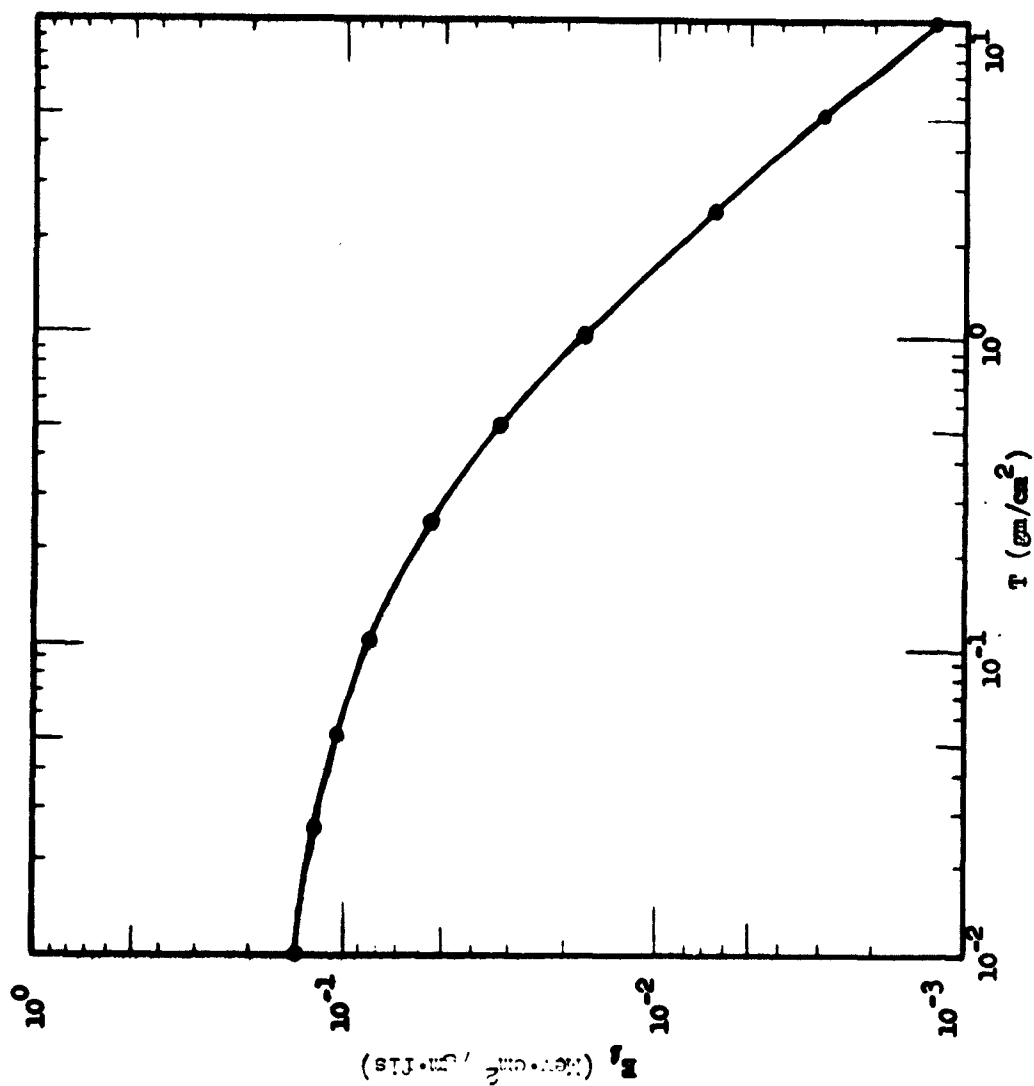


Figure 2.14 The energy of escape per unit path length as a function of thickness for prompt fission gamma radiation (9.1  $\gamma/\text{fis}$ ).

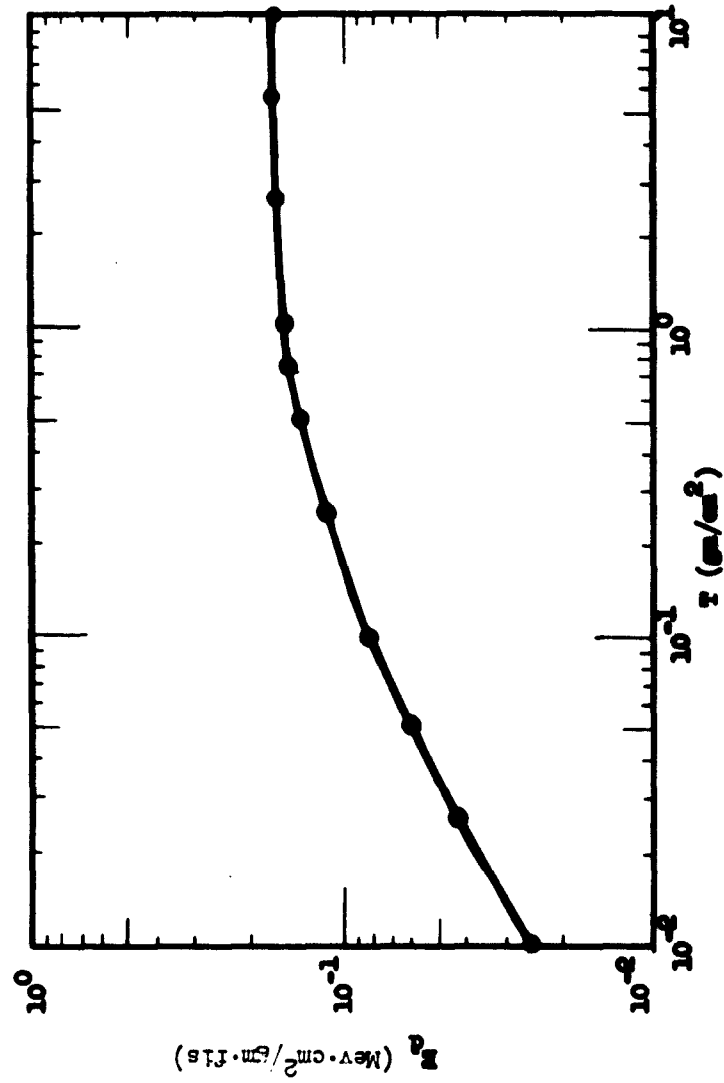


Figure 2.15 The energy deposited per unit path length as a function of thickness for prompt fission gamma radiation (9.1  $\gamma$ /fis).

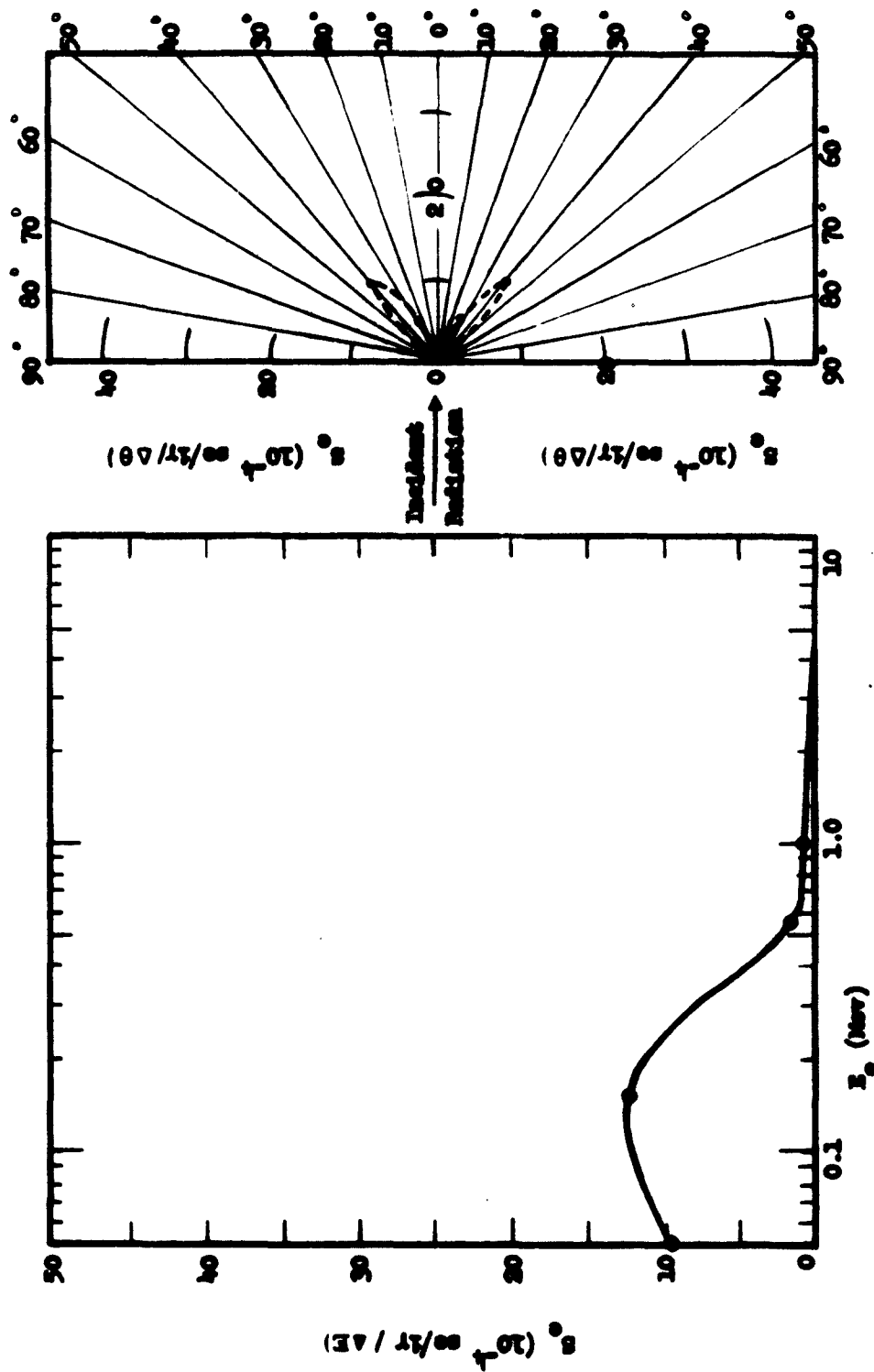


Figure 2.16 Energy and angle of emission spectra for prompt fission gamma radiation incident on a sample of thickness  $0.01 \text{ gm/cm}^2$  ( $\Delta E = 0.1 \text{ MeV}$ ;  $\Delta \theta = 2^\circ$ )



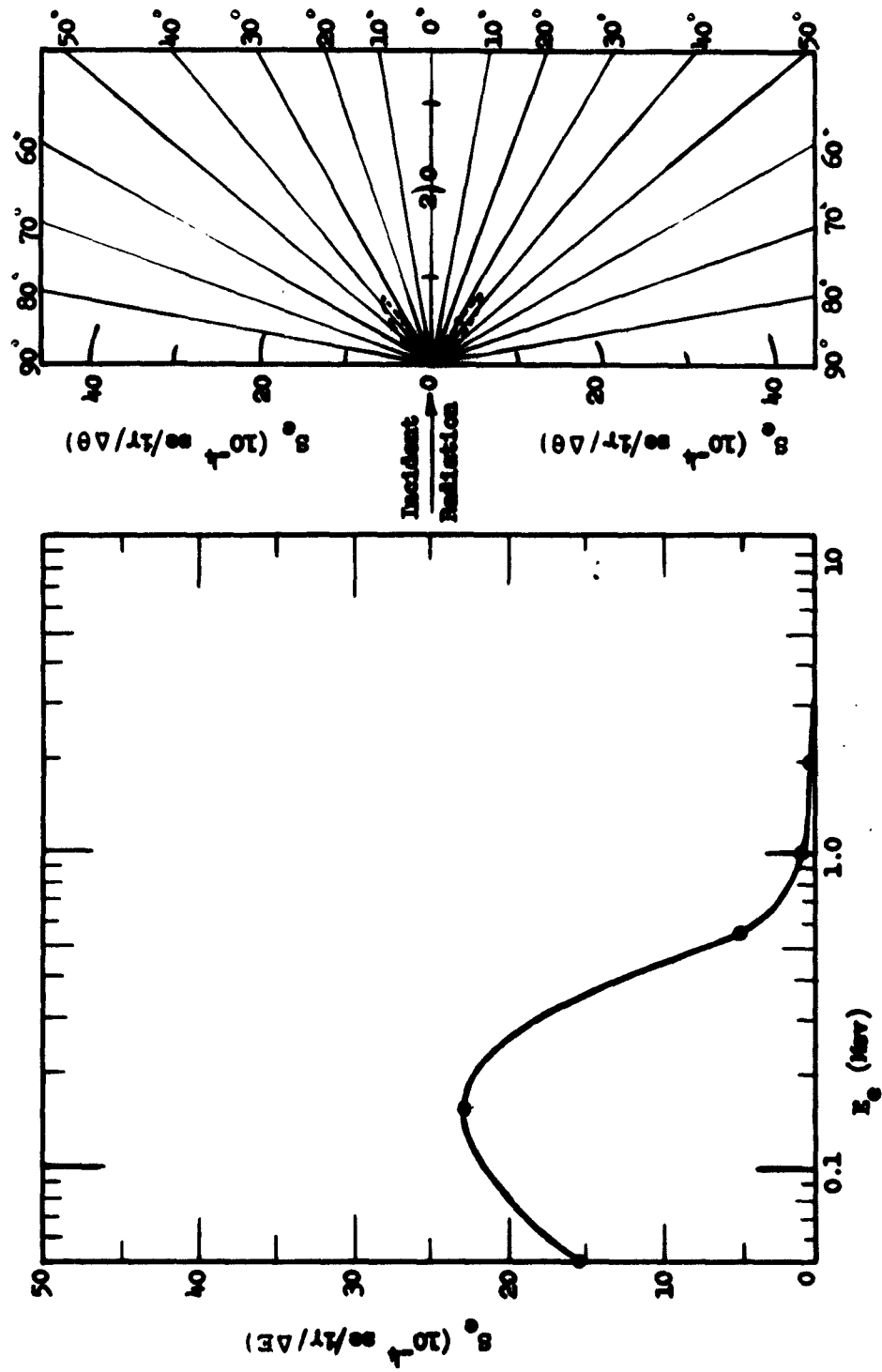


Figure 2.17 Energy and angle of emission spectra for prompt fission gamma radiation incident on a sample of thickness  $0.025 \text{ gm/cm}^2$

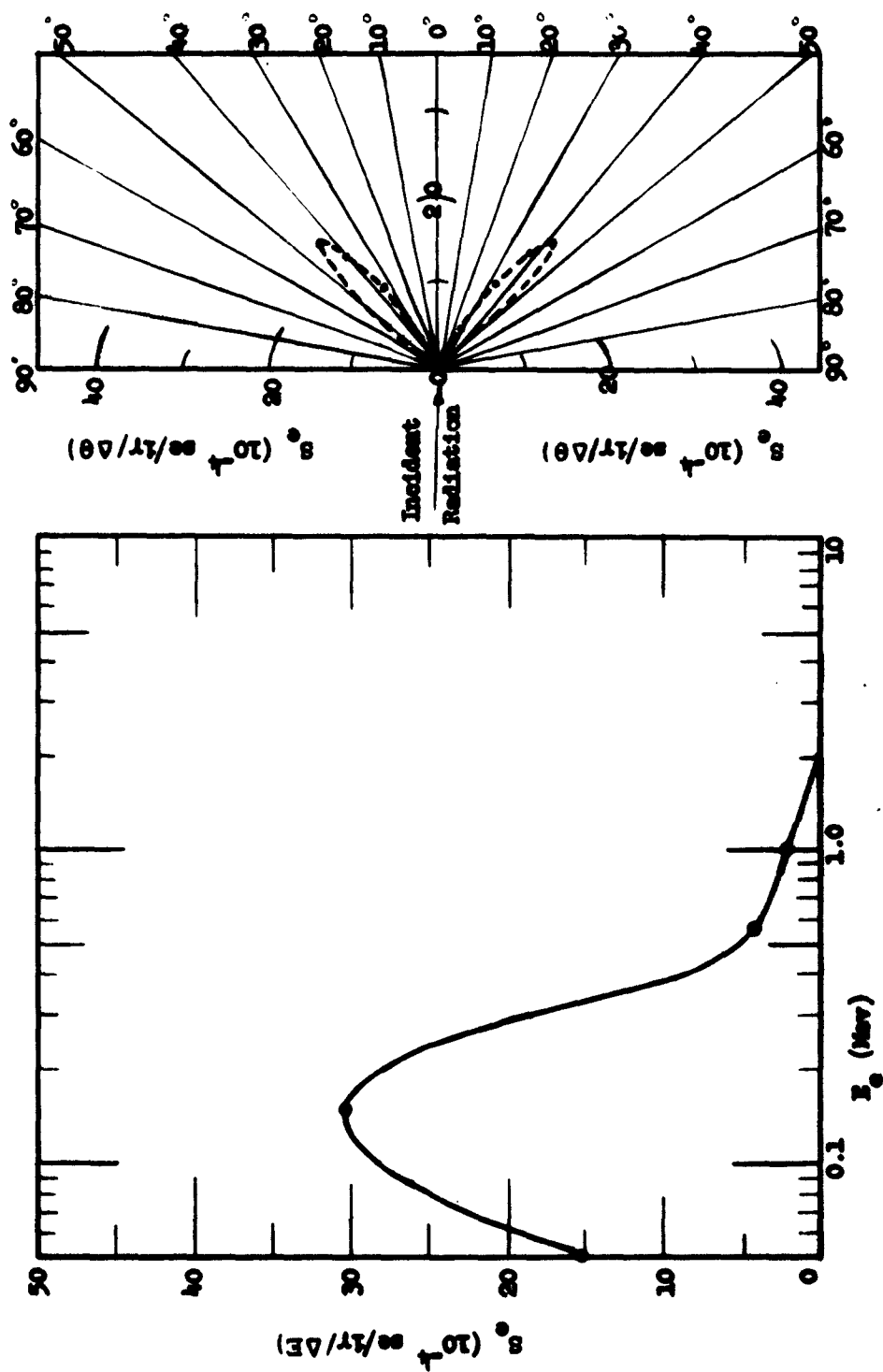


Figure 2.18 Energy and angle of emission spectra for prompt fission gamma radiation incident on a sample of thickness  $0.05 \text{ gm/cm}^2$

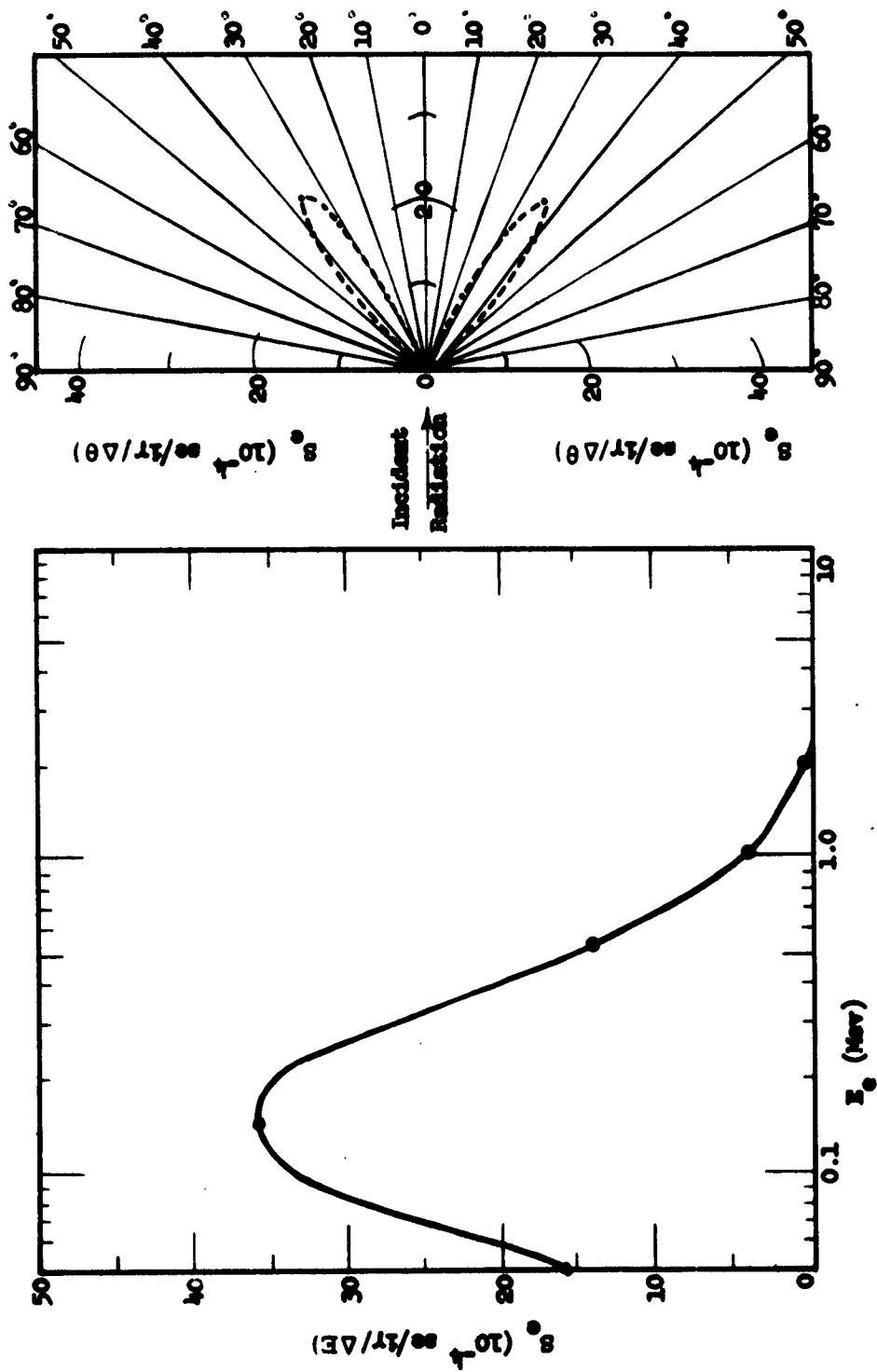


Figure 2.19 Energy and angle of emission spectra for prompt fission gamma radiation incident on a sample of thickness 0.10 gm/cm<sup>2</sup>

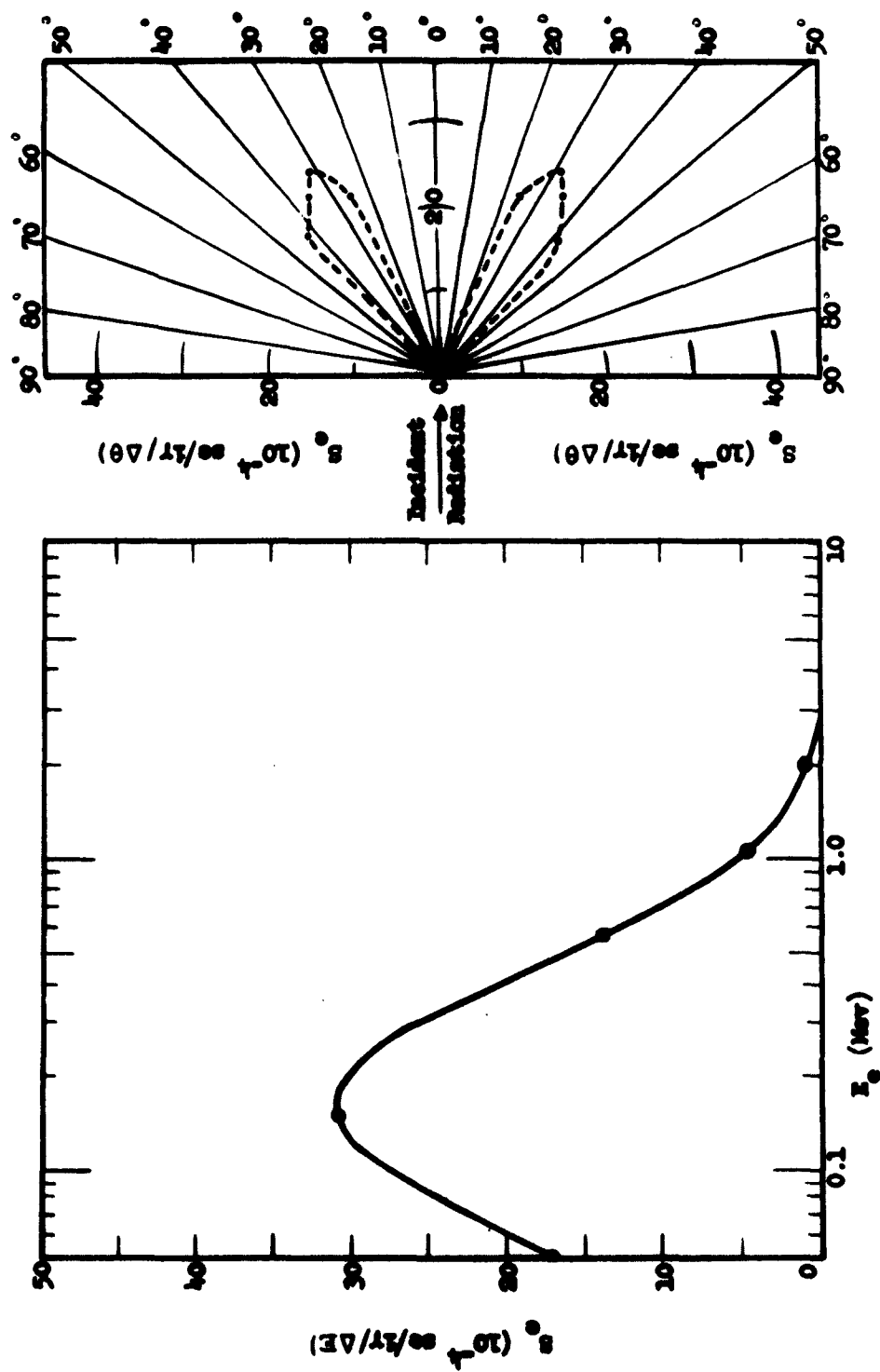


Figure 2.20 Energy and angle of emission spectra for prompt fission gamma radiation incident on a sample of thickness 0.25 gm/cm<sup>2</sup>

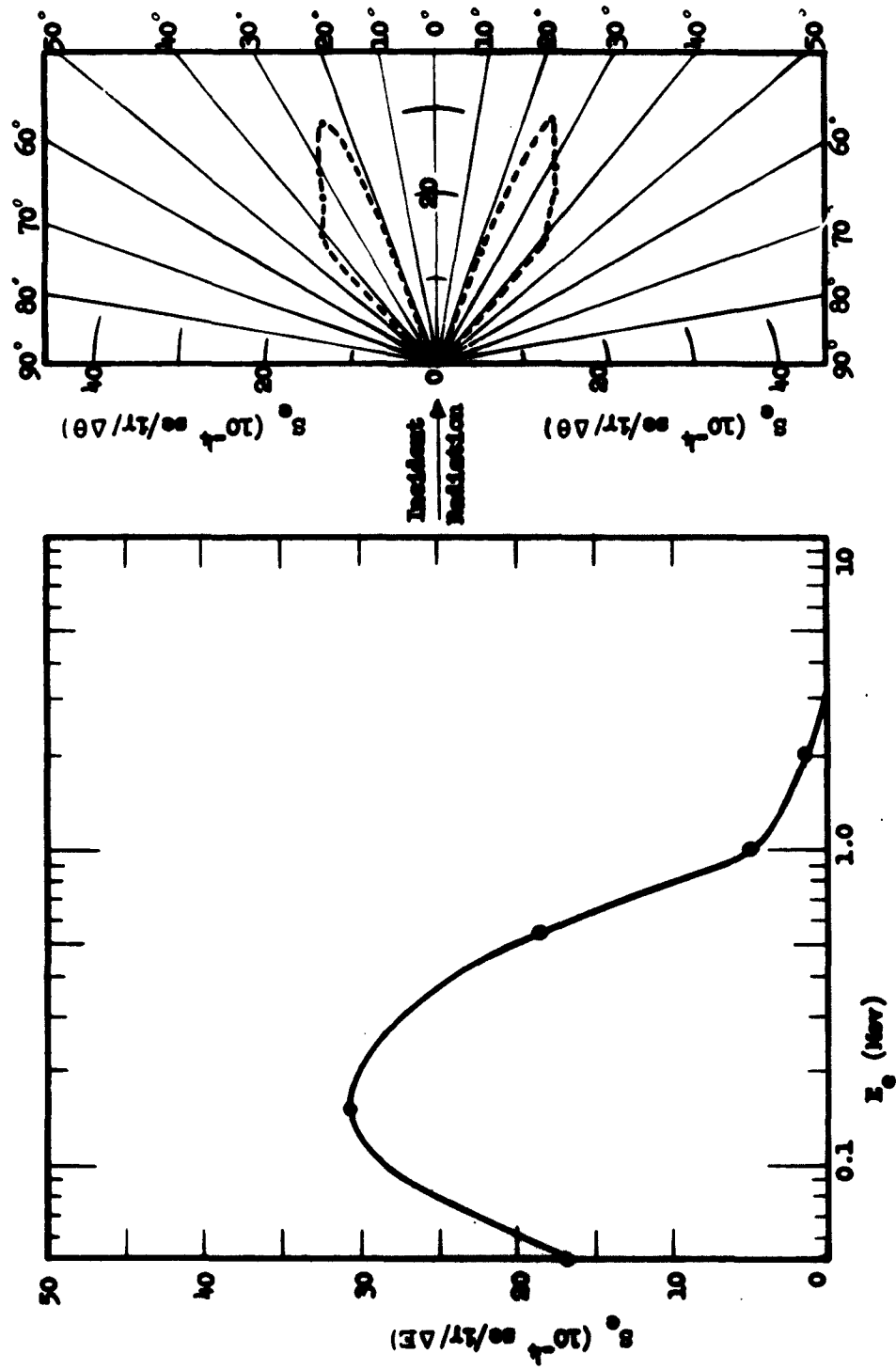


Figure 2.21 Energy and angle of emission spectra for prompt fission gamma radiation incident on a sample of thickness 0.50 gm/cm<sup>2</sup>

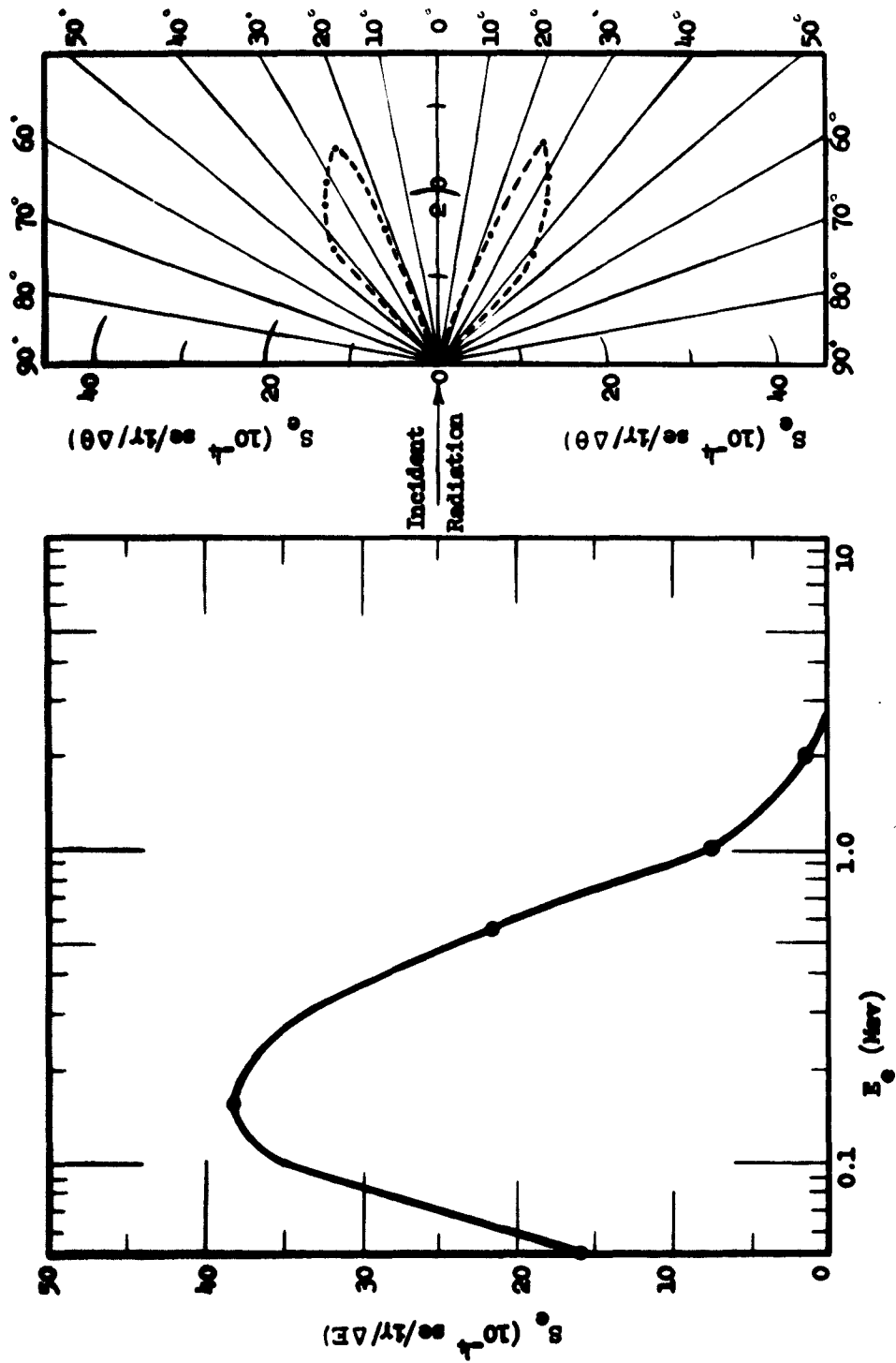


Figure 2.22 Energy and angle of emission spectra for prompt fission gamma radiation incident on a sample of thickness 0.75 gm/cm<sup>2</sup>

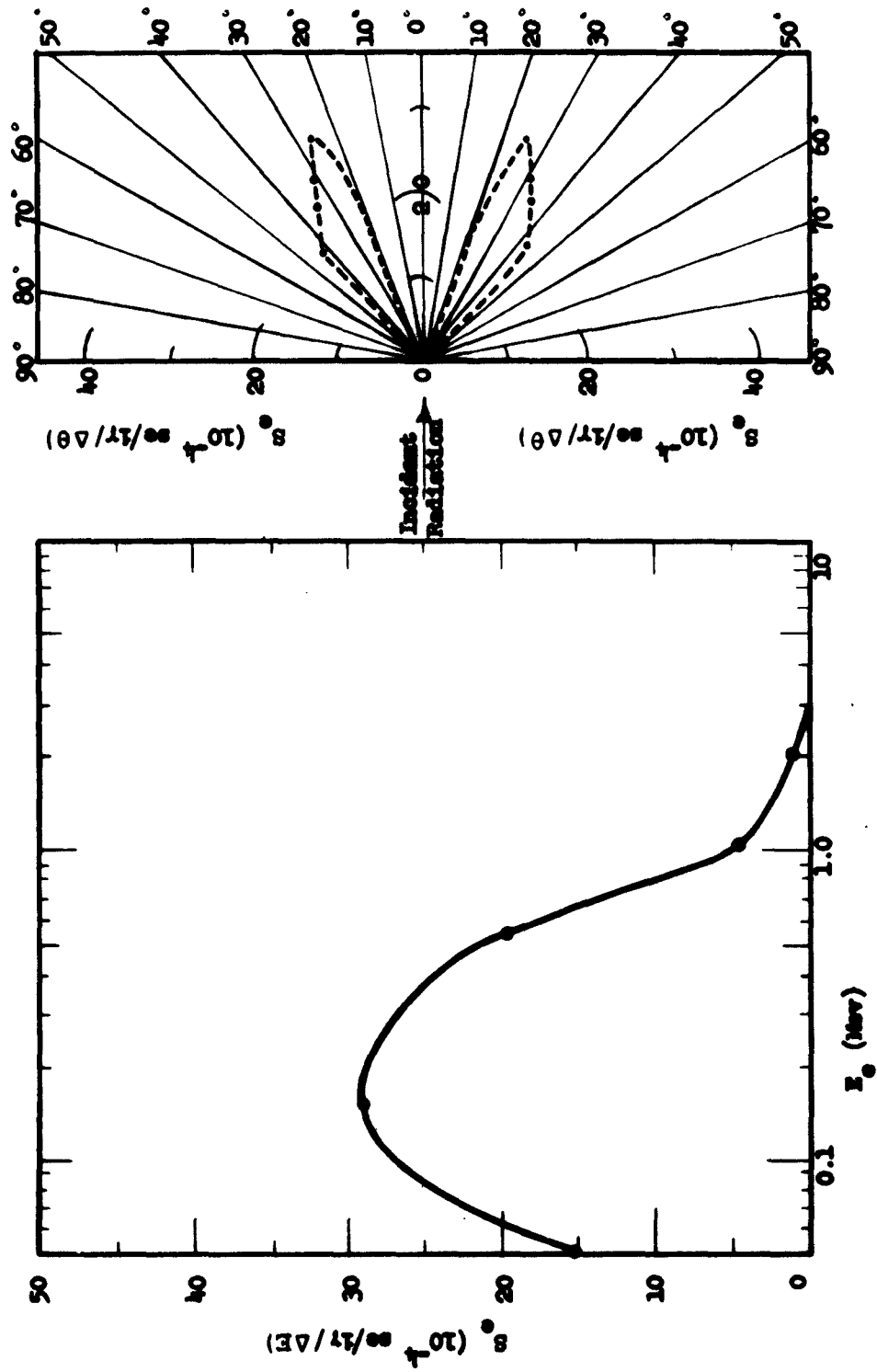


Figure 2.23 Energy and angle of emission spectra for prompt fission gamma radiation incident on a sample of thickness 1.0 gm/cm<sup>2</sup>

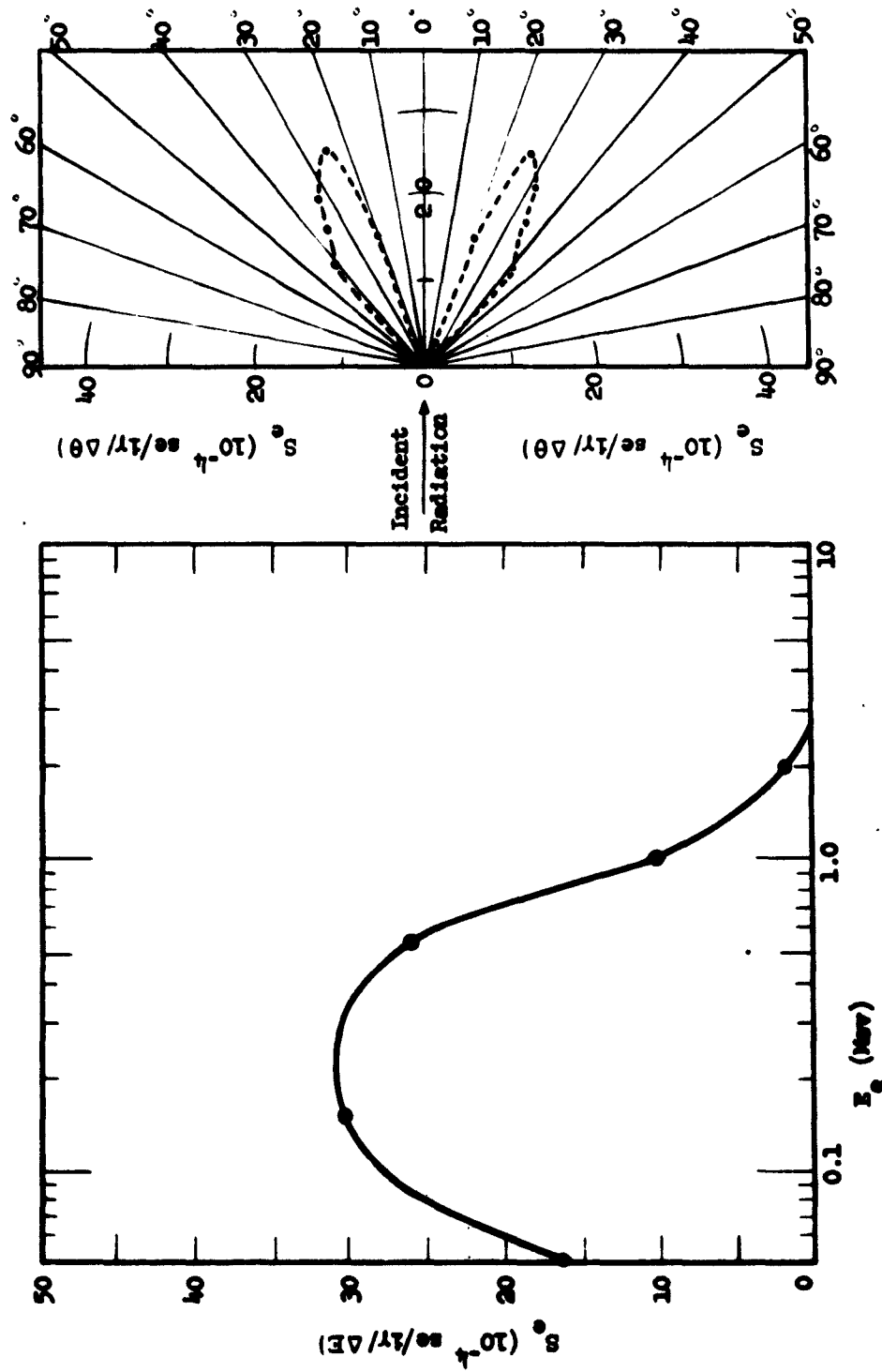


Figure 2.24 Energy and angle of emission spectra for prompt fission gamma radiation incident on a sample of thickness 2.5 gm/cm<sup>2</sup>



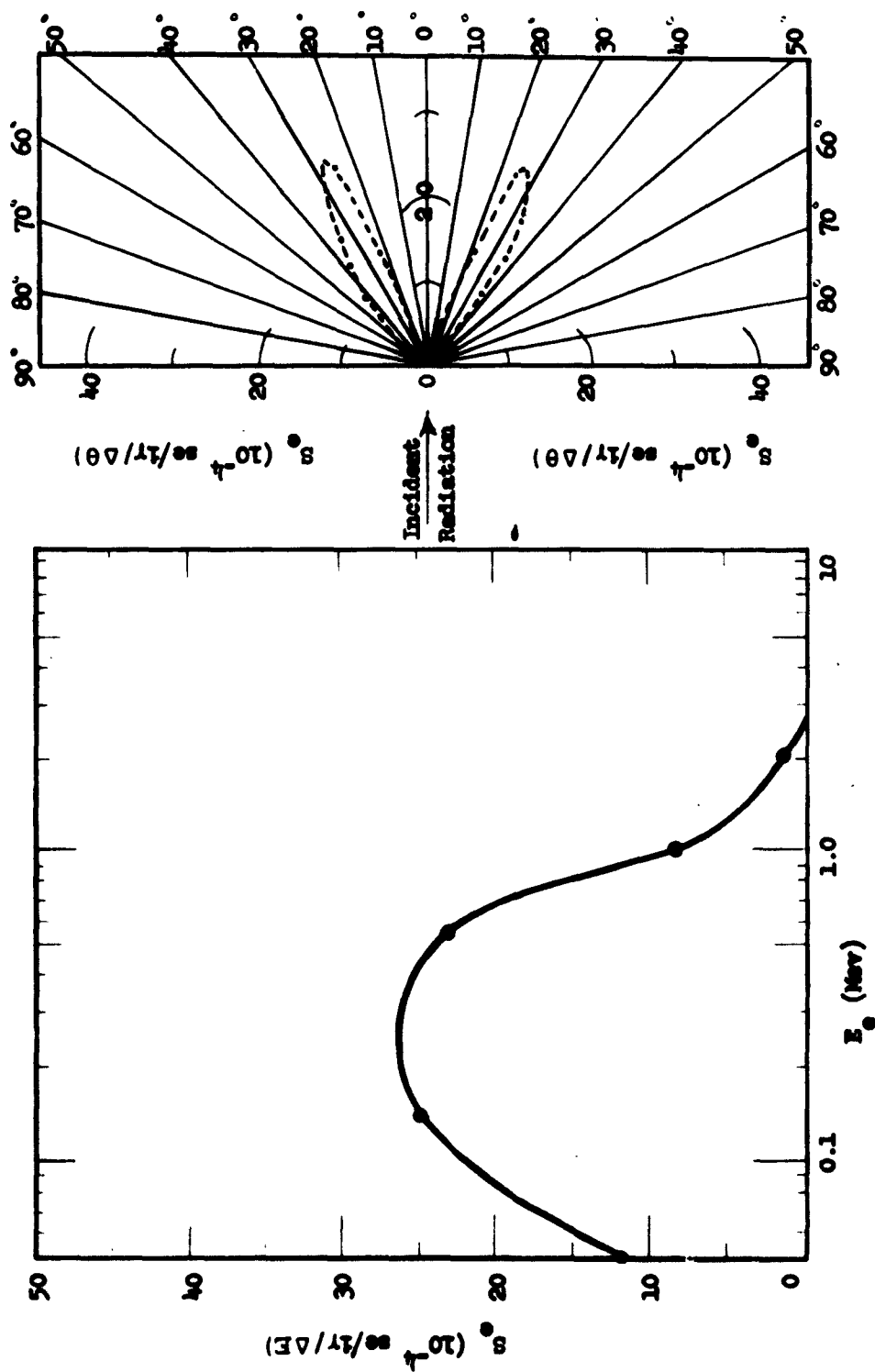


Figure 2.25 Energy and angle of emission spectra for prompt fission gamma radiation incident on a sample of thickness 5.0 gm/cm<sup>2</sup>

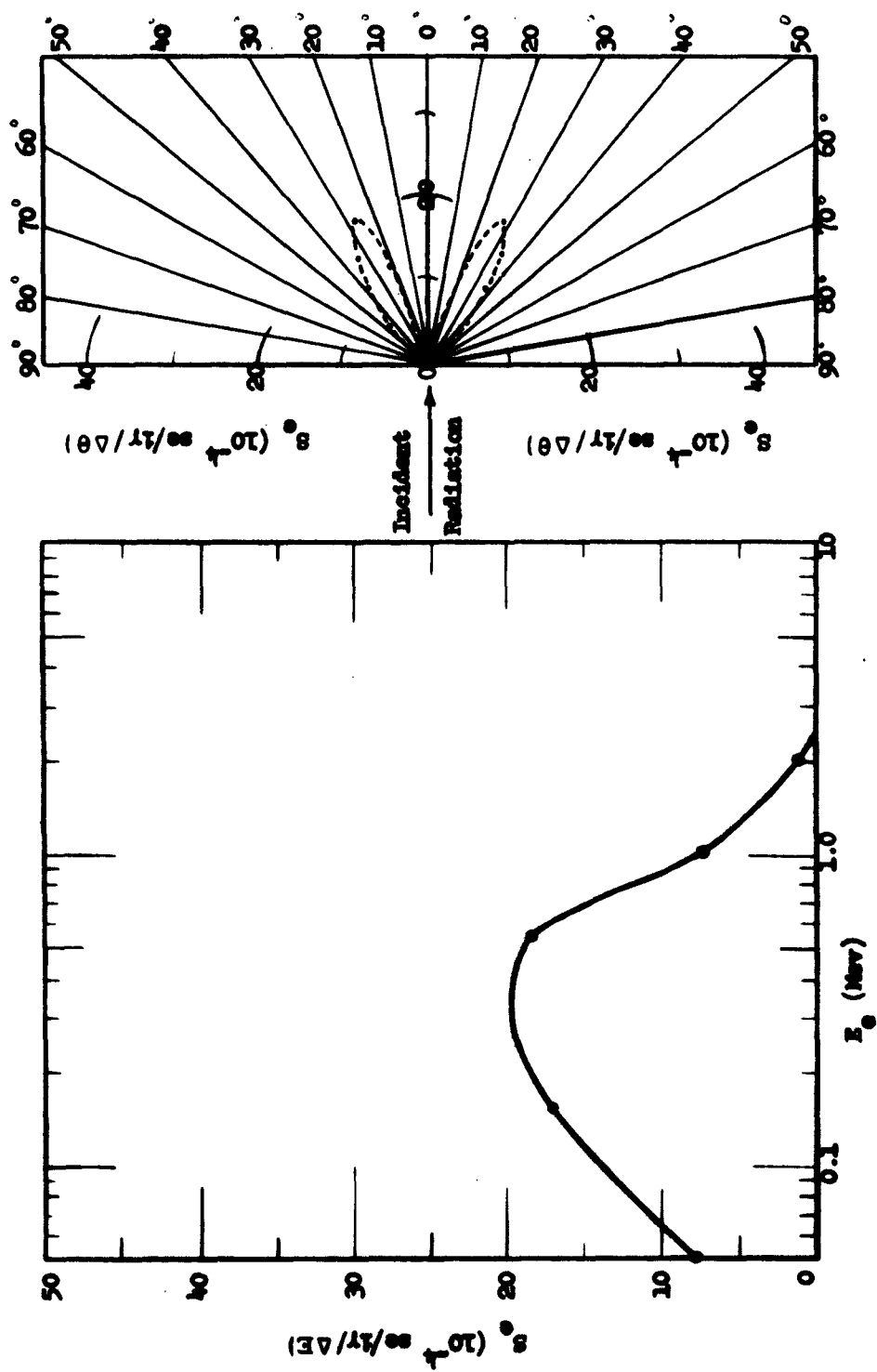


Figure 2.26 Energy and angle of emission spectra for prompt fission gamma radiation incident on a sample of thickness  $10 \text{ gm/cm}^2$

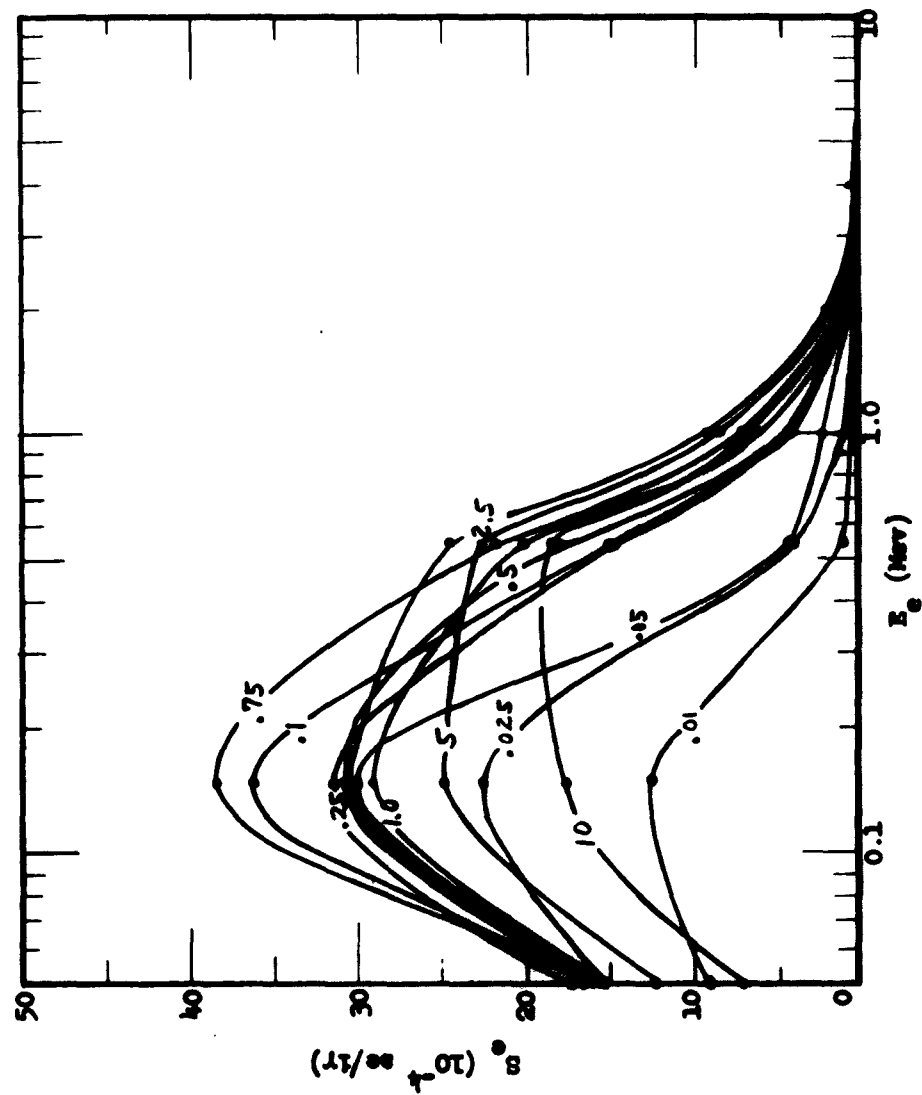


Figure 2.27 Energy spectra for prompt fission gamma radiation for thicknesses in the range from 0.01 to 10 gm/cm<sup>2</sup>

### 3. SECONDARY ELECTRON EMISSION BY 25-MEV ELECTRONS

#### a. General remarks

Let us very briefly look at the electromagnetic phenomena that are of importance in the interaction with matter of high-energy charged particles, such as 25-Mev electrons from a linear accelerator (linac). We will consider first the phenomena that occur when a charged particle passes in the neighborhood of an atom.

(1) If the distance of closest approach is large compared with the dimensions of the atom ( $10^{-8}$  cm), the atom reacts as a whole to the variable field set up by the passing particle. The result is an excitation or an ionization of the atom. The phenomenon can be treated by the ordinary methods of quantum mechanics without direct reference to radiation. For these comparatively distant collisions, the magnetic moment of the particle is of secondary importance, because the forces associated with the magnetic moment decrease as the third power of the distance, whereas the Coulomb forces decrease as the square of the distance. Therefore the passing particle can be considered as a point charge.

(2) If the distance of closest approach is of the order of atomic dimensions, the interaction no longer involves the passing particle and the atom as a whole, but rather the passing particle and one of the atomic electrons. As a consequence of the interaction, the electron is ejected from the atom with considerable energy. This phenomenon is often described as a knock-on process. If the energy acquired by the secondary electron is large compared with the binding energy, the phenomenon can be treated as an interaction between the passing particle and a free electron. Radiation phenomena can still be neglected, and the ordinary methods of quantum mechanics can be used. However, one can no longer neglect the magnetic moments or spins of the interacting particles. When the particles are identical, exchange phenomena occur and acquire special importance when the minimum distance of approach becomes comparable with the DeBroglie wavelength. This collision process will be described as an elastic collision with atomic electrons.

(3) When the distance of closest approach becomes smaller than the atomic dimensions, the deflection of the trajectory of the passing particle in the electric field of the nucleus becomes the most important effect. Classically, each deflection results in the emission of a weak electromagnetic radiation with a continuous frequency spectrum. Numerous soft quanta, whose total energy is usually a very small fraction of the particle energy, accompany the deflection. In few cases, however, one photon of energy comparable with that of the particle is emitted. Because of the comparatively small probability of this effect, the problem of the scattering of particles can be treated separately from that of radiation or bremsstrahlung.

(4) The problem of computing the probability of photon emission by the passage of a charged particle through an atom requires the application of quantum electrodynamics. As in the scattering problem, the atom is still represented schematically by a central field of force. However, the Hamiltonian of the system, which in the scattering problem consisted of the Hamiltonian of the particle exclusively, now contains also the Hamiltonian of the electromagnetic field and a small interaction term that depends on the coordinates of both the particle and the field. This interaction term produces transitions corresponding to energy transfers between the particle and the electromagnetic field.

It will be shown that the predominant mechanism for energy loss by 25-Mev electrons is by ionization. This will be described as an elastic collision process between the incident electron and the atomic electrons. Also, this collision mechanism could be considered as an inelastic collision between an incident electron and the atom as a whole.

For this discussion we will put methods (1) and (2) into one group and call it energy loss by ionization. Methods (3) and (4) will be put into another group and called energy loss by radiation or bremsstrahlung. As was mentioned above, we will show that energy loss by ionization collisions is much greater than energy losses by radiative-type collisions which give rise to the emission of photons.

The energy loss by ionization collisions and that loss by radiative-type collisions have a strikingly different behavior. The energy

loss due to radiation collisions is nearly proportional to  $Z^2$  and the increase is nearly linear with energy, while ionization energy losses are proportional to  $Z$  and increase only logarithmically with energy. Therefore, when the energy of the incident electron  $E_o$  becomes much greater than  $E_c$  then the radiation collision process predominates. If  $E_o < E_c$ , then the ionization process predominates. Table 3.1 was taken from Segre (1953), p. 266.

Segre (1953) gives this relationship

$$\frac{(dE_o/dx) \text{ rad}}{(dE_o/dx) \text{ ion}} \approx \frac{E_o Z}{1600 m_o c^2}$$

for the ratio of the radiative loss to the ionization loss. The above relationship was used to determine the ratio  $\frac{(dE_o/dx) \text{ rad}}{(dE_o/dx) \text{ ion}}$ , found in table 3.1. The incident electron energy is given to be 25 Mev.

One can see from table 3.1 that  $E_c \approx E_o$  for iron ( $Z = 26$ ). This means that radiative and ionization losses should be approximately equal at this point. Indeed, this is shown to be true by observation of the ratio of losses for iron. At this point the approximation  $A = 2Z$  begins to break down. Therefore, the concern will be with lower  $Z$  materials where the ionization losses are at least a factor of 2 greater than the radiative losses.

#### b. Theory

##### (1) Conservation laws for elastic collisions

For purposes of calculating the angular distribution, it is assumed that the theory of elastic collisions holds for the interaction of the incident electron and the atomic electrons. Whatever the forces involved, the principles of the conservation of energy and momentum must be satisfied, so that the consequences of these principles remain applicable under all circumstances.

Such consequences may now be considered by studying the

disturbance created by the passage of one particle through the field of force of another particle.

Conservation of momentum in the direction of the incident electron is

$$p_0 = p \cos \theta + p' \cos \phi \quad (3.1)$$

and normal to the direction of the incident electron is

$$0 = p \sin \theta - p' \sin \phi. \quad (3.2)$$

A third relationship between these variables is obtained from the conservation of energy,

$$E_0 = E + E'. \quad (3.3)$$

Using the relativistic relationship

$$pc = \sqrt{T(T + 2m_0c^2)} \quad (3.4)$$

where  $T$  is the kinetic energy, and some algebra, one can solve for the  $\cos \theta$  by using the momentum vector diagram in figure 3.1 and the law of cosines. The  $\cos \theta$  becomes

$$\cos \theta = \frac{E(E_0 + 2m_0c^2)}{(p_0c)(pc)} \quad (3.5)$$

where

$$p_0c = \sqrt{E_0(E_0 + 2m_0c^2)} \quad (3.6)$$

and

$$p c = \sqrt{E (E + 2 m_0 c^2)}. \quad (3.7)$$

If one evaluates equations (3.5) and (3.6) for  $E_0 = 25$  Mev, the  $\cos \theta$  becomes in its simplest form

$$\cos \theta = 1.0206 \frac{E}{p c} \quad (3.8)$$

where

$$p c = \sqrt{E (E + 1.022)} \quad (3.9)$$

where the secondary electron is born with energy  $E$  in Mev.

## (2) Collision cross sections for identical particles

The collision between an incident electron and an atomic electron requires special treatment because the two electrons are indistinguishable after the collision. Consider the collision of an incident electron of kinetic energy  $E_0$  with an atomic electron which was initially free and stationary. After the collision one of the electrons will have energy  $E$ , the other,  $(E_0 - E)$ . It cannot be determined which electron was the incident electron. Arbitrarily, the faster electron after the collision is defined as the incident electron insofar as future collisions are concerned. This is equivalent to restricting the energy transfer  $E$  to values up to  $E_0/2$ . Thus, the maximum energy transferred to the secondary electron by the incident electron will be  $E_{\max} = E_0/2$ .

To understand the quantum-mechanical cross sections for collisions between two electrons, it is helpful to evaluate the classical cross section first. Evans (1955) gives the classical differential cross section as



$$d\sigma(E_0, E) = \frac{2\pi e^4}{m_0 v^2} \frac{dE}{E^2} \quad (3.10)$$

This represents the probability that the incident electron loses energy  $E$  and has kinetic energy  $(E_0 - E)$  after the collision. But to this must be added the classical probability that the incident electron loses energy  $(E_0 - E)$  and has kinetic energy  $E$  after the collision, which is

$$d\sigma(E_0, E_0 - E) = \frac{2\pi e^4}{m_0 v^2} \frac{dE}{(E_0 - E)^2} \quad (3.11)$$

Thus the classical differential cross section for the collision between identical particles, i. e., the probability that one particle will have kinetic energy  $E$  after the collision, is the sum of the two probabilities, or

$$d\sigma(E_0, E) = \frac{2\pi e^4}{m_0 v^2} \frac{dE}{E^2} \left( \frac{E_0}{E_0 - E} \right)^2 \left[ 1 - 2 \frac{E}{E_0} + 2 \frac{E^2}{E_0^2} \right] \quad (3.12)$$

This cross section applies only for  $E \geq (E_0 - E)$ , i. e., for  $E \leq E_0/2$ . For  $E \geq E_0/2$ , the corresponding cross section is zero, because these collisions are already included in equation (3.12).

To introduce into the cross section the effects of quantum-mechanical exchange, and of relativity, Möller treated the problem of the collision between two free electrons, using the relativistic Dirac theory of the electron. In Möller's theory the spin (measured in units of  $\hbar$ ) and its magnetic moment (measured in units of  $e\hbar/2m_0c$ ) were assumed to take on the normal values, namely, magnetic moment 0 for particles of spin 0, and 1 for charged particles of spin  $1/2$  or 1.

Möller's cross section for extremely relativistic electrons ( $E_0 \gg m_0 c^2$ ) is

$$d\sigma = \frac{2\pi e^4}{m_0 v^2} \frac{dE}{E^2} \left( \frac{E_0}{E_0 - E} \right)^2 \left[ 1 - \frac{E}{E_0} + \frac{E^2}{E_0^2} \right]^2 \quad (3.13)$$

Equation (3.13) can be found in Evans (1955), p. 577, and Rossi (1952), p. 15. It has the same limits as equation (3.12) and represents the probability that the slower electron will have energy  $E$  after the collision. In equation (3.10) through (3.13),  $v$  represents the velocity of the incident electron. In this case the incident electrons have an energy of 25 Mev, which have a velocity equivalent to the speed of light for all practical purposes.

Equation (3.13) can be integrated from  $E$  to  $E_0/2$  to get

$$\sigma(E_0, E) = \frac{2\pi e^4}{m_0 c^2} \left[ \frac{1}{2E_0} + \frac{1}{E} - \frac{E}{E_0^2} - \frac{1}{E_0 - E} \right] \quad (3.14)$$

where  $\sigma(E_0, E)$  is the probability of producing a secondary electron with energy between  $E$  and  $E_0/2$ . The integration is somewhat tedious, but straightforward, and is not presented in this paper because of its length and lack of contribution. Thus, the cross section as given in equation (3.14) will be used in equation (2.18) to give the number of secondary electrons produced while the incident electron passes through the thickness  $T$ . Concern is only with the interactions of the incident electrons and the atomic electrons producing secondary electrons. It will be assumed that the tertiary electrons produced by the secondary electrons can be neglected in comparison with the secondary electron production.

The theory of the secondary electron production, the probability of escape and deposition, the range of electrons, and the number and energy losses shall be the same for incident electrons as for photons as described in section 2. The theoretical energy losses for charged particles will be presented next so that we can later compare the calculated and predicted theoretical numbers.

## (3) Energy losses determined theoretically

The average energy loss by an electron initially with energy  $E_o$  per unit path length is defined by

$$\frac{dE_o}{ds} = NZ \int_{E_L}^{E_{MAX}} E d\sigma(E_o, E) \quad (3.15)$$

where  $N$  is the number of atoms per  $\text{cm}^3$  and  $E_{MAX}$  is defined to be equal  $E_o/2$ . To evaluate the above integral collisions will be divided into hard and soft collisions. Namely, hard collisions will be defined as energy transfer between  $E_{MAX}$  and some arbitrary value  $E_H$ , where the only restriction on  $E_H$  is that it be large compared with the binding energy of the electron. Soft collisions are defined to be collisions where the energy transfer extends from the arbitrary value  $E_H$  to the minimum possible energy transfer  $E_L$ , which is generally of the order of an excitation energy or the ionization energy of one atomic electron. The hard collision contribution was determined by substituting equation (3.13) for  $d\sigma(E_o, E)$  in equation (3.15) and integrating the straightforward but tedious function term by term to find

$$\frac{dE_{oH}}{ds} = \frac{2\pi e^4}{m_o c^2} NZ \left[ \left( \ln \frac{E_o}{E_H} \right) - 0.261 \right] \quad (3.16)$$

Since interest is only in high energy secondary electrons, the soft component will not be considered. Evaluating equation (3.16) for 25-Mev incident electrons and using  $E_H$  as the ionization potential for aluminum (165 ev), gives

$$\frac{dE_{oH}}{ds} = 0.881 \text{ Mev/gm/cm}^2.$$

This number will be compared with the results of the computer calculation in the section on discussion of results.

c. Procedure

(1) Energy groups

Since the calculations were made on the CDC 1604 high-speed digital computer, the energy groups can be made as small as desired. However, it was found that  $\Delta E = 10^{-2}$  Mev was as small as needed. Any further reduction in  $\Delta E$  only increased the computer time proportionately and did not improve the calculation significantly to warrant the change. Thus, the energy groups used are shown in figure 3.2.

The first energy group starts at  $E_0/2$  for reasons discussed in the theory. The lower bound was chosen to be the K shell ionization potential (165 ev) for aluminum for all runs. This does not present a serious error for two reasons. (a) Interest is only in high-energy secondary electron emission. (b) The ionization potential varies linearly with  $Z$ , so for low  $Z$  materials the above number is a good average.

(2) Sample division

Sample division is the same as described in section 2.c(2).

(3) Attenuation

The energy of the incident electron is reduced as it passes through a sample material. The incident electron is attenuated by calculating (using methods outlined in section 2.c(4)) the energy of the particle at the center of the  $\Delta R$  in question and this is assumed to be the incident electron energy for the entire  $\Delta R$ .

(4) Sample problem

The calculational method is the same as described in section 2.c (4) except for the differences mentioned above. Therefore, no sample problem will be given in this section.

#### d. Results

The results are contained in table 3.2 (Energy Losses and Secondary Electron Emission Efficiencies as a Function of Thickness for 25 MEV Electrons) and table 3.3 (Number of Secondaries which Escape as a Function of Energy, Average Angle of Emission and Thickness for 25 MEV Electrons). The data contained in table 3.2 can be found plotted on figures 3.3 - 3.6, and table 3.3 and 3.4 data are plotted on figures 3.7 - 3.18.

#### e. Discussion

Figure 3.3 gives  $S_e$  versus thickness. At a thickness of  $0.01 \text{ gm/cm}^2$ ,  $S_e$  is  $7 \times 10^{-3} \text{ se/ie}$  with a constant increase with thickness to approximately  $8 \times 10^{-2} \text{ se/ie}$  (8 percent) maximum at about  $4 \text{ gm/cm}^2$  and then a decrease to  $4.8 \times 10^{-2} \text{ se/ie}$  at  $10 \text{ gm/cm}^2$ . The increase is due to more atomic electrons being made available and the decrease is due to the attenuation of the incident beam.

Figure 3.4 forms a straight line on log-log paper and is a plot of  $S_d$  versus thickness. The values range from  $46 \text{ se/ie}$  at  $0.01 \text{ gm/cm}^2$  to  $4600 \text{ se/ie}$  at  $10 \text{ gm/cm}^2$ . One would expect the number to become larger with thickness.

Figures 3.5 and 3.6 will be considered together. The former is a plot of the energy of escape  $E_g$  and the latter is a plot of the energy deposited  $E_d$  per unit path length as a function of thickness. Adding these two curves point for point gives the energy liberated by the incident beam; this value ranges from  $0.849$  to  $0.904 \text{ Mev/gm/cm}^2$ . The predicted value as given by section 3.b(3) is  $0.881 \text{ Mev/gm/cm}^2$ . This is an indication that the calculational method is correct.

Figures 3.7 to 3.17 contain the energy and angle of emission spectra for 25-Mev electrons for thicknesses in the range from  $0.01$  to  $10 \text{ gm/cm}^2$ . The energy spectrum is a plot of the number of secondaries escaping per incident electron as a function of the energy of escape.

Figure 3.18 is a plot of all the energy spectra as a relative perspective of their intensities as a function of thickness. The intensity

TDR-63-50

increases with thickness in general. The most probable energy of escape  $E_e$  occurs at about 0.15 Mev for almost all the thicknesses.

Table 3.1

Critical Energy  $E_c$  and the Ratio of the  
Radiative Loss to the Ionization Loss for  
Various Materials

Materials	Z	$E_c$ (Mev)	$\frac{(dE_o/dx) \text{ rad}}{(dE_o/dx) \text{ ion}}$
Hydrogen	1	340	0.0313
Carbon	6	103	0.133
Aluminum	13	47	0.407
Iron	26	24	0.513
Copper	29	21.5	0.507
Lead	82	0.9	2.570
Air	7.36	83.0	0.230
Water	7.23	93	0.227

Table 3.2

Energy Losses and Secondary Electron  
Emission Efficiencies as a Function of  
Thickness for 25 Mev Electron

T (gm/cm <sup>2</sup> )	E <sub>g</sub> (Mev/gm/cm <sup>2</sup> )	E <sub>d</sub> (Mev/gm/cm <sup>2</sup> )	S <sub>e</sub> (se/ie)	S <sub>d</sub> (se/ie)
10.0	4.17-3*	8.45-1	4.83-2	4.67 + 3
5.0	2.55-2	8.53-1	7.38-2	2.34 + 3
2.5	6.85-2	8.21-1	7.51-2	1.17 + 3
1.0	1.32-1	7.67-1	6.01-2	4.67 + 2
0.75	1.51-1	7.50-1	5.46-2	3.51 + 2
0.5	1.76-1	7.24-1	4.71-2	2.34 + 2
0.25	2.17-1	6.05-1	3.56-2	1.17 + 2
0.1	2.65-1	6.37-1	2.35-2	4.67 + 1
0.05	3.00-1	6.04-1	1.63-2	2.34 + 1
0.025	3.29-1	5.73-1	1.17-2	1.17 + 1
0.01	3.66-1	5.35-1	7.06-3	4.68 + 0

\* 4.17 x 10<sup>-3</sup>



Table 3.3  
Number of Secondaries Which Escape as a Function of  
Energy, Average Angle of Emission and Thickness for 25 Mev Electrons

$E_e^*$ (Mev)	T = 10 gm/cm <sup>2</sup>		T = 5 gm/cm <sup>2</sup>		T = 2.5 gm/cm <sup>2</sup>		T = 1 gm/cm <sup>2</sup>	
	$S_e(10^{-4} \frac{se}{ie})$	$\theta$ (deg)	$S_e(10^{-4} \frac{se}{ie})$	$\theta$ (deg)	$S_e(10^{-4} \frac{se}{ie})$	$\theta$ (deg)	$S_e(10^{-4} \frac{se}{ie})$	$\theta$ (deg)
0.05	25.44	61.35	25.370	64.03	25.130	66.62	27.010	70.01
0.15	35.35	39.07	35.060	43.80	39.140	48.38	36.950	54.14
0.55	31.03	32.72	27.010	33.39	28.510	44.43	27.640	46.47
1.0	24.20	39.17	14.420	31.71	20.340	36.77	16.440	39.74
2.0	6.375	32.65	4.703	27.98	10.330	29.93	7.524	31.61
4.0	---	---	0.661	23.12	5.041	22.44	3.103	23.27
6.0	---	---	---	---	4.073	18.06	1.834	18.63
8.0	---	---	---	---	1.191	15.63	1.334	15.55
10.0	---	---	---	---	---	---	1.217	13.17
12.0	---	---	---	---	---	---	---	---

\* $\Delta E_e = 0.10$  Mev

Table 3.3 (Cont'd)

Number of Secondaries Which Escape as a Function of  
Energy, Average Angle of Emission and Thickness for 25 Mev Electrons

$E_e$ (Mev)	$T = 0.75 \text{ gm/cm}^2$		$T = 0.50 \text{ gm/cm}^2$		$T = 0.25 \text{ gm/cm}^2$		$T = 0.10 \text{ gm/cm}^2$	
	$S_e (10^{-4} \frac{\text{se}}{\text{ie}})$	$\theta$ (deg)	$S_e (10^{-4} \frac{\text{se}}{\text{ie}})$	$\theta$ (deg)	$S_e (10^{-4} \frac{\text{se}}{\text{ie}})$	$\theta$ (deg)	$S_e (10^{-4} \frac{\text{se}}{\text{ie}})$	$\theta$ (deg)
0.05	26.850	71.16	26.440	71.73	26.200	73.14	26.990	74.65
0.15	37.610	56.24	37.290	57.69	37.63	60.68	35.140	63.50
0.55	26.680	47.70	24.140	48.77	19.47	50.16	12.570	51.40
1.0	14.670	40.46	12.920	41.08	9.075	41.98	5.115	42.69
2.0	6.406	32.03	5.229	32.34	3.373	32.82	1.571	33.22
4.0	2.475	23.50	1.876	23.68	1.044	23.92	0.470	24.10
6.0	1.456	18.82	1.036	18.94	0.546	19.10	0.235	19.21
8.0	1.059	15.65	0.726	15.74	0.378	15.85	0.155	15.93
10.0	0.912	13.26	0.604	13.33	0.303	13.42	0.122	13.48
12.0	---	---	---	---	0.143	11.48	0.112	11.49

Table 3.3 (Cont'd)

Number of Secondaries Which Escape as a Function of  
Energy, Average Angle of Emission and Thickness for 25 Mev Electrons

$E_e$ (Mev)	$T = 0.05 \text{ gm/cm}^2$		$T = 0.025 \text{ gm/cm}^2$		$T = 0.01 \text{ gm/cm}^2$	
	$S_e (10^{-4} \frac{se}{ie})$	$\theta$ (deg)	$S_e (10^{-4} \frac{se}{ie})$	$\theta$ (deg)	$S_e (10^{-4} \frac{se}{ie})$	$\theta$ (deg)
0.05	26.940	75.14	25.450	75.43	22.390	75.73
0.15	31.420	65.01	25.920	66.12	16.340	66.86
0.55	8.289	51.93	4.887	52.35	2.242	52.57
1.0	2.732	42.99	1.535	43.20	0.686	43.32
2.0	0.869	33.34	0.451	33.44	0.184	33.49
4.0	0.243	24.15	0.124	24.20	0.050	24.21
6.0	0.121	19.24	0.061	19.26	0.024	19.27
8.0	0.079	15.96	0.040	15.97	0.016	15.97
10.0	0.061	13.49	0.031	13.50	0.012	13.50
12.0	0.059	11.50	0.028	11.51	0.011	11.51

Table 3.4  
Number of Secondaries Which Escape as a Function  
of Angle and Thickness for 25 Mev Electrons

* $\theta$ (deg)	$T = 10 \text{ gm/cm}^2$	$T = 5 \text{ gm/cm}^2$	$T = 2.5 \text{ gm/cm}^2$	$T = 1 \text{ gm/cm}^2$	$T = 0.75 \text{ gm/cm}^2$	$T = 0.50 \text{ gm/cm}^2$
	$S_e(10^{-4} \frac{\text{se}}{\text{ie}})$	$S_e(10^{-4} \frac{\text{se}}{\text{ie}})$	$S_e(10^{-4} \frac{\text{se}}{\text{ie}})$	$S_e(10^{-4} \frac{\text{se}}{\text{ie}})$	$S_e(10^{-4} \frac{\text{se}}{\text{ie}})$	$S_e(10^{-4} \frac{\text{se}}{\text{ie}})$
15	0.006	24.81	53.03	23.09	17.17	11.36
25	1.976	41.61	37.41	29.40	23.17	16.15
35	33.77	27.32	26.63	26.57	27.16	23.95
45	20.66	19.30	19.81	16.77	19.24	19.13
55	13.81	13.59	13.29	13.29	13.42	13.47
65	7.30	3.52	3.17	3.33	3.25	7.63
75	3.66	3.72	3.75	3.71	3.71	3.61

\*  $\Delta\theta = 2^\circ$

Table 3.4 (Cont'd)  
 Number of Secondaries Which Escape as a Function  
 of Angle and Thickness for 25 Mev Electrons

$\theta$ (deg)	T = 0.25gm/cm <sup>2</sup>	T = 0.10gm/cm <sup>2</sup>	T = 0.05gm/cm <sup>2</sup>	T = 0.025gm/cm <sup>2</sup>	T = 0.01gm/cm <sup>2</sup>
	$S_e(10^{-4} \frac{se}{ie})$	$S_e(10^{-4} \frac{se}{ie})$	$S_e(10^{-4} \frac{se}{ie})$	$S_e(10^{-4} \frac{se}{ie})$	$S_e(10^{-4} \frac{se}{ie})$
15	5.62	2.241	1.12	0.56	0.224
25	3.11	3.277	1.64	0.83	0.330
35	14.00	5.709	2.36	1.42	0.569
45	13.31	10.61	5.51	2.81	1.129
55	12.86	13.60	10.77	5.37	2.392
65	7.35	7.61	7.44	6.56	6.413
75	3.61	3.72	3.68	3.61	3.625

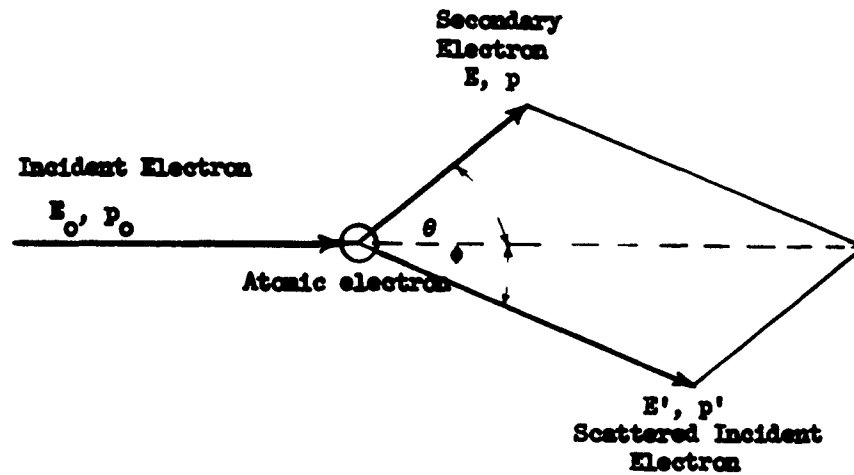


Figure 3.1 Trajectories in the scattering plane for the incident electron  $E_0$ , the scattered electron  $E'$ , and the secondary electron  $E$ . The momentum is represented by  $p$

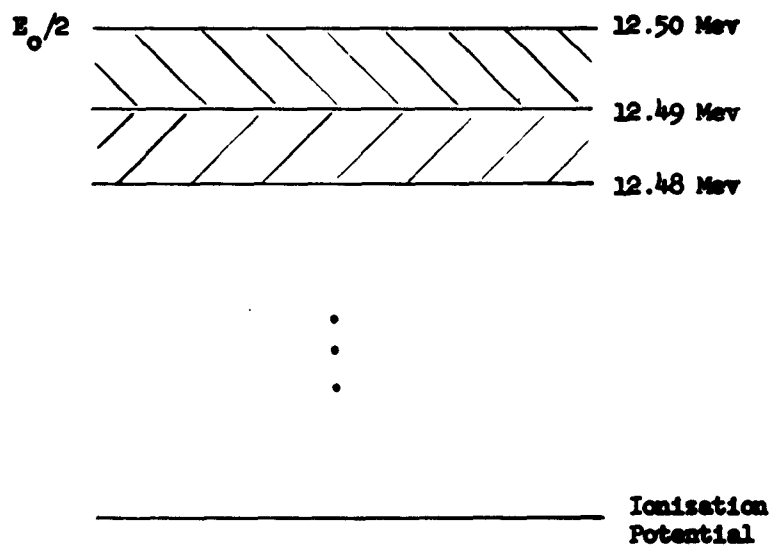


Figure 3.2 Energy groups for the 25 Mev electron program

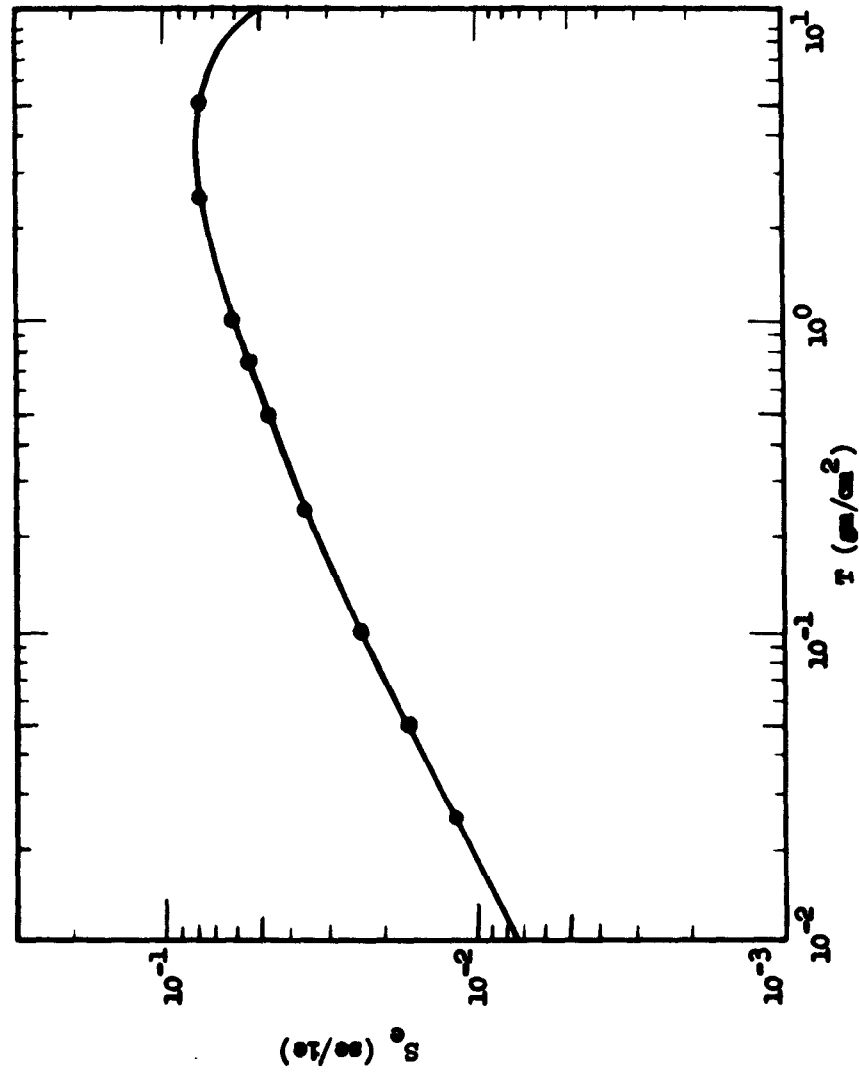


Figure 3.3 The number of secondaries escaping  $S_e$  as a function of thickness for 25-Mev electrons



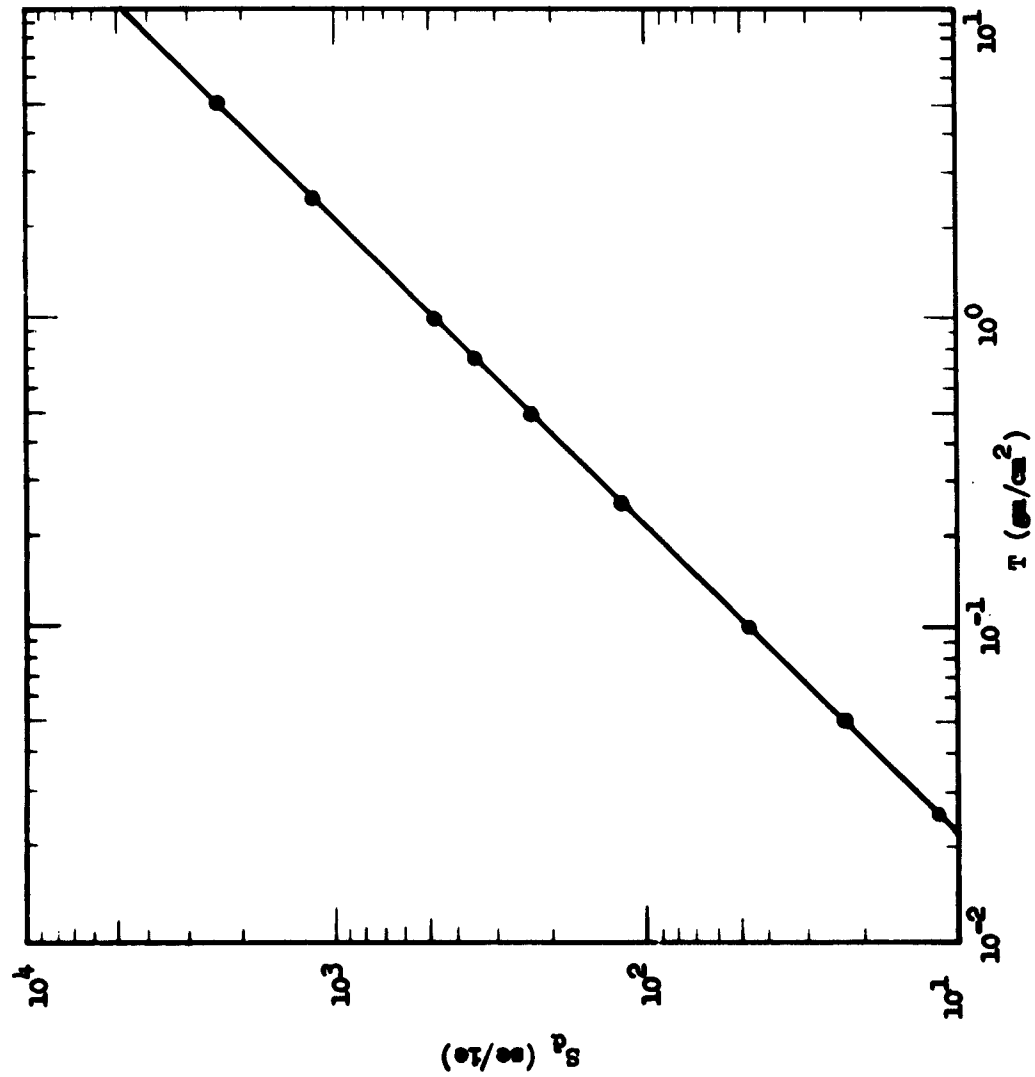


Figure 3.4 The number of secondaries deposited  $S_d$  as a function of thickness for 25-Mev electrons

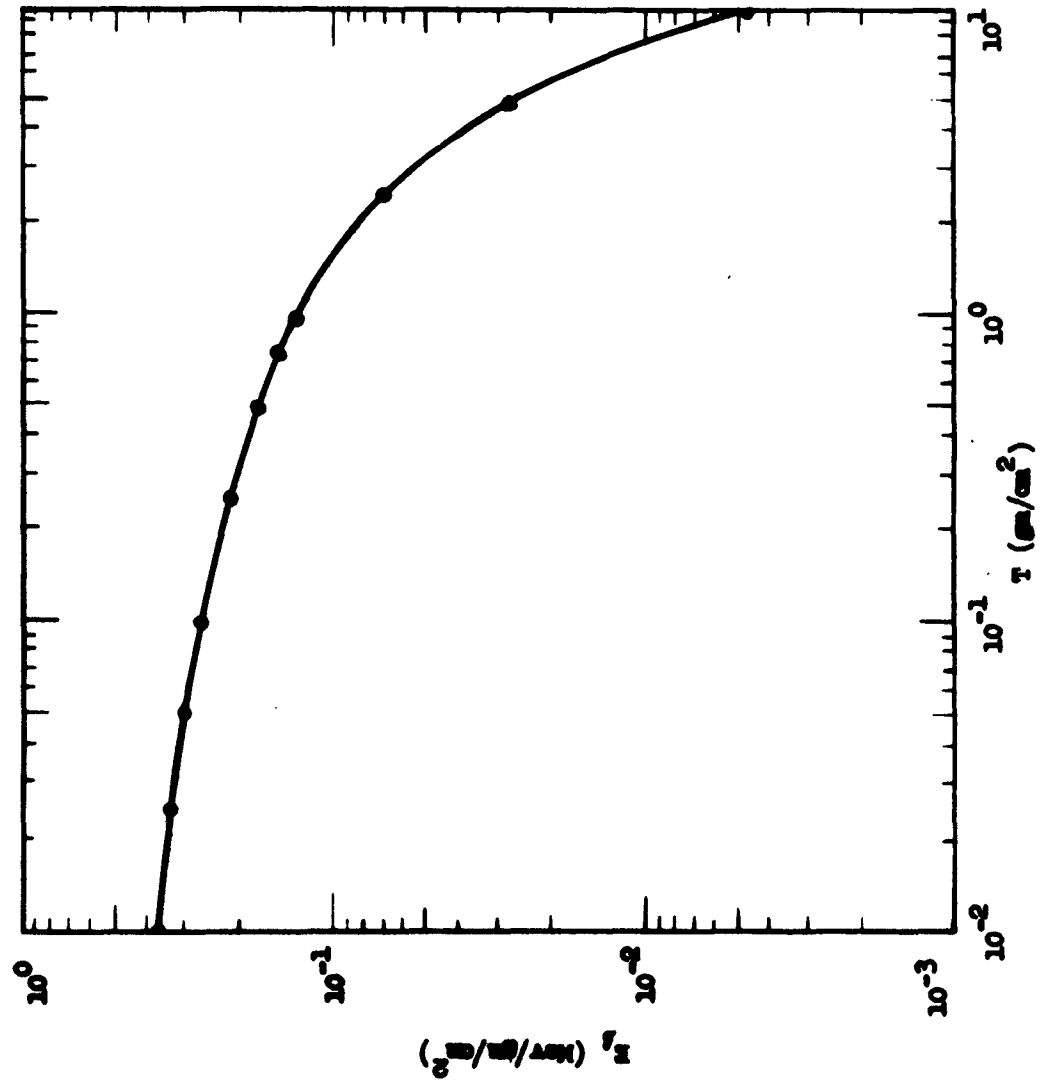


Figure 3.5 The energy of escape per unit path length as a function of thickness for 25-Mev electrons

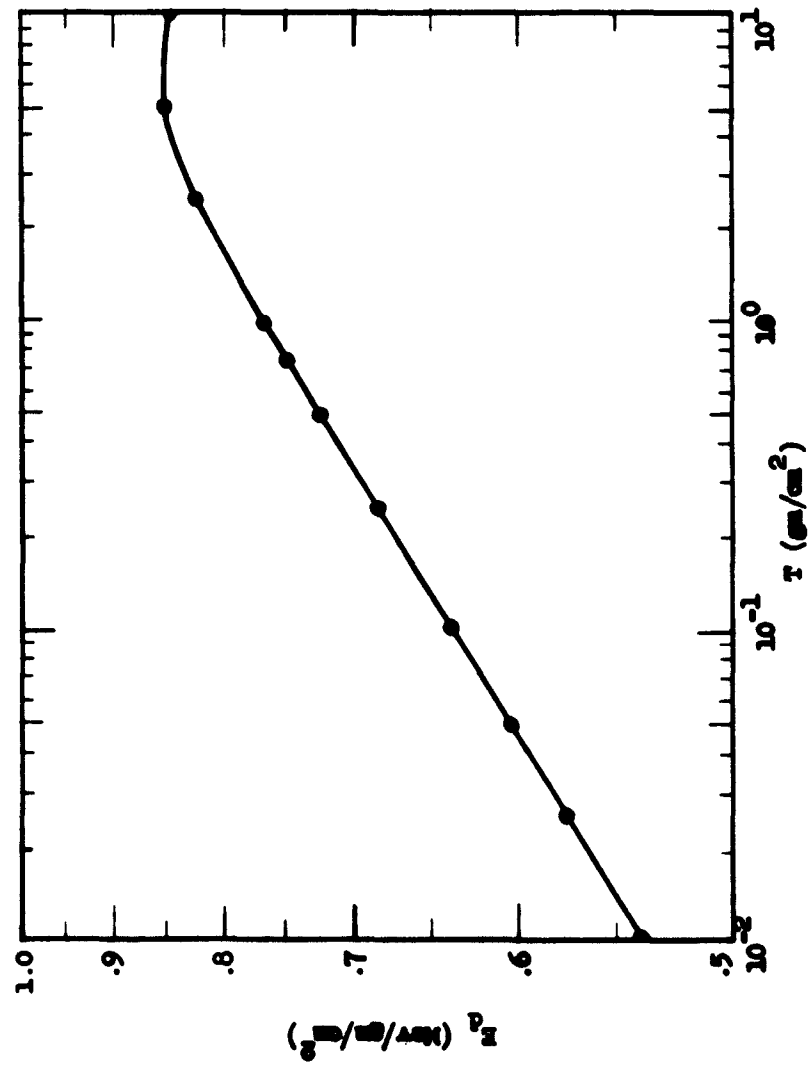


Figure 3.6 The energy deposited per unit path length as a function of thickness for 25-Mev electrons

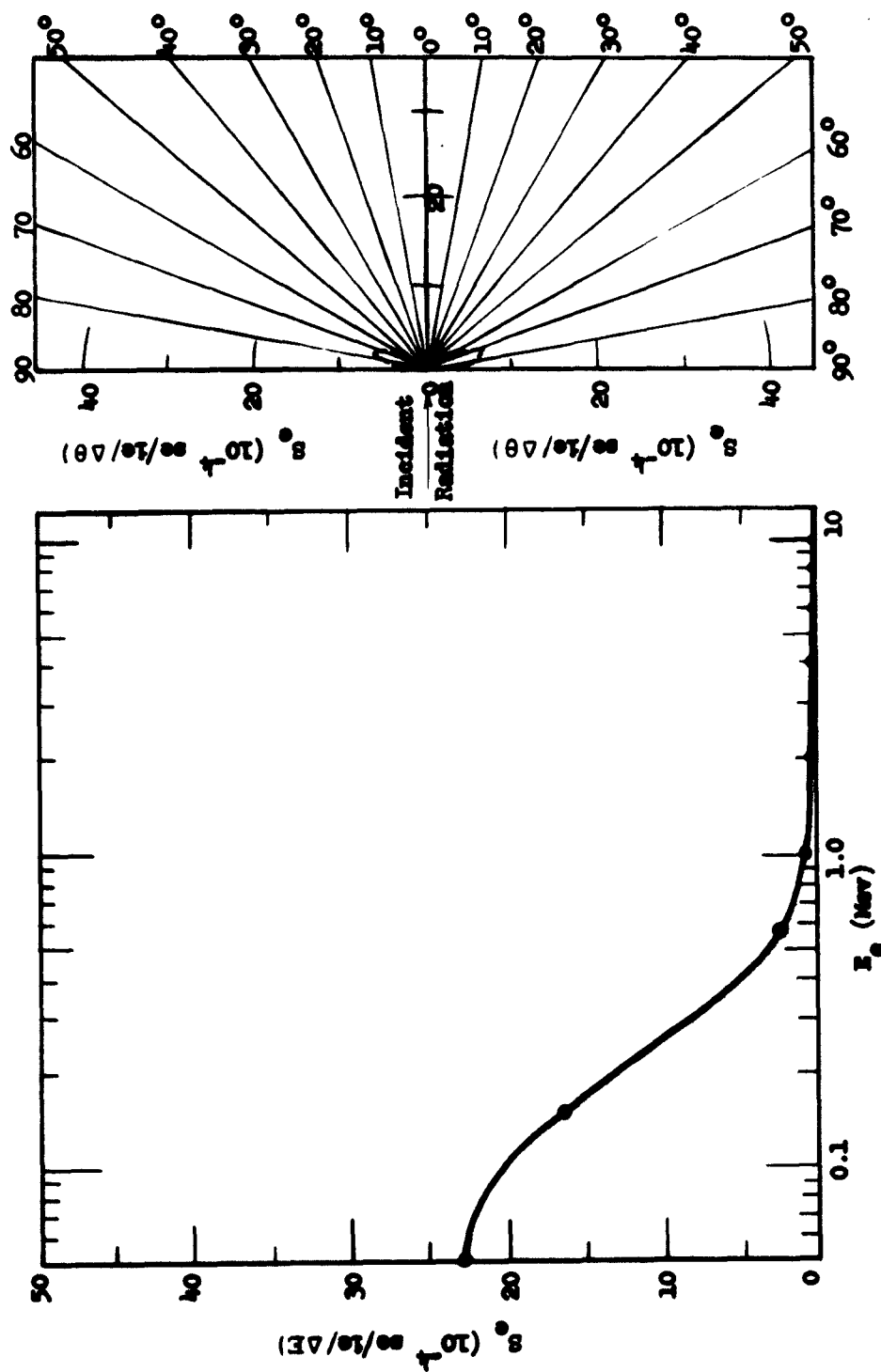


Figure 3.7 Energy and angle of emission spectra for 25-Mev electrons incident on a sample of thickness 0.01 gm/cm<sup>2</sup>

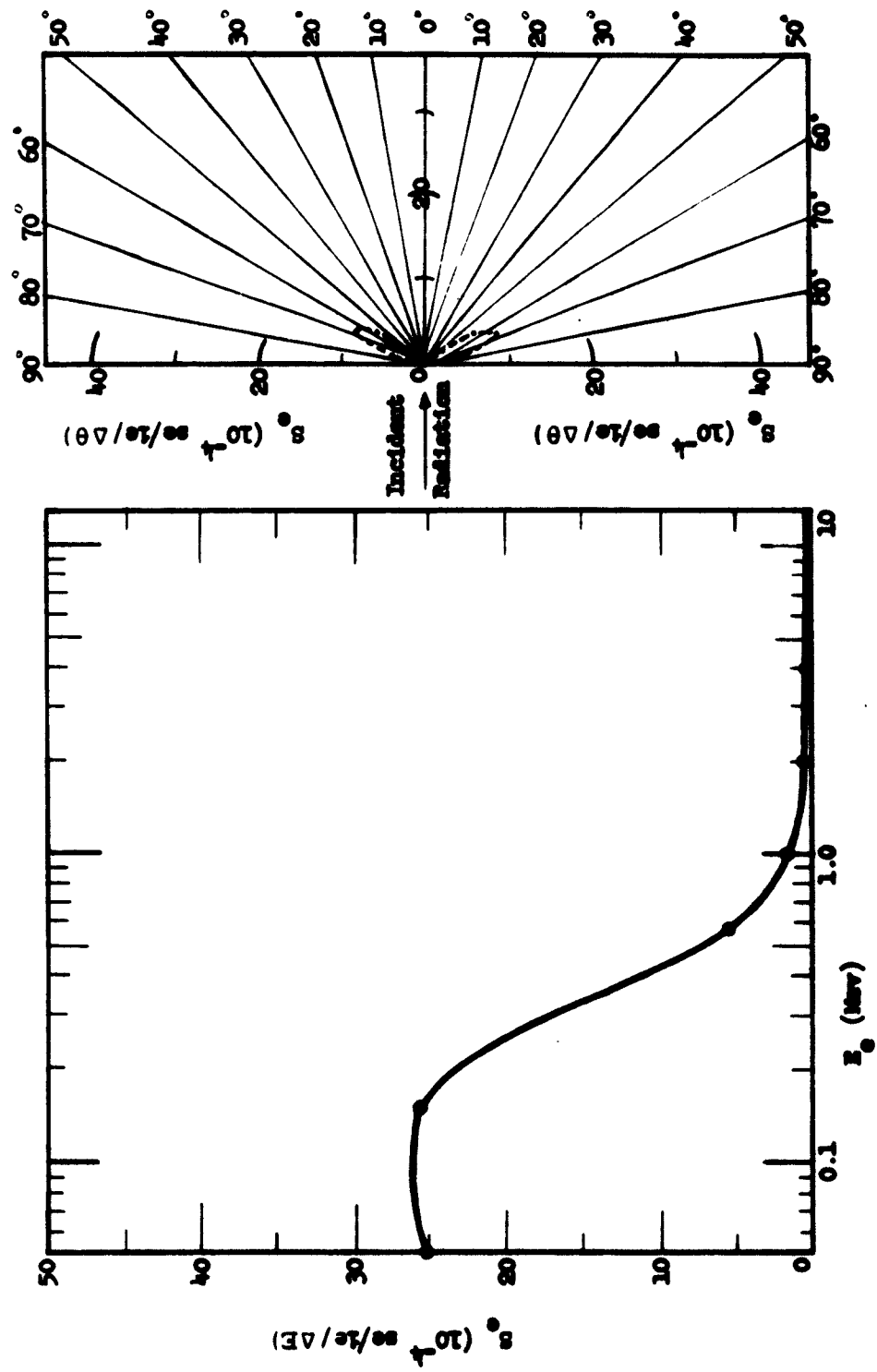


Figure 3.8 Energy and angle of emission spectra for 25-Mev electrons incident on a sample of thickness 0.025 gm/cm<sup>2</sup>

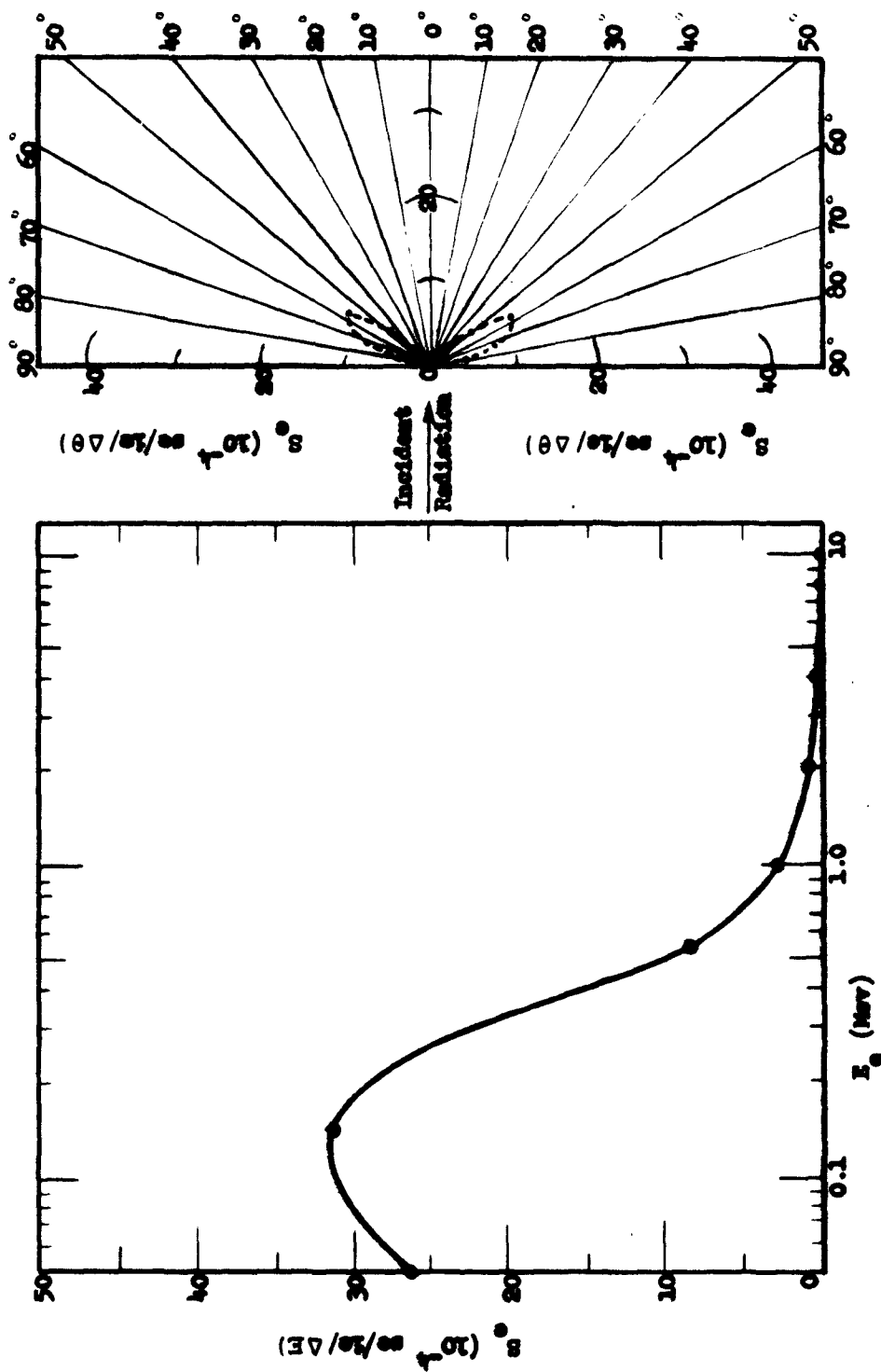


Figure 3.9 Energy and angle of emission spectra for 25-Mev electrons incident on a sample of thickness 0.05 gm/cm<sup>2</sup>

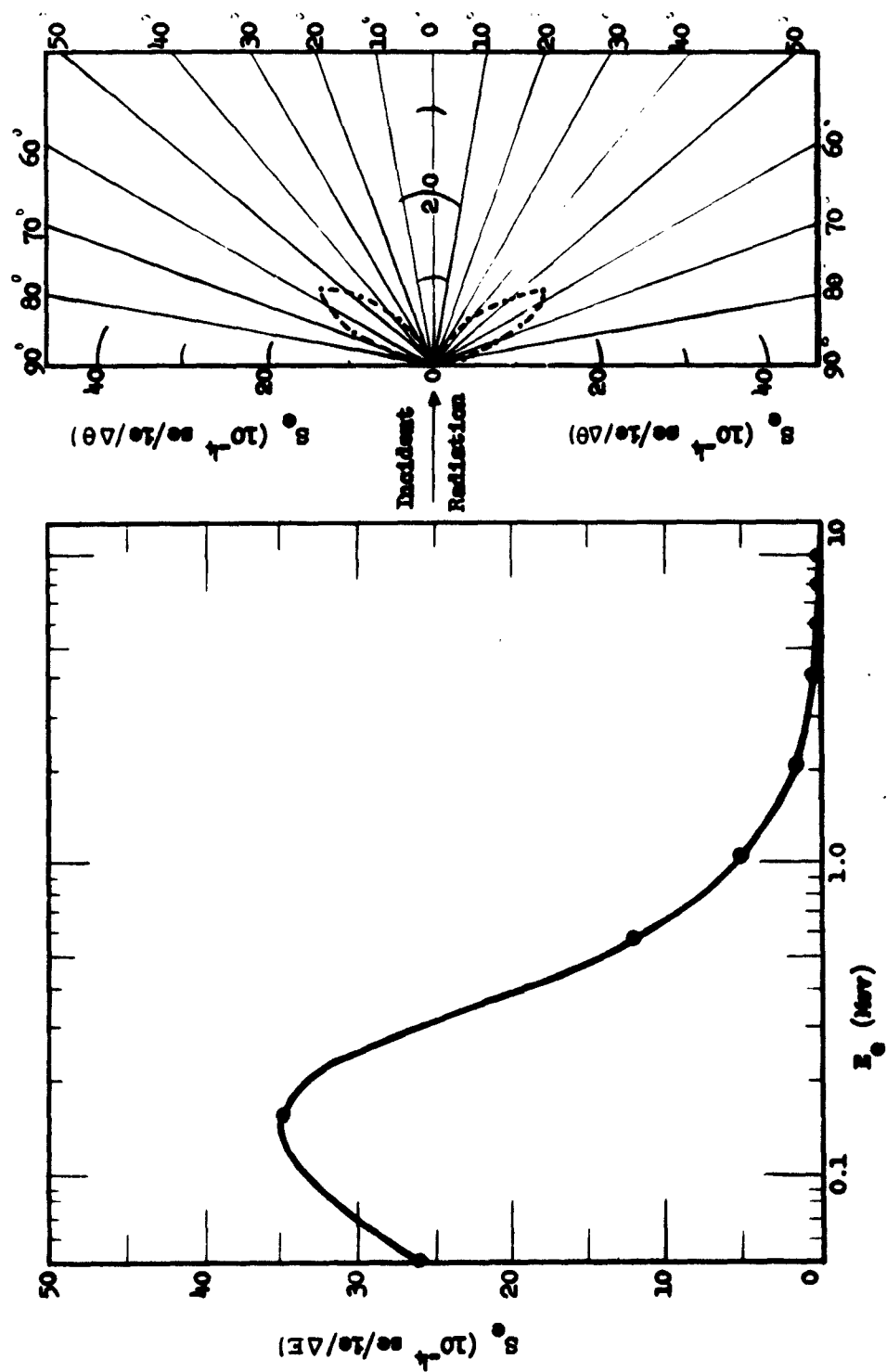


Figure 3.10 Energy and angle of emission spectra for 25-Mev electrons incident on a sample of thickness 0.10 gm/cm<sup>2</sup>

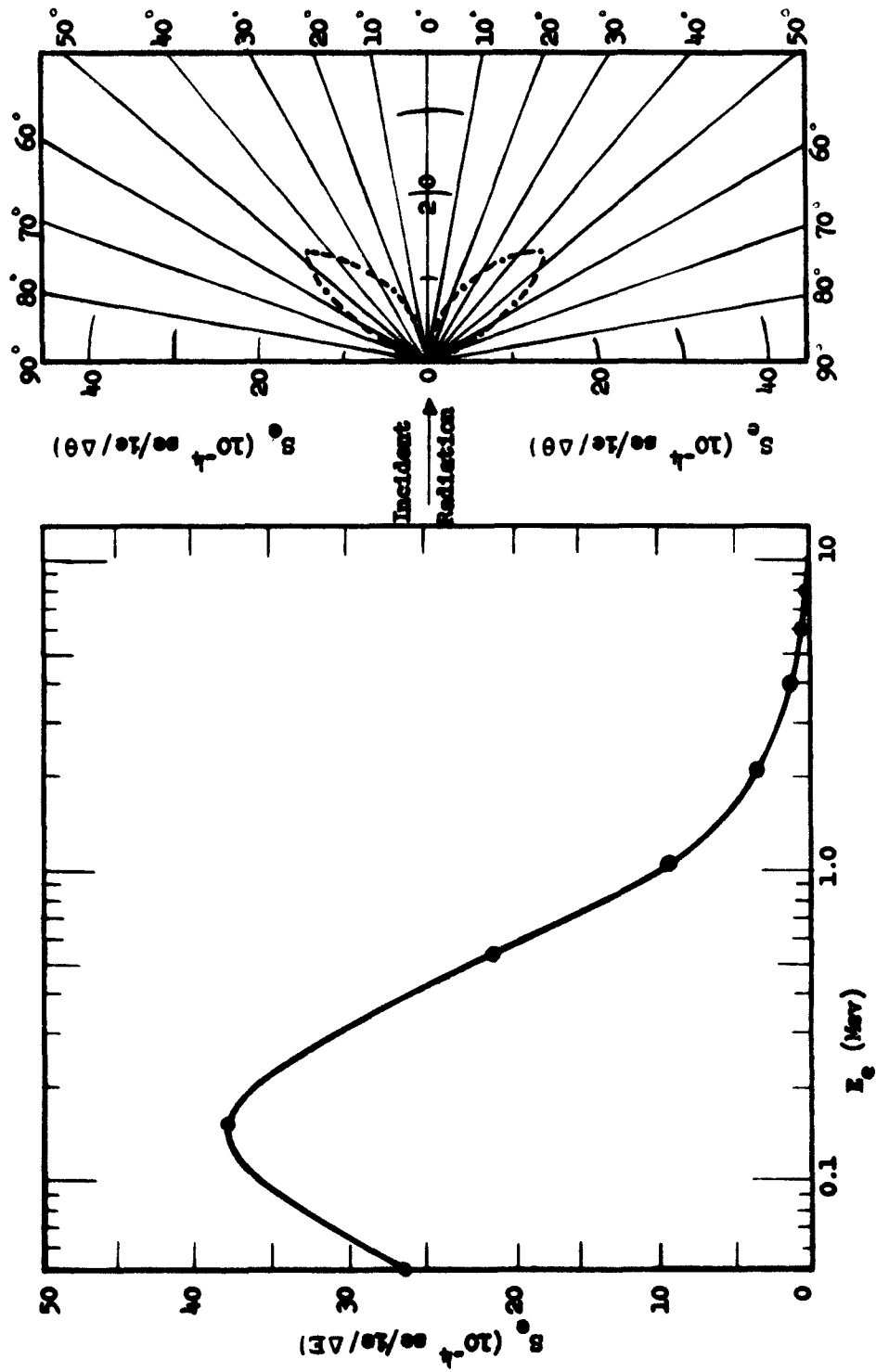


Figure 3.11 Energy and angle of emission spectra for 25-Mev electrons incident on a sample of thickness 0.25 gm/cm<sup>2</sup>



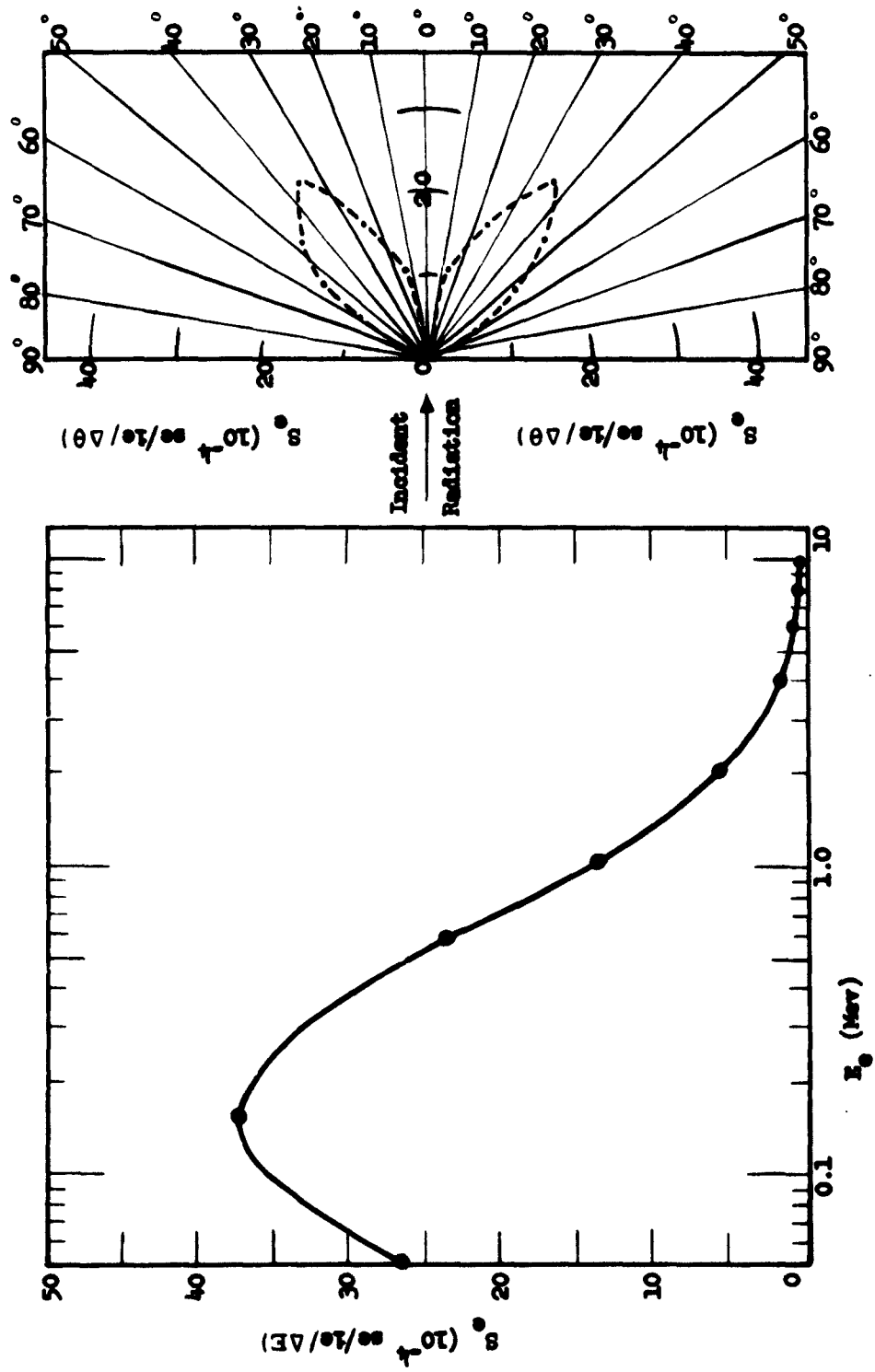


Figure 3.12 Energy and angle of emission spectra for 25-Mev electrons incident on a sample of thickness 0.50 gm/cm<sup>2</sup>

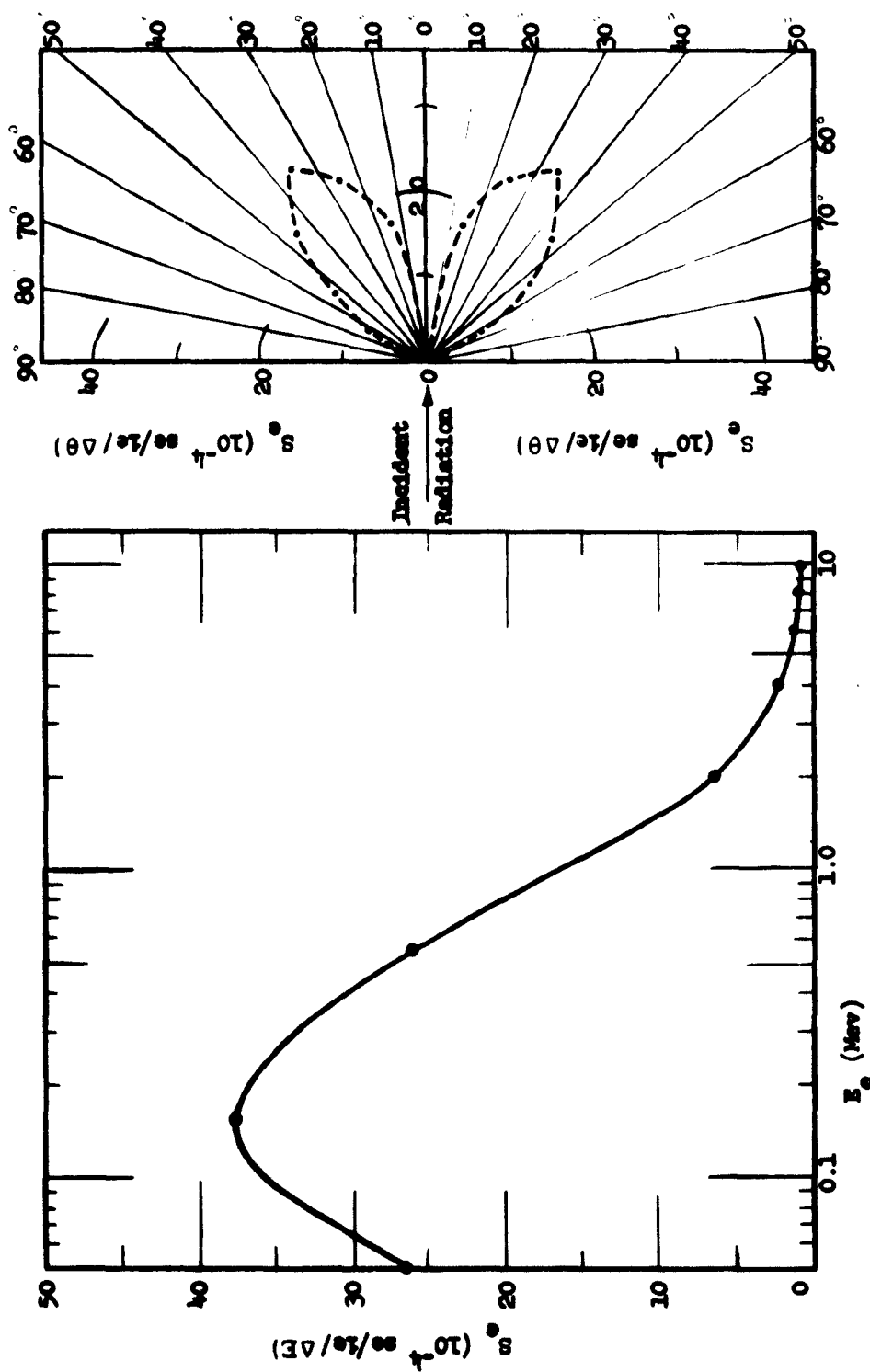


Figure 3.13 Energy and angle of emission spectra for 25-Mev electrons incident on a sample of thickness 0.75 gm/cm<sup>2</sup>

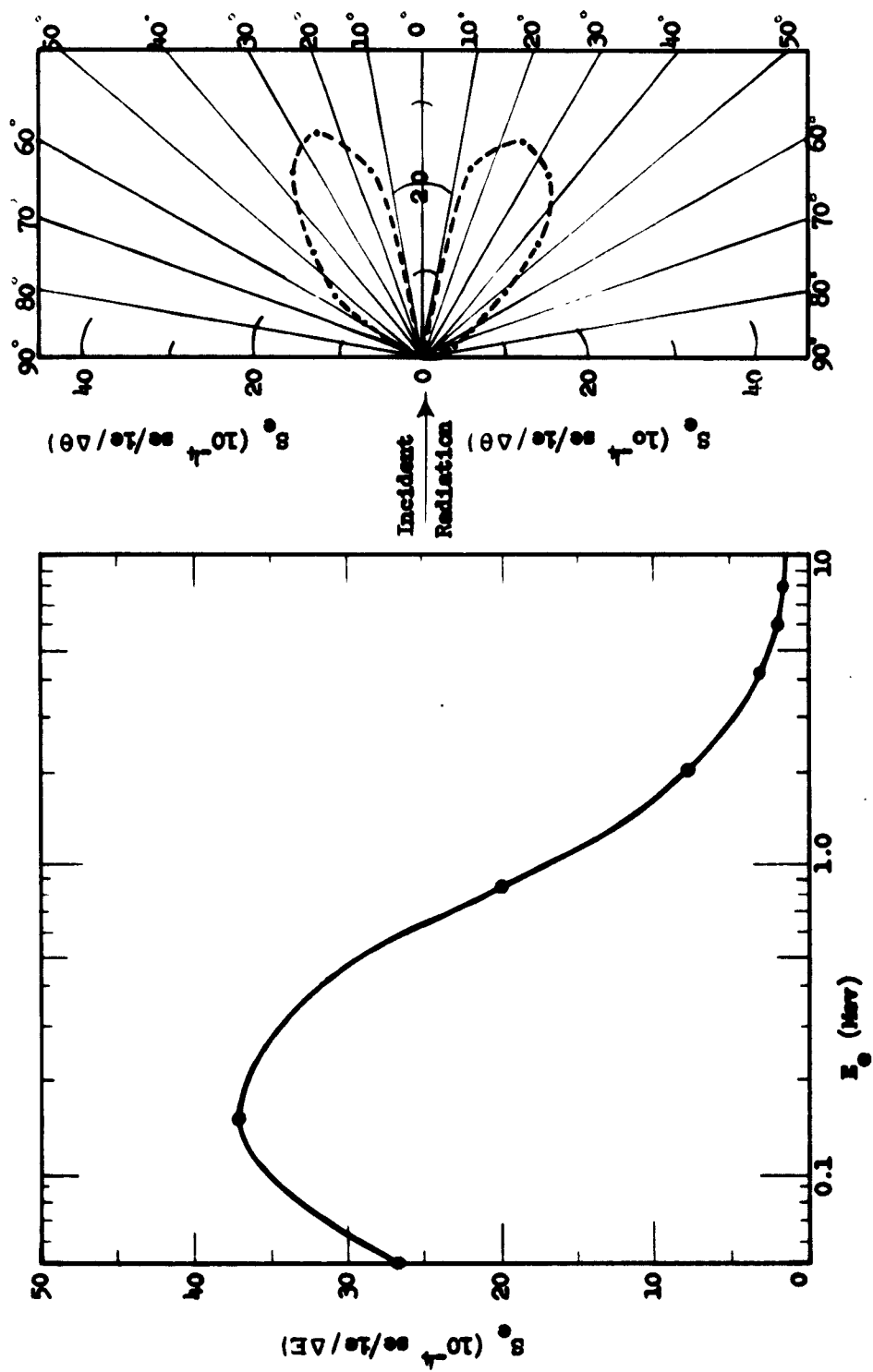


Figure 3.14 Energy and angle of emission spectra for 25-Mev electrons incident on a sample of thickness 1.0 gm/cm<sup>2</sup>

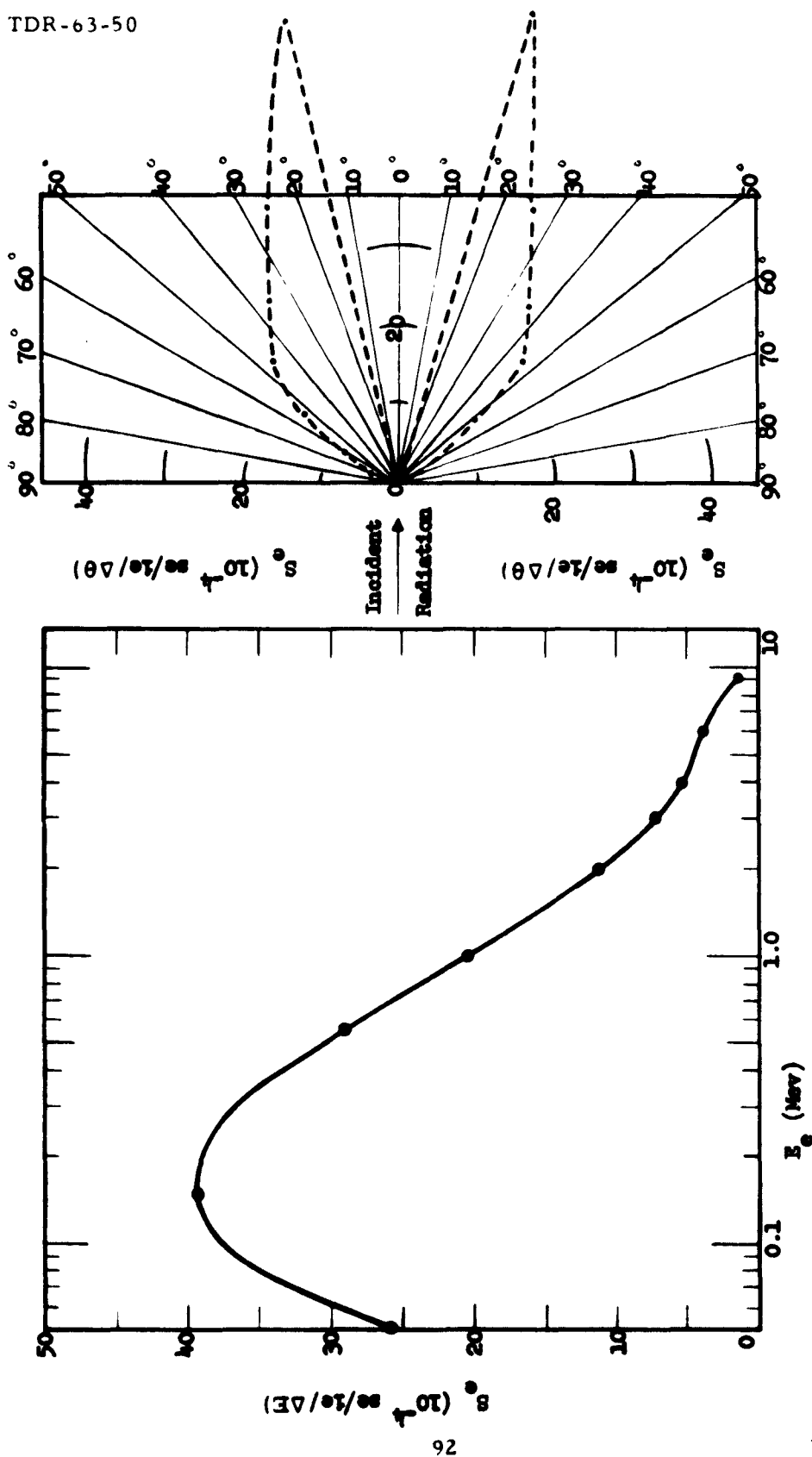


Figure 3.15 Energy and angle of emission spectra for 25-Mev electrons incident on a sample of thickness 2.5 gm/cm<sup>2</sup>

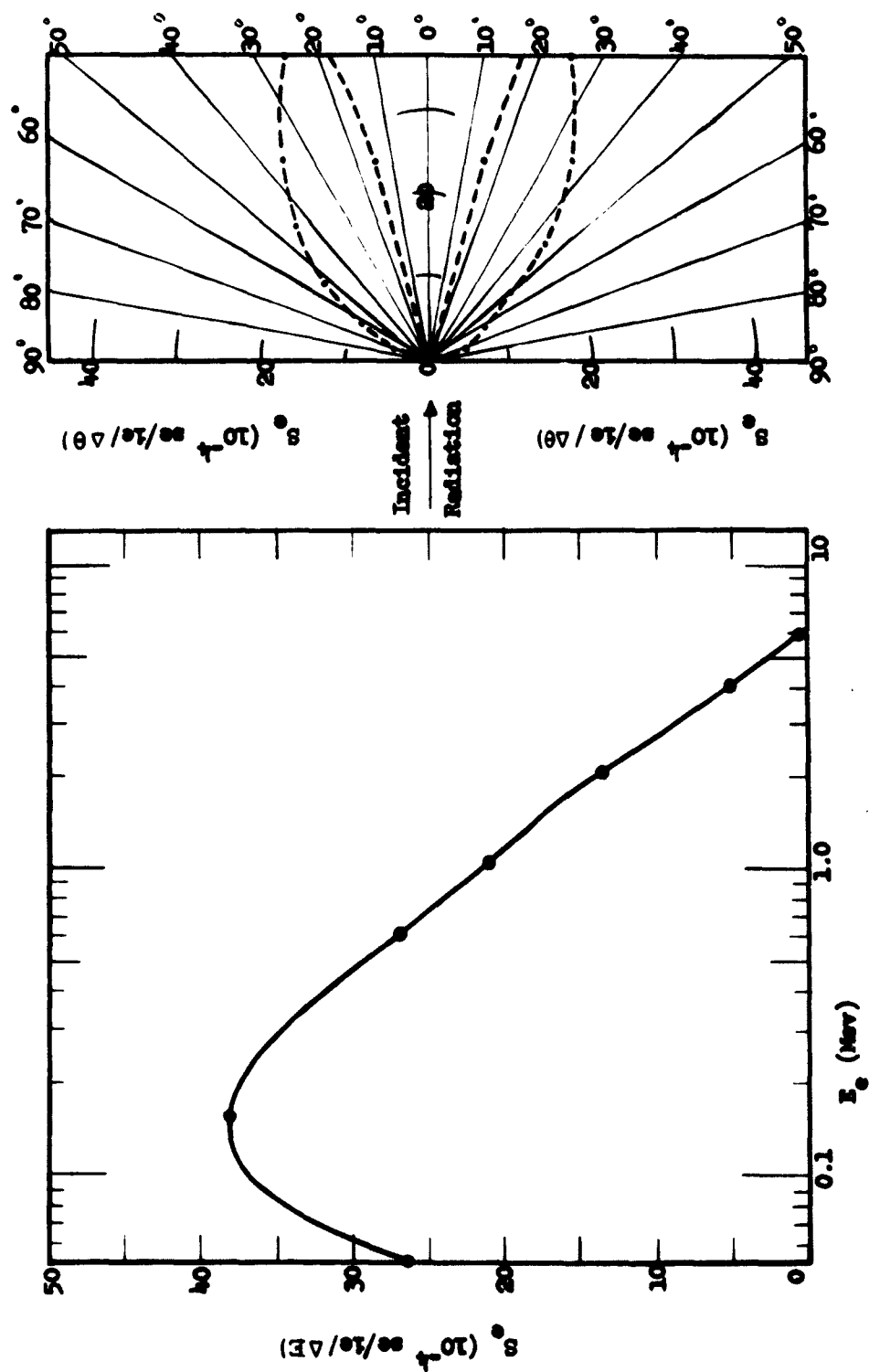


Figure 3.16 Energy and angle of emission spectra for 25-Mev electrons incident on a sample of thickness 5.0 gm/cm<sup>2</sup>

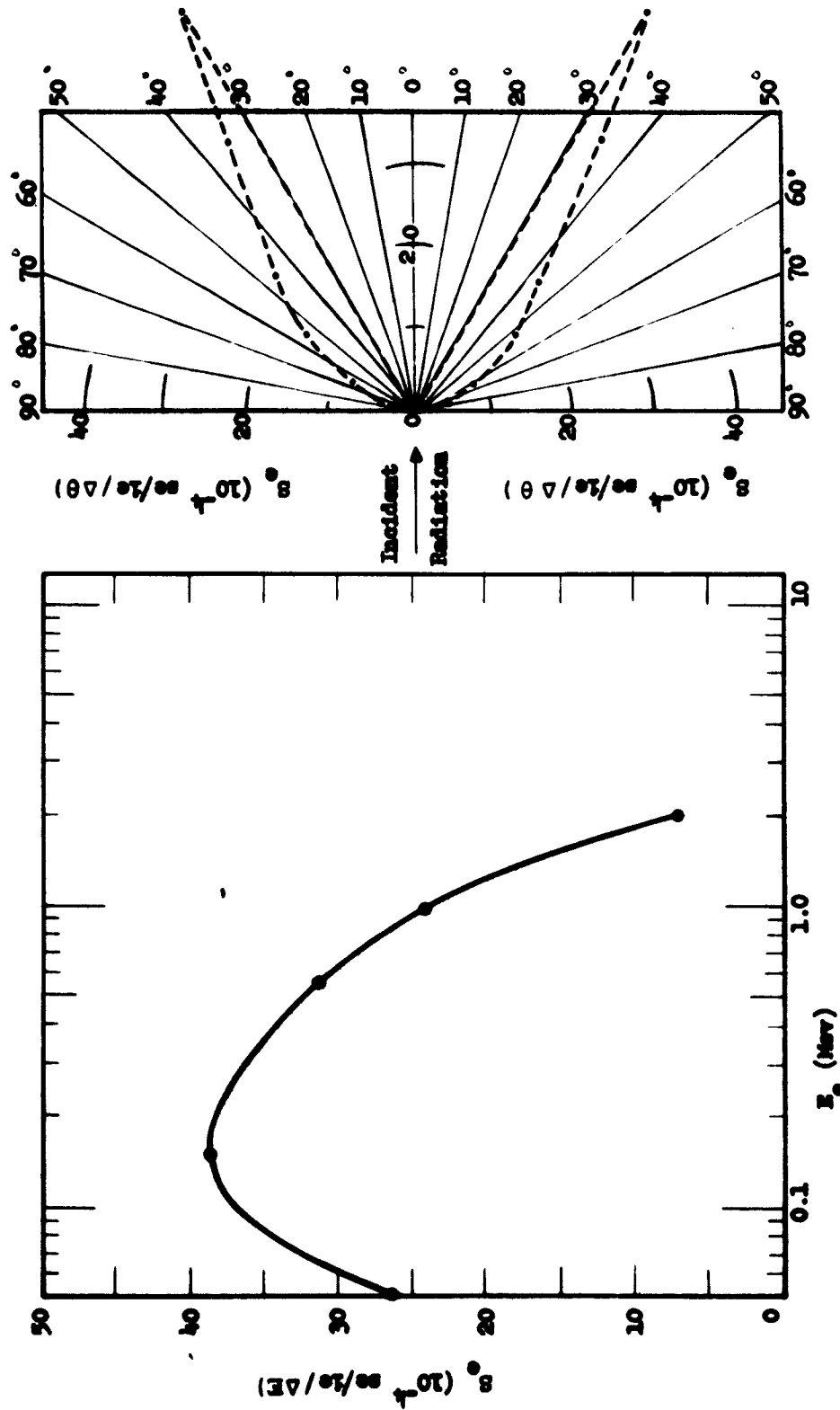


Figure 3.17 Energy and angle of emission spectra for 25-Mev electrons incident on a sample of thickness 10 gm/cm<sup>2</sup>

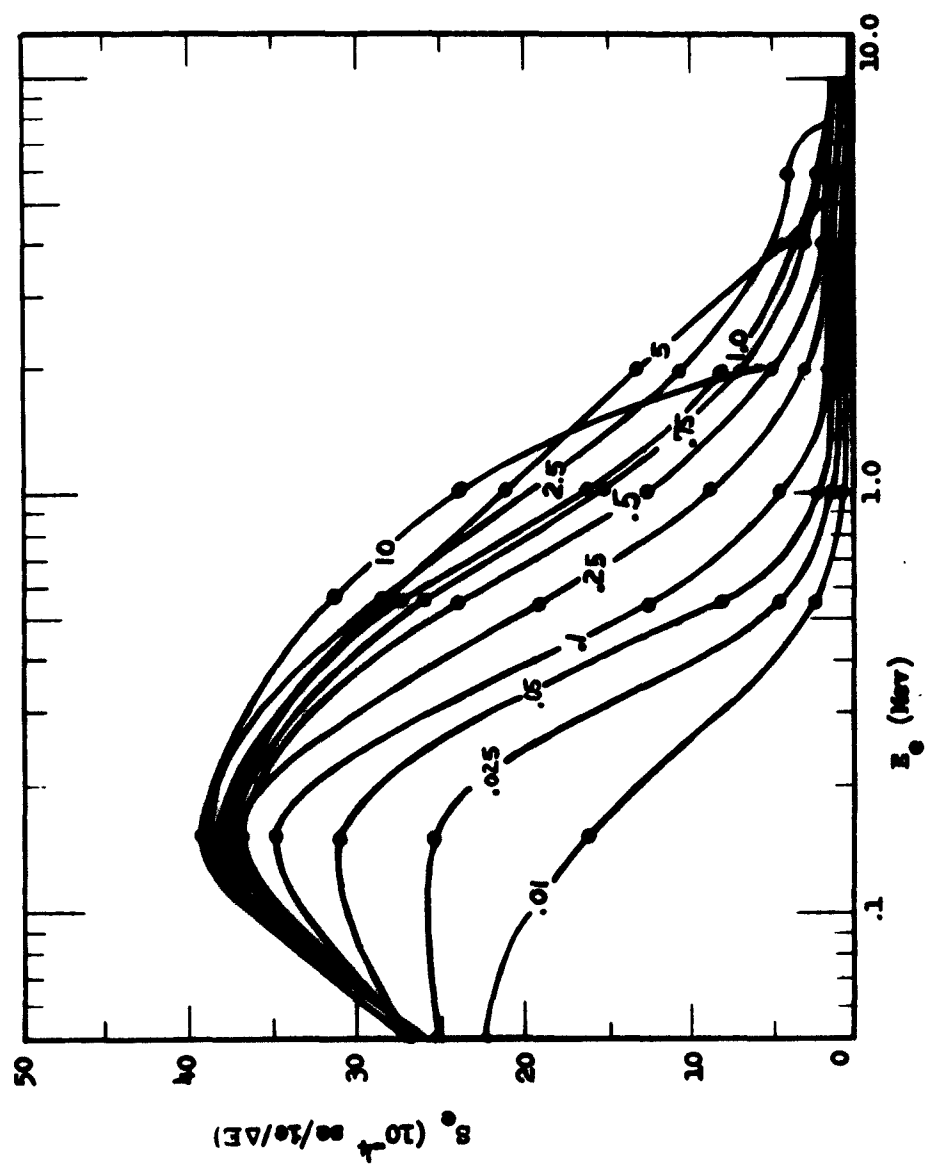


Figure 3.18 Energy spectra for 25-Mev electrons for thicknesses in the range from 0.01 to 10  $\text{gm}/\text{cm}^2$

4. SECONDARY ELECTRON EMISSION BY A 600 KV PULSED X-RAY SOURCE.

a. General remarks

The remarks in this section concern a 600-kv Fexitron Flash X-Ray System manufactured by Field Emission Corporation, McMinnville, Oregon. The spectrum used for the calculations to follow was measured on the Fexitron located at Sandia Corporation, Albuquerque, New Mexico. It is capable of delivering 1200 megawatts in 0.1  $\mu$ sec with impulse currents of 2,000 amperes at 600-kv anode potential.

b. Theory

The theory for this section shall be the same as section 2. b.

c. Procedure

(1) Energy groups

The Bouchard (1962) energy spectrum, figure 4. 1, measured at the Sandia Corporation 600-kv Flash X-Ray System was used to determine the weighting as a function of energy group. Table 4. 1 contains the energy groups and the spectrum weighting factors as taken from figure 4. 1.

The quantity  $E N(E)$  in table 4. 1 is used in this section in the same context as  $N_m$  in section 2. c(1).

(2) Sample division

The sample division in this section is the same as section 2. c(2).

(3) Attenuation

The attenuation is the same as section 2. c(3).

(4) Sample problem

The calculations were done in a very similar manner to those



in section 2. c(4) except for different energy groups and weighting factors.

#### d. Results

The results are contained in table 4.2 (Energy Losses and Secondary Electron Emission Efficiencies as a Function of Thickness for 600 KV X-rays), table 4.3 (Number of Secondaries which Escape as a Function of Energy, Average Angle of Emission and Thickness for 600 KV X-rays) and table 4.4 (Number of Secondaries which Escape as a Function of Angle and Thickness for 600 KV X-rays). The data contained in table 4.2 can be found plotted on figures 4.2 - 4.5, and table 4.3-4.4 data are in figures 4.6-4.7.

#### e. Discussion

Tables 4.2 and 4.3 contain the data from the computer. The results of these tables are plotted in figures 4.2 - 4.7.

Figure 4.2 gives the  $S_e$  versus the thickness. For small thicknesses the value  $S_e$  increases to a maximum of  $5 \times 10^{-4}$  and stays at this value over a large range of thicknesses. However, it begins to decrease for the larger thicknesses to a value of  $2 \times 10^{-4}$  at  $10 \text{ gm/cm}^2$ .

$S_d$  versus thickness forms a straight line on log-log paper, figure 4.3. It increases from  $10^{-3}$  at  $0.01 \text{ gm/cm}^2$  to 1 at  $10 \text{ gm/cm}^2$ .

The sum of figures 4.4 and 4.5 gives  $8.08 \times 10^{-3} \text{ Mev/gm/cm}^2$  for the energy loss by the incident beam which is a factor of three less than the total energy loss. Since we are only concerned with the high energy component this seems reasonable for 600 KV X rays.

In figures 4.6 and 4.7, one will find the energy spectra and angle-of-emission spectrum plotted. The angle-of-emission spectra were all almost the same value (see table 4.3); therefore only one is presented. In figure 4.6, the intensities increase with decreasing thicknesses in general. However, there is a striking difference in these spectra from the previous ones because these do not reach a maximum up to 0.05 Mev. The spectra are presented together so one can get a relative perspective of their intensities.

Table 4.1

Energy Groups and Weighting Factors  
For 600 KV X-rays

$h\nu_0$ (Mev)	$E N(E) \left( \frac{\text{Mev}}{\text{Mev} \cdot \text{cm}^2} \right)$
.00 - .05	0.000
.05 - .10	1.050
.10 - .15	2.300
.15 - .20	2.600
.20 - .25	2.750
.25 - .30	2.800
.30 - .35	2.625
.35 - .40	2.300
.40 - .45	1.850
.45 - .50	1.350
.50 - .55	0.800
.55 - .60	0.250

Table 4.2

Energy Losses and Secondary Electron  
Emission Efficiencies as a Function of  
Thickness for 600 KV X- rays

T (gm/cm <sup>2</sup> )	E <sub>l</sub> (Mev/gm/cm <sup>2</sup> )	E <sub>d</sub> (Mev/gm/cm <sup>2</sup> )	S <sub>e</sub> (se/i γ )	S <sub>d</sub> (se/i γ )
10.0	1.70-6	8.08-3	1.95-4	1.13 0
5.0	5.42-6	8.08-3	3.17-4	5.63- 1
2.5	1.37-5	8.08-3	4.04-4	2.81- 1
1.0	3.94-5	8.08-3	4.67-4	1.12- 1
0.75	5.37-5	8.03-3	4.80-4	8.39- 2
0.50	8.28-5	7.98-3	4.91-4	5.50- 2
0.25	1.69-4	7.93-3	5.03-4	2.76- 2
0.10	4.29-4	7.69-3	5.11-4	1.07- 2
0.05	8.62-4	7.26-3	5.14-4	5.11- 3
0.025	1.72-3	6.39-3	5.13-4	2.30- 3
0.01	3.64-3	4.46-3	4.28-4	6.96- 4

\*  $3.51 \times 10^{-5}$

Table 4.3  
Number of Secondaries Which Escape as a Function of  
Energy, Average Angle of Emission and Thickness  
For 600 KV X-rays

$E_e$ (Mev)	$T = 10 \text{ gm/cm}^2$		$T = 5 \text{ gm/cm}^2$		$T = 2.5 \text{ gm/cm}^2$		$T = 1.0 \text{ gm/cm}^2$	
	$S_e(10^{-4} \frac{\text{se}}{\text{ly}})$	$\theta$ (deg)	$S_e(10^{-4} \frac{\text{se}}{\text{ly}})$	$\theta$ (deg)	$S_e(10^{-4} \frac{\text{se}}{\text{ly}})$	$\theta$ (deg)	$S_e(10^{-4} \frac{\text{se}}{\text{ly}})$	$\theta$ (deg)
.05	27.17	42.4	44.95	42.4	57.89	42.4	66.77	42.5
.15	13.01	40.3	20.32	40.3	25.41	40.3	29.44	40.4
.25	0.11	39.1	0.17	39.1	0.20	39.1	0.37	39.1
<hr/>								
	$T = 0.75 \text{ gm/cm}^2$		$T = 0.50 \text{ gm/cm}^2$		$T = 0.25 \text{ gm/cm}^2$		$T = 0.10 \text{ gm/cm}^2$	
.05	64.06	42.7	70.26	42.5	72.07	42.5	72.55	42.6
.15	32.79	40.4	30.83	40.4	31.53	40.4	32.73	40.4
.25	0.28	39.1	0.38	39.1	0.39	39.1	0.32	39.1
<hr/>								
	$T = 0.05 \text{ gm/cm}^2$		$T = 0.025 \text{ gm/cm}^2$		$T = 0.01 \text{ gm/cm}^2$			
.05	72.92	42.7	72.67	43.0	57.49	43.3		
.15	32.93	40.4	33.00	40.4	30.75	40.4		
.25	0.32	39.1	0.32	39.1	0.26	39.1		

Table 4.4  
Number of Secondaries Which Escape as a Function  
of Angle and Thickness for 600 KV X-rays

$\theta$ (deg)	$T = 10.0 \text{ gm/cm}^2$	$T = 5.0 \text{ gm/cm}^2$	$T = 2.5 \text{ gm/cm}^2$	$T = 1.0 \text{ gm/cm}^2$	$T = 0.75 \text{ gm/cm}^2$	$T = 0.50 \text{ gm/cm}^2$
	$S_e(10^{-4} \frac{\text{se}}{\text{iy}})$	$S_e(10^{-4} \frac{\text{se}}{\text{iy}})$	$S_e(10^{-4} \frac{\text{se}}{\text{iy}})$	$S_e(10^{-4} \frac{\text{se}}{\text{iy}})$	$S_e(10^{-4} \frac{\text{se}}{\text{iy}})$	$S_e(10^{-4} \frac{\text{se}}{\text{iy}})$
39	7.22	11.01	13.60	15.65	15.80	16.32
41	21.09	33.62	42.45	48.69	50.10	51.02
43	10.84	18.62	24.41	28.59	29.43	30.18
45	1.14	2.19	3.04	3.71	3.80	3.96

Table 4.4 (Cont'd)

Number of Secondaries Which Escape as a Function  
of Angle and Thickness for 600 KV X-rays

$\theta$ (deg)	$T = 0.25 \text{ gm/cm}^2$	$T = 0.10 \text{ gm/cm}^2$	$T = 0.05 \text{ gm/cm}^2$	$T = 0.025 \text{ gm/cm}^2$	$T = 0.01 \text{ gm/cm}^2$
	$S_e(10^{-4} \frac{\text{se}}{\text{iy}})$	$S_e(10^{-4} \frac{\text{se}}{\text{iy}})$	$S_e(10^{-4} \frac{\text{se}}{\text{iy}})$	$S_e(10^{-4} \frac{\text{se}}{\text{iy}})$	$S_e(10^{-4} \frac{\text{se}}{\text{iy}})$
39	16.67	16.76	16.83	16.44	6.57
41	52.22	53.20	53.45	53.57	43.75
43	31.01	31.53	31.70	31.78	31.97
45	4.09	4.19	4.19	4.20	4.20

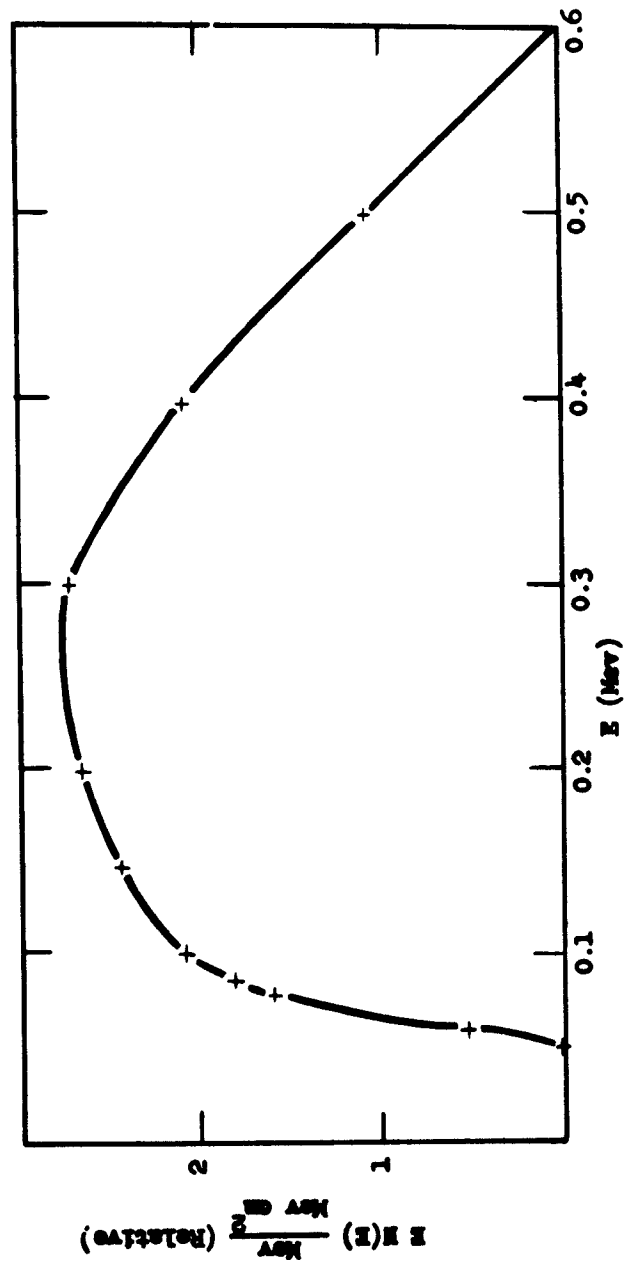


Figure 4.1 Energy spectrum from 600-kv flash X-ray machine as a function of photon energy

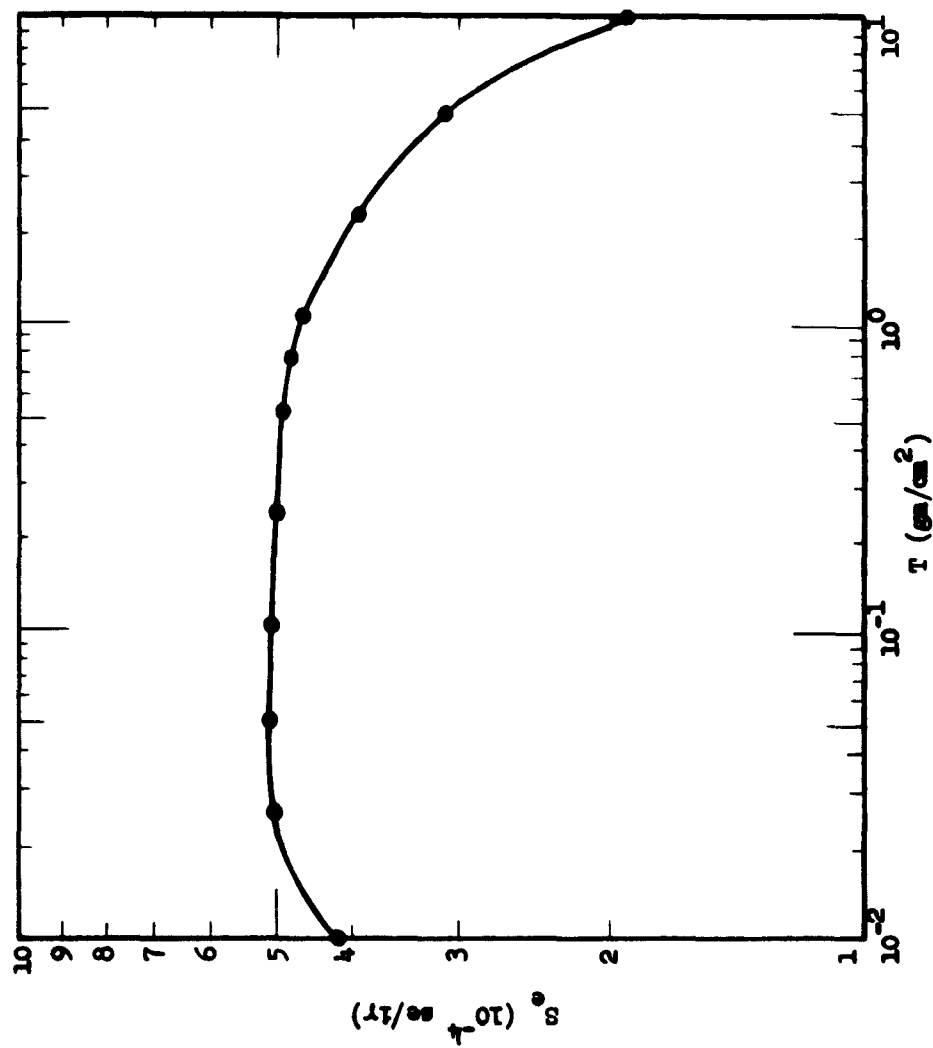


Figure 4.2 The number of secondaries escaping  $S_e$  as a function of thickness for 600-kv X rays



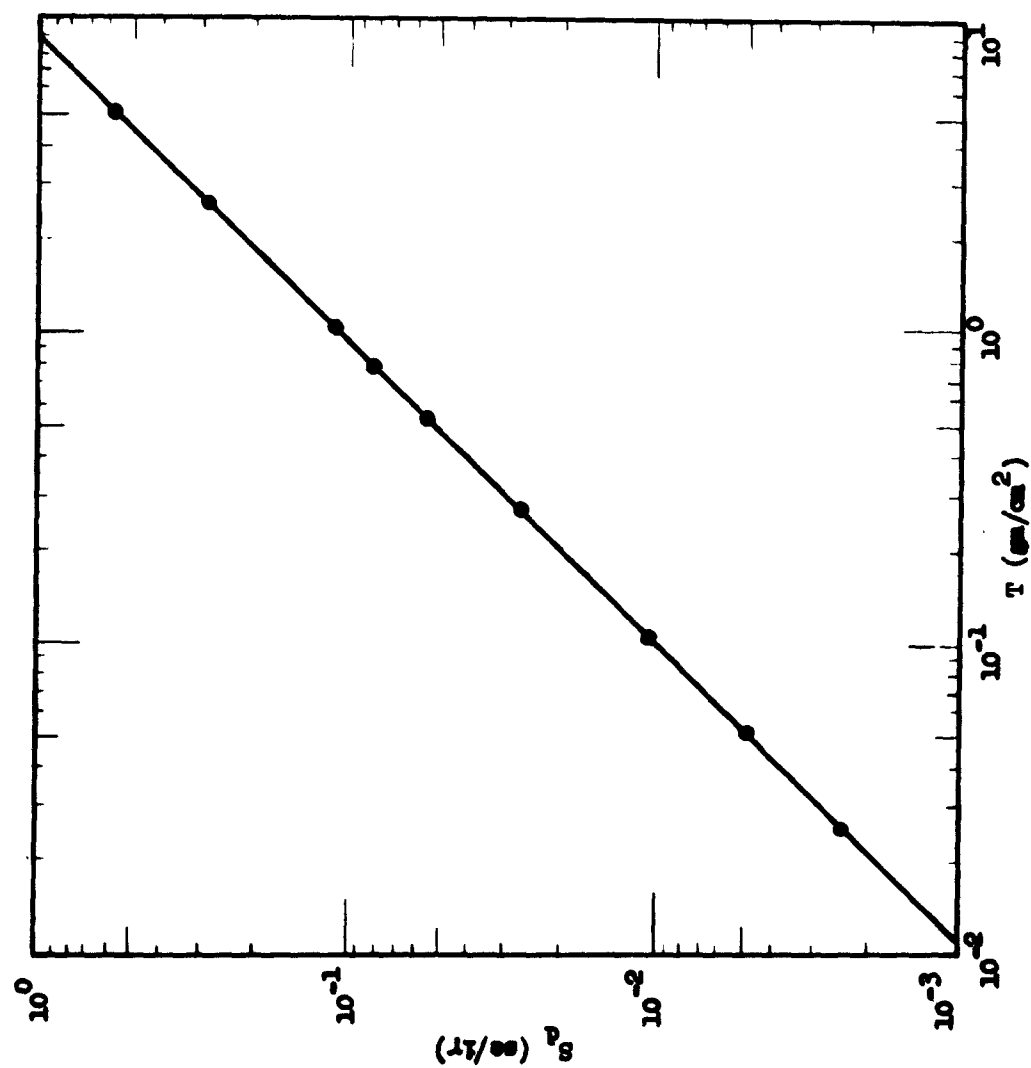


Figure 4.3 The number of secondaries deposited  $S_d$  as a function of thickness for 600-kv X rays

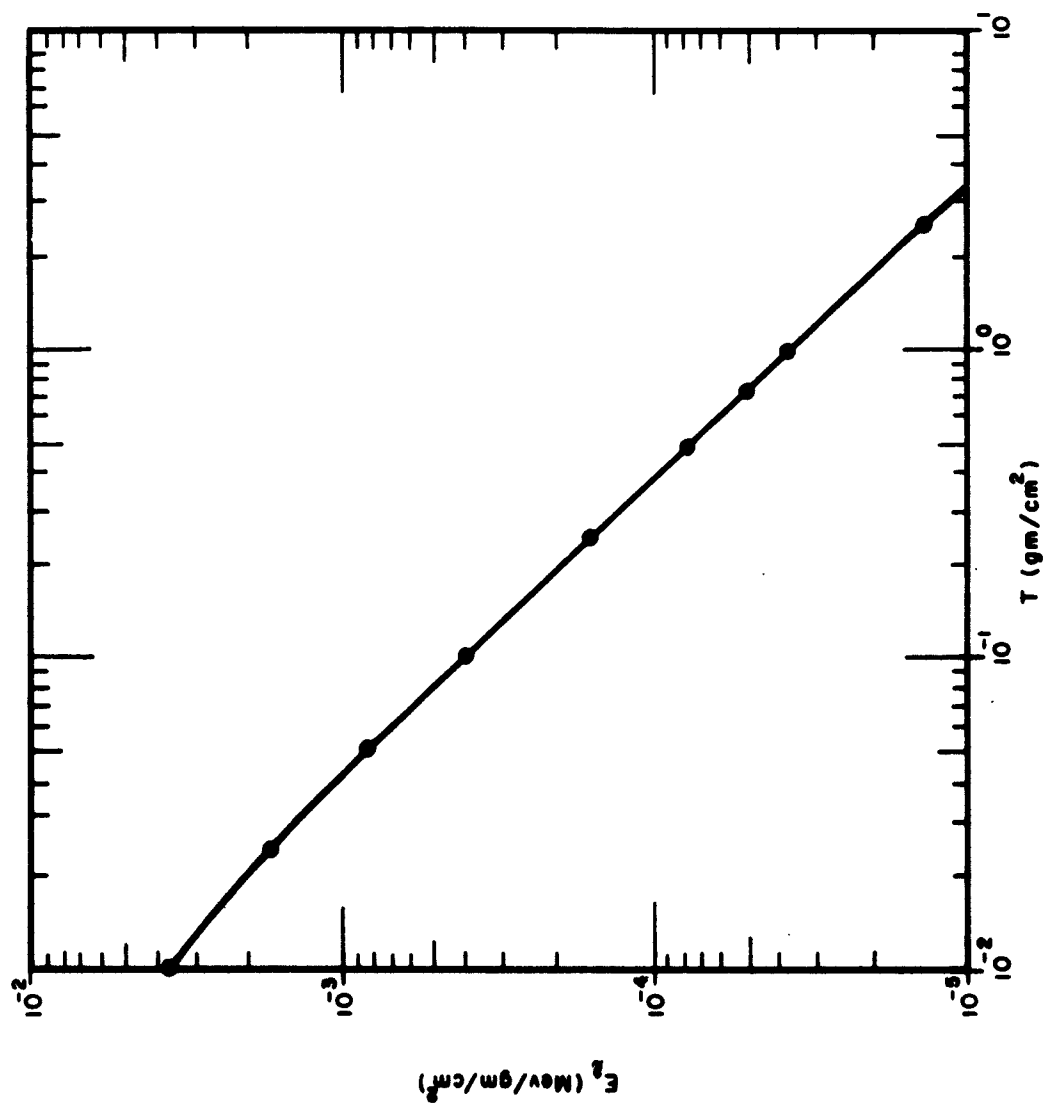


Figure 4.4 The energy of escape per unit path length as a function of thickness for 600-kv X rays

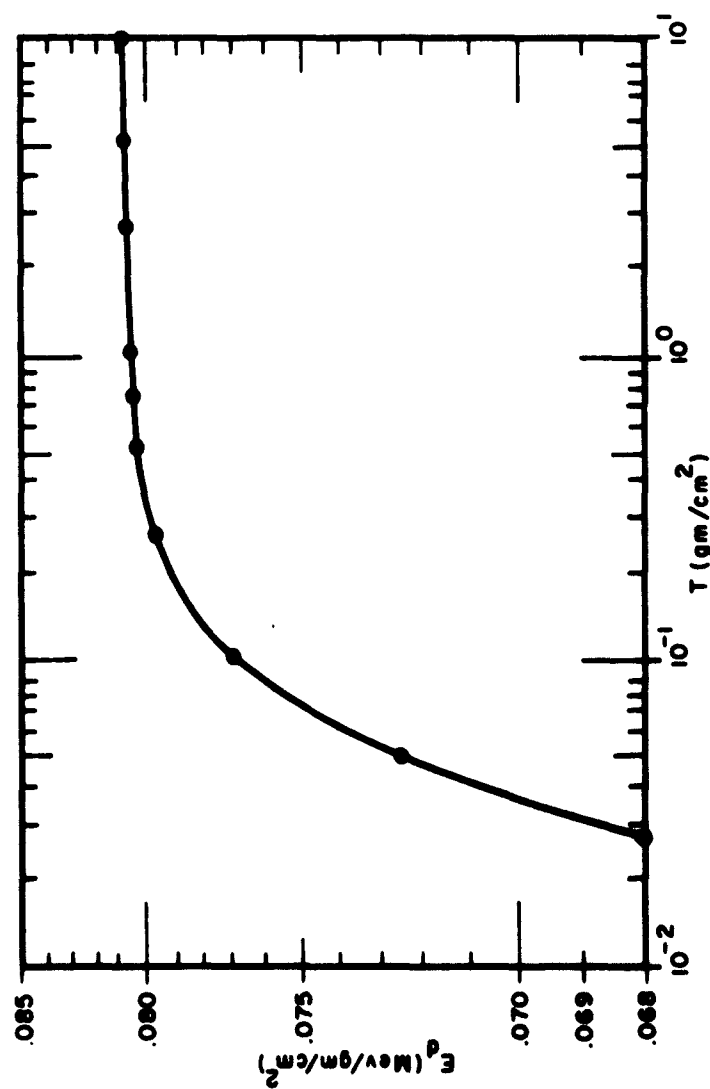


Figure 4.5 The energy deposited per unit path length as a function of thickness for 600-kv X rays

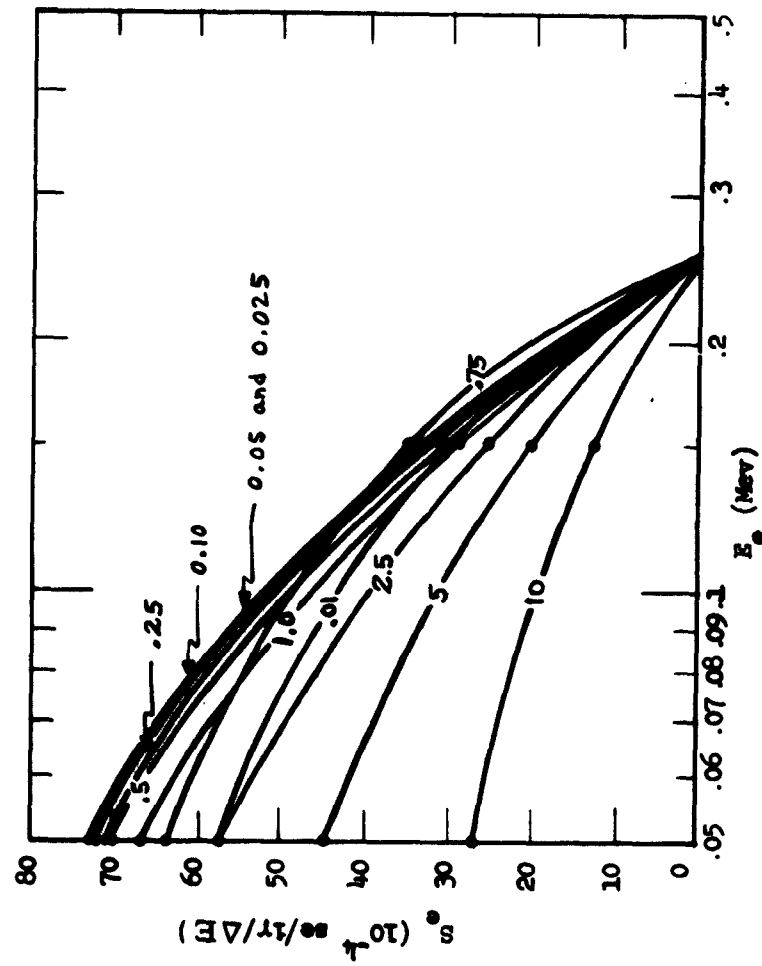


Figure 4.6 Energy spectra for 600-kv X rays for thicknesses in the range from 0.01 to 10  $\text{gm/cm}^2$

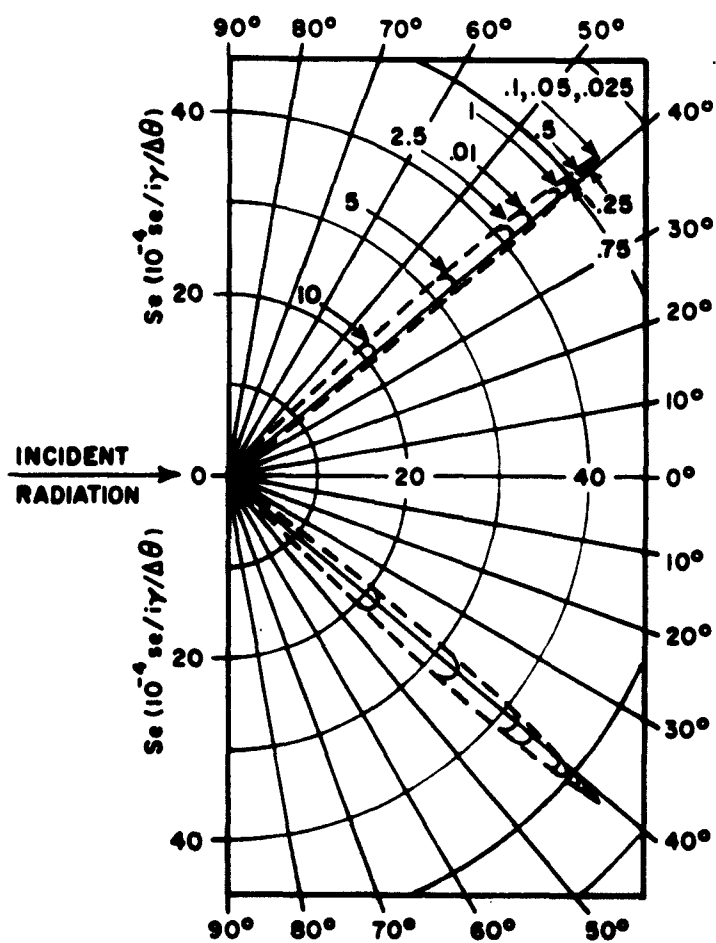


Figure 4.7 Angle of emission spectrum for 600-kv X rays. The numbers 10, 5, 2.5 .... etc., are thicknesses in  $gm/cm^2$

5. ASSUMPTIONS AND PERCENT ERRORS.

a. Low-Z materials were assumed ( $A = 2Z$ ), that is, materials where the atomic mass is equal to two times the atomic number. However, these calculations apply for materials where atomic mass is not identically equal to two times the atomic number because there is a cancelling effect on atomic number and atomic mass because of the range-energy relationships used. There is essentially no error involved.

b. Interactions are described by straight-line motion using semi-empirical range-energy curves for aluminum. This is not considered to be an error of any consequence for low-Z materials. However, it would be better to make the calculations for the range-energy curves for whatever material is being used.

c. The angular distribution was taken into account assuming elastic collisions with the incident particle and the atomic electrons. No error is anticipated.

d. Attenuation of the incident beam was also evaluated and included in the calculations. No error is anticipated.

e. Plates were used which are thin ( $0.01$  to  $10 \text{ gm/cm}^2$ ) compared with the range of 25-Mev electrons ( $13 \text{ gm/cm}^2$ ).

f. Only secondaries (delta rays) produced by the primary electrons are considered. Thus the low-energy secondary electron ionizations, which are proportional to the total number of low-energy electrons produced have been ignored. The error here is very small; and the best calculation is about 3 - 4 percent.

g. The integral of the cross section for production of a secondary electron times the probability for escape from the surface has been calculated, assuming the latter to be proportional to the range of the secondary. No error is anticipated.

h. The atomic electrons have been assumed to be free (kinetic energy after the collision is much greater than the binding energy) and stationary (the kinetic energy before the collision is much smaller than the kinetic

energy after the collision). No error is anticipated.

i. The density effect was not taken into account. Each atom was considered as an isolated event with no interference from other atoms in the neighborhood. In other words, the collisions were considered as close collisions. No error is anticipated.

j. The Compton interaction was assumed to be the predominant mechanism for energy loss in the prompt fission gamma and 600-kv X-ray calculation. The error is negligible for prompt fission gammas; however, the photoelectric effect should be included for higher  $Z$  materials in the X-ray calculation.

## 6. RESULTS

A summary of some of the most important results is given in table 6.1. As can be observed from this table, the secondary electron emission efficiency for 600-kv X rays is 0.05 percent with the prompt fission photon efficiency approximately an order of magnitude greater and the 25-Mev electron efficiency about two orders of magnitude greater.

The energy losses by the incident photon beams are approximately the same and agree very well with the predicted value. The energy loss by the incident 25-Mev electron beam agrees almost identically with the predicted value. The energy loss by the 25-Mev electron beam is about a factor of five greater than the energy losses by the photon beams.

The number of secondary electrons deposited per incident particle  $S_d$  is 1 for the two photon beams but 4,600 for the 25-Mev electron beam. This indicates that the electron beam has a stronger tendency to produce low-energy secondaries that do not escape.

The energy and angle-of-emission spectra are given in the various sections.

The results of this paper give the experimenter the basic parameters necessary for comparing the transient radiation effects on electronic components for various types of radiation fields. With a slight modification of the results, one can plot curves for the proper dose for irradiating a sample

Table 6.1  
Summary

Quantity	Prompt Fission Photons	25 Mev Electrons	600 KV X-rays
$S_e$ max (se/i particle)	0.3%	8%	0.05%
$S_d$ at 10 gm/cm <sup>2</sup> (se/i particle)	1.0	4600	1.0
$E_d$ max (Mev/gm/cm <sup>2</sup> )	0.170 per fis. (0.126)	0.693 (0.831)*	0.00803
$E_e$ Most probable (Mev)	0.15	0.15	< 0.05

\* Predicted Value



with the machine to give the same effects one would expect from a prompt fission gamma radiation field. In this way one is able to properly simulate in the laboratory the effects expected in a nuclear environment, since an important part of a nuclear environment is the prompt fission gamma radiation field.

## 7. CONCLUSIONS AND RECOMMENDATIONS.

An accurate method has now been established for determining the secondary electron emission efficiencies as a function of energy of escape, their angle of emission, and many other basic parameters for comparing different radiation fields for transient radiation effects work in the laboratory.

It has been found that the secondary electron emission efficiency for 25-Mev electrons is 8.0 percent followed by the prompt fission gamma efficiency of 0.3 percent and finally the 600-kv X-ray efficiency is 0.05 percent.

The energy spectra were about the same for all three types of radiation fields with respect to their intensities. The shapes were approximately the same for 25-Mev electrons and prompt fission gamma. However, the 600-kv X-ray spectra did not reach a maximum down to 0.05 Mev.

Since these are basic parameters, they will be useful in many ways. The individual experimenter is left the task of adapting these parameters to best fit his needs. For example, if one is interested in keeping the secondary electron emission efficiency the same for his laboratory radiation field and for a nuclear environment, it will be necessary to plot a curve relating these parameters. On the other hand, if an experimenter is interested in keeping the energy deposited equal, another curve can be plotted, etc.

The 600-kv X-ray calculation should be used only for low-Z material because no photoelectric effect was considered.

APPENDIX A

PROMPT FISSION GAMMA PROGRAM

This appendix contains the computer program and a sample printout for prompt fission gamma radiation from  $U^{235}$  fissions. The program was written for the CDC 1604 high-speed digital computer at AFSWC.

```

COMMON T,PT,RATIO
DIMENSION D(130),W(130),C(130),AQ(130)
CALL FTHFON
T=-1./15762
RATIO=1.
CALL PRON
RATIO=PT
CONST=0.30125
ACC=.5
ACC1=1.-ACC
ACC2=1.-ACC*.5
ACC3=.5/ACC2
700 READ 3,TT
IF (EOF) 44,701
701 PRINT 1,TT
RSTART=TT*ACC2
DELRST=TT*ACC
XPQ7=0.0
DO 60 J=1,125
O(J)=0.0
W(J)=0.0
AQ(J)=0.
60 C(J)=0.0
K=0
IX=0
SUMF=0.0
SEL=0.0
SEDP=0.0
SUMI=0.0
SUMP=0.0
4 READ 3,E1,F2,EN
IX=IX+1
IF (EOF) 20,5
5 F=(E1+F2)*.5
SUMF=SUMF+F
A=E/.511
A11=1.0+A
A12=A11+A
A13=A12+A
A121=LOGF(A12)
SIG=0.49896*(A11/A/A*(1.0+1.0/A12-A121/A)+A121/(A+A)-A13/A12/A12)
SIGA=.49896*(2.*A11*A11/A/A/A12-A13/A12/A12-A11*(2.*A*(A-1.0)-1.0)
1/A/A/A12/A12-4.0*A*A/3.0/A12/A12/A12-(A11/A/A-0.5*0.5/A/A)/A*A121)
EHAR=E*SIG/SIG
IF (EHAR-2.4) 7,6,6
6 RHAR=.351*EHAR-.0702
GO TO 8
7 RHAR=.273*(EHAR*(1.265-.0954*LOGF(EHAR)))
8 SE=(CONST*SIG*EN
DELR=DFLRST
N=1
R=RSTART
SSD=0.0
SSL=0.0

```

```

EDP=0.0
EL=0.0
AL=F/.510984
COSTH=Y1.+AL)*SQRT(SIGA/(SIGA+AL+2.*SIG)/AL)
THETA=ACOS(COSTH)*57.2957795
ALPHA=PHAR+.5762
IF (SE) 17,17.9
9 T=(R/CNSTH-RBAR)/ALPHA
T1=T
CALL PRUP
PE=PT
TIO=EXP(-CONST*SIG*(R-T1))
SI=SE*PE*DELR*TIO
SD=SE*(1.-PE)*DELR*TIO
PXE=.5+PE
DELY=1.
IF (SL-Y.F-20) 10,10,11
10 RSTANT=HSTANT+ACC1
XPQ7=XPQ7+DELRST
DELRST=DELRST+ACC1
GO TO 500
11 T=T+DEIX
CALL PRUB
IF (PT-PXE) 12,13,14
12 T=T-DEIX
DELY=DELY+.5
IF (J.E=6-DELY) 11,11,13
13 RLBAR=(T-T1)*ALPHA
IF (RLBAR=.77) 14,15,15
14 B=EXP(-1.665-SQRT(1.6-.3814+.06F(RLBAR+.273)))/.1986)
GO TO 16
15 B=(RLBAR+.0702)/.351
16 XQ=SI*B
J=XINTF(R+10.)+1
Q(J)=Q(J)+1.
W(J)=W(J)+THETA
C(J)=C(J)+SL
J=XINTF(THETA+.5)+1
AO(J)=AO(J)+SL
EL=EL+YQ
FDP=EDP+SE*EBAR*DELR-XQ
SSL=SSI+SL
SSD=SSN+SD
500 R=R+ACC1
DELR=DELR+ACC1
IF (R-51.F=4) 2000,2000,9
2000 GO TO (2001,17) ,N
2001 N=2
R=R+ACC3
DELR=R+2.
GO TO 9
17 SUMI=SUMI+SSL
XPQ=SE*XPQ7
SSD=SSD+XPQ
EDP=FDP+XPQ*EBAR
SUMI=SUMI+SSD

```

```

SEDPP=SEDPP+EDP
SEL=SEL+EL
IF (IX-24) 19,18,18
18 PRINT 1,TT
IX=0
19 XXX=SUMPL/SUME
XXY=SUMU/SUME
PRINT 2,F1,E2,EL,SEL,EDP,SEDPP,SSL,XXX,SSD,XXY
GO TO 4
20 CONTINUE
PRINT 1,TT
DO 43 J=1,130
IF (C(J)) 43,43,39
39 K=K+1
FJ=J-1
X=FJ/10.
Y=X+.1
XX=(X+.05)+C(J)
40 Z=W(J)/U(J)
41 PRINT 500,X,Y,C(J),7,XX
IF (XMODF(K,25)) 43,42,43
42 PRINT 1,TT
43 CONTINUE
K=0
PRINT 1,TT
DO 50 J=1,50
IF (A0(J)) 50,50,51
51 K=K+1
X=J+2
Y=X-2.
PRINT 550,Y,X,A0(J)
IF (K-25) 50,50,52
52 K=0
PRINT 1,TT
50 CONTINUE
GO TO 700
44 CONTINUE
CALL TIMEOFF
500 FORMAT(10X,2F10.3,E13.3,F11.2,F13.3/)
550 FORMAT(10X,2F10.2,E13.3/)
600 FORMAT(1H1)
1 FORMAT(1H1,8X3HT=F7.3//)
2 FORMAT(2F8.3,8F12.3/)
3 FORMAT(2F5.0,F10.0)
END
SUBROUTINE PROB
COMMON T,PT,RATIO
LDA T
AJP M (1)
STA XX
LAC C2
STA SIGN
LDA XX
SIJ (4)
(1) LDA C2
STA SIGN

```

	IAC	T
	STA	XX
(4)	FMU	XX
	STA	X2
	LDA	XX
	FSB	C3
	AJP	M (2)
	IDA	C2
	FDV	X2
	STA	X22
	FMU	C4
	FSH	C5
	FMU	C6
	FMU	X22
	FAD	C5
	FMU	C7
	FMU	X22
	FSH	C5
	FMU	C8
	FMU	X22
	FAD	C5
	FMU	C9
	FMU	X22
	FSR	C5
	FMU	X22
	FAD	C5
	STA	ERF
	IAC	X2
	STA	X2
+	ENA	X2
+	RTJ	EXPF
+	RTJ	ERROR.
	FMU	C10
	FDV	XX
	FMU	ERF
	FAD	C5
	SLJ	(3)
(2)	IAC	X2
	FDV	D1
	FAD	D2
	FMU	X2
	FDV	D3
	FSB	D4
	FMU	D5
	FMU	X2
	FAD	D6
	FMU	X2
	FMU	D7
	FSB	D8
	FMU	X2
	FAD	D9
	FMU	C2
	FMU	X2
	FSR	C5
	FMU	X2
	FDV	C9

```

      FAD      C5
      FNU      XX
      FNU      D10
(3)   FNU      SIGN
      FAD      C2
      EDV      RATIO
      STA      PT
      RETURN
C2    DEC      .5
C3    DEC      1.447704
C4    DEC      11.
C5    DEC      1.
C6    DEC      9.
C7    DEC      7.
C8    DEC      5.
C9    DEC      3.
C10   DEC      -5641806
D1    DEC      105.
D2    DEC      .07692308
D3    DEC      6.
D4    DEC      .090909091
D5    DEC      .2
D6    DEC      .11111111
D7    DEC      .25
D8    DEC      .142857143
D9    DEC      .6
D10   DEC      1.1283792
SIGN  RSS      1
XX     RSS      1
X2     RSS      1
X22    RSS      1
FRF     RSS      1
EXPF    LIB     EXPF
      END
      SUBROUTINE TIMEON
+      FNA      00000      CLEAR ACCUMULATOR.
+      EXF      7 000110  TEST CHANNEL 1 FOR ACTIVE.
      STA      00000      CLEAR CLOCK CONTENTS TO ZERO.
+      EXF      010000  START CLOCK.
      RETURN
      END
      SUBROUTINE TIMEOFF
+      NOP
-      EXF      7 000110  DUMMY STATEMENT.
      EXF      020000  TEST CHANNEL 1 FOR ACTIVE.
      LDA      00000  STOP THE REAL-TIME CLOCK.
      STA      KLOCK  CLOCK CONTENTS TO ACCUMULATOR.
      TIME=DATE(KLOCK)/3600.0
      PRINT *,TIME
      RETURN
1      FORMAT(11H1RUN TIME =F9.2,9H MINUTES,/)
      END
      END
      END

```

T = 0.500									
	$\frac{R}{T}$	$\frac{E_R}{T}$	$\frac{R}{T}$	$\frac{E_R}{T}$	$\frac{R}{T}$	$\frac{E_R}{T}$	$\frac{R}{T}$	$\frac{E_R}{T}$	$\frac{R}{T}$
	(MeV)	(MeV)	(MeV)	(MeV)	(MeV)	(MeV)	(MeV)	(MeV)	(MeV)
7.00	1.50	3.2078	0.5	1.2078	0.05	1.7928	0.06	1.7928	0.06
7.06	7.00	1.5918	0.5	2.8778	0.05	2.8948	0.06	4.0498	0.06
7.20	7.40	3.2048	0.5	6.1018	0.05	6.1108	0.06	1.0708	0.05
7.06	7.20	3.9018	0.5	1.0008	0.04	7.4398	0.06	1.0218	0.05
6.80	7.00	3.3938	0.5	2.3098	0.04	6.0378	0.06	2.5038	0.05
6.60	6.80	2.9978	0.5	3.6098	0.04	6.2138	0.06	3.1298	0.05
6.40	6.60	3.1008	0.5	1.9908	0.04	6.9918	0.06	3.8248	0.05
6.20	6.40	3.9428	0.5	2.3008	0.04	6.1318	0.06	4.6378	0.05
6.00	6.20	5.8148	0.5	2.8008	0.04	1.3008	0.05	6.3048	0.05
5.80	6.00	7.7078	0.5	3.6008	0.04	1.9038	0.05	7.9908	0.05
5.60	5.80	1.1108	0.4	4.7098	0.04	2.9778	0.05	1.0908	0.04
5.40	5.60	1.3048	0.4	6.1208	0.04	3.7798	0.05	1.4798	0.04
5.20	5.40	1.5908	0.4	7.0008	0.04	4.9708	0.05	1.9338	0.04
5.00	5.20	1.6478	0.4	8.1028	0.04	4.5198	0.05	2.3098	0.04
4.80	5.00	1.2028	0.4	1.0418	0.03	4.2618	0.05	2.8118	0.04
4.60	4.80	1.7978	0.4	1.2418	0.03	6.3708	0.05	3.4008	0.04
4.40	4.60	2.7028	0.4	1.4418	0.03	1.238	0.04	4.4718	0.04
4.20	4.40	3.2108	0.4	1.8128	0.03	1.3098	0.04	5.7708	0.04
4.00	4.20	3.4938	0.4	2.1048	0.03	1.6928	0.04	7.4608	0.04
3.80	4.00	6.3208	0.4	2.6008	0.03	2.1198	0.04	9.5038	0.04
3.60	3.80	9.2028	0.4	3.1078	0.03	2.8048	0.04	1.2418	0.03
3.40	3.60	9.7308	0.4	3.7008	0.03	3.4218	0.04	1.5038	0.03
3.20	3.40	6.4508	0.4	4.3798	0.03	4.3808	0.04	2.8198	0.03





$E_L$ (Mev)	$E_u$ (Mev)	$S_e$ (se/ly)	$\theta_{AV}$ (deg.)	$E_{AV} S_e$ (Mev·Se/ly)
.00	.1	1.674E-003	40.32	8.371E-005
.10	.2	3.054E-003	36.99	4.581E-004
.20	.3	4.094E-003	34.37	1.024E-003
.30	.4	3.414E-003	32.86	1.195E-003
.40	.5	3.258E-003	31.23	1.466E-003
.50	.6	1.820E-003	28.80	1.001E-003
.60	.7	1.328E-003	29.29	8.631E-004
.70	.8	1.839E-003	27.99	1.379E-003
.80	.9	1.328E-003	26.71	1.128E-003
.90	1.0	8.912E-004	25.98	8.466E-004
1.00	1.1	4.214E-004	24.86	4.425E-004
1.10	1.2	8.462E-004	24.48	9.732E-004
1.20	1.3	8.299E-004	23.66	7.874E-004
1.30	1.4	4.104E-004	23.12	5.540E-004
1.40	1.5	1.893E-004	22.28	2.744E-004
1.50	1.6	3.589E-004	21.96	5.562E-004
1.60	1.7	3.290E-004	21.44	5.428E-004
1.70	1.8	9.881E-005	20.76	1.729E-004
1.80	1.9	1.732E-004	20.84	3.204E-004
1.90	2.0	1.811E-004	20.11	3.531E-004
2.00	2.1	1.890E-004	19.75	2.235E-004
2.10	2.2	5.829E-005	19.19	1.253E-004
2.20	2.3	1.100E-004	18.96	2.475E-004
2.30	2.4	7.989E-005	18.72	1.877E-004
2.40	2.5	5.652E-005	17.99	1.385E-004

$E_L$ (Mev)	$E_u$ (Mev)	$S_e$ (se/ly)	$\theta_{AV}$ (deg.)	$E_{AVSe}$ (Mev·Se/ly)
2.50	2.6	4.664E-005	18.16	1.189E-004
2.60	2.7	5.676E-005	17.66	1.504E-004
2.70	2.8	2.057E-005	17.46	5.657E-005
2.80	2.9	2.921E-005	16.99	8.325E-005
2.90	3.0	3.413E-005	16.88	1.007E-004
3.00	3.1	1.222E-005	16.69	3.728E-005
3.10	3.2	1.964E-005	16.28	6.188E-005
3.20	3.3	2.140E-005	16.13	6.957E-005
3.30	3.4	1.548E-005	15.98	5.186E-005
3.40	3.5	1.153E-005	15.39	3.980E-005
3.50	3.6	4.756E-006	15.65	3.463E-005
3.60	3.7	9.817E-006	15.34	3.583E-005
3.70	3.8	7.686E-006	14.92	2.882E-005
3.80	3.9	5.122E-006	15.03	1.972E-005
3.90	4.0	4.200E-006	14.79	1.659E-005
4.00	4.1	2.878E-006	14.70	1.166E-005
4.10	4.2	4.277E-006	14.30	1.775E-005
4.20	4.3	1.900E-006	14.45	8.077E-006
4.30	4.4	2.498E-006	14.21	1.087E-005
4.40	4.5	2.978E-006	13.84	1.325E-005
4.50	4.6	1.883E-006	13.97	8.567E-006
4.60	4.7	6.071E-007	13.83	2.823E-006
4.70	4.8	1.216E-006	13.55	5.776E-006
4.80	4.9	4.837E-007	13.59	2.346E-006
4.90	5.0	2.338E-007	13.41	1.157E-006

$E_L$ (Mev)	$E_u$ (Mev)	$S_e$ (se/ly)	$\theta_{AV}$ (deg.)	$E_{AVSe}$ (Mev Se/ly)
5.00	5.1	1.177E-006	12.05	5.945E-006
5.60	5.7	5.918E-007	12.05	3.344E-006
5.80	5.9	2.960E-007	12.05	1.732E-006
6.00	6.1	2.225E-007	12.05	1.346E-006
6.10	6.2	7.421E-008	12.05	4.564E-007

T=	0.500		
	$\theta_L$	$\theta_u$	Se
	(deg.)	(deg.)	(se/ly)
	12.00	14.00	2.362E-005
	14.00	16.00	1.643E-004
	16.00	18.00	3.749E-004
	18.00	20.00	9.564E-004
	20.00	22.00	1.438E-003
	22.00	24.00	2.923E-003
	24.00	26.00	3.054E-003
	26.00	28.00	1.685E-003
	28.00	30.00	3.747E-003
	30.00	32.00	2.594E-003
	32.00	34.00	2.614E-003
	34.00	36.00	2.272E-003
	36.00	38.00	2.373E-003
	40.00	42.00	1.953E-003
	42.00	44.00	8.961E-004
	44.00	46.00	7.688E-004

APPENDIX B

25-MEV ELECTRON PROGRAM

This appendix contains the computer program and a sample printout for 25-Mev electrons from a linear accelerator. The program was written for the CDC 1604 high-speed digital computer at AFSWC.

```

COMMON T,PT,RATIO
DIMENSION A(130),B(130),C(130),AQ(130)
DIMENSION YEL(130),YEDP(130),XSSL(130),XSSD(130)
CALL TIMEON
F00=22.
RHA25=.351*E00-.0702
ALPHA25=.5702*RHA25
ACC=.5
ACC1=1.-ACC
ACC2=1.-ACC*.5
ACC3=.5/ACC2
DELF1=.01
IXX=10
CONST=.30125
RATIO=1.
T=-1./5762
CALL PRON
RATIO=PI
1 READ 41,TT
IF(EOF) 40,2
2 DO 3 J=1,130
A(J)=0.
H(J)=0.
C(J)=0.
AQ(J)=0.
YEL(J)=0.
YEDP(J)=0.
XSSL(J)=0.
3 XSSD(J)=0.
KKK=0
SENSE=1 IGH 2
RSTART=T1*ACC2
DELF1=T1*ACC
R=RSTART
DELF=DELF1
4 FL=0.
KKK=KKK+1
DELF=DELF1
T=(T1-R-RHA25)/ALPHA25
CALL PRON
I1=1
PXE=I1*.5
DELY=10.
5 T=T+DELY
6 CALL PRON
DELY=DELY*.5
IF(I1-PXE) 7,8,5
7 T=T-DELY
IF(I1-P=0-DELY) 6,6,8
8 RHA=(T-I1)*ALPHA25
R0=(RHA+.0702)/.351
R0=1/N1F(E0,R00)
R02=R0*R0
TE0=1./R02

```

```

E2=E1*.7
FDP=1.
SSD=0.
SSI=1.
LAG=2/
LIP=LXY=1
SENSE=LIGHT 1
9 E1=E2
E2=E1-DELE
10 SIG12=.206*DELE*(TF0+1./E1/E2+1./E0-E1)/(E0-E2)
EBAR=(E1+E2)/2.
COSTH=1.0206*EBAR/SQRT(EBAR*(1.022+EBAR))
THETA=ACOS(COSTH)*.577795
IF(EBAR-.4) 12,11,11
11 RBAR=.321*EBAR-.0702
GO TO 13
12 RBAR=.273*(EBAR*(1.265-.0954*LOGF(EBAR)))
13 SE=CONST*SIG12*LFLP
ALPHA=RBAR*.5762
T=(1/COSTH-RBAR)/ALPHA
T1=T
CALL PRON
PF=0.1
PD=1.-PI
SD=SE*PD
SL=SE*PT
SSL=SSI+SL
SSD=SSD+SD
PXF=.5*PI
DELY=10.
IF(SI) 14,14,15
14 SI=0.
F=0.
A(1)=A(1)-1.
THETA=0.
GO TO 21
15 T=T+DEIX
16 CALL PRON
DELY=DELY*.5
IF(F-PXF) 17,18,15
17 T=T-DEIX
IF(1.F-0-DEIX) 16,16,18
18 RBAR=(T-T1)*ALPHA
IF(RBAR-.77) 19,20,20
19 F=EXP((1.265-SQRT(1.6-.3814*LOGF(RBAR/.273)))/.1908)
GO TO 21
20 F=(RBAR+.0702)/.351
21 F=1-IF(F,EBAR)
YU=1-F
XU/=(SE-EBAR-YU)
FL=FI+YU
FDP=FDP+YU7
K=1,50-XI:IF(EBAR*10.)
XFL(K)=XFL(K)+XU
XFD(K)=XFD(K)+XU7
XSL(K)=XSL(K)+SL

```



```

XSSD(K)=XSSD(K)+SD
J=XI*IF(TH*10.)+1
A(J)=A(J)+1.
R(J)=B(J)+THETA
C(J)=C(J)+SL
I=XI*IF(THETA*.5)+1
AQ(J)=AQ(J)+SL
IIP=IIP+1
IF(IIP-1>X) 25,22,22
22 IIP=0
LAG=LAG+1
IF(LAG-25) 24,24,23
23 LAG=0
PRINT 42,TT,E0,DELF,PKK,R
24 PRINT 43,E1,PE,F,X0,FL,X0Z,ENP,SL,SSL,SD,SSD
25 IF(1-F2) 9,9,26
26 DELF=DELF/10.
IF(01-F2) 9,9,27
27 DELF=DELF/100.
IF(00021-F2) 9,9,28
28 IF(SENSE LIGHT 1) 29,30
29 E1=F2
F2=.0001*5
DELF=E1-F2
GO TO 10
30 PRINT 43,E1,PE,F,X0,FL,X0Z,ENP,SL,SSL,SD,SSD
R=R+ACC1
DELF=DELF+ACC1
IF(1-5.E-4) 31,31,4
31 IF(SENSE LIGHT 2) 32,33
32 R=R+ACC5
DELF=R*2.
GO TO 4
33 PRINT 46,TT
SEDP=0.
SUMI=0.
SUML=0.
DO 35 J=1,130
IF(XSSL(J)+XSSD(J)) 36,36,34
34 FJ=131-J
I=L+1
E1=FJ/10.
E2=F1-.1
SEL=SEL+E1(J)
SEDP=SEDP+XEDP(J)
SUMI=SUMI+XSSL(J)
SUML=SUML+XSSD(J)
PRINT 44,E1,F2,XFL(J),SEL,XEDP(J),SEDP,XSSL(J),SUML,XSSD(J),QUMD
IF(I-25) 36,36,35
35 I=0
PRINT 40,TT
36 CONTINUE
I=0
PRINT 40,TT
DO 37 J=1,130

```

```

37      IF(A(J)) 39,39,37
        L=L+1
        FJ=J-1
        v=FJ/10.
        Y=X+.1
        XX=(Y+.05)*C(J)
        Z=R(J)/A(J)
        PRINT 45,X,Y,C(J),7,XX
        IF(I-25) 39,39,34
38      L=0
        PRINT 40,TT
39      CONTINUE
        I=0
        PRINT 46,TT
        DO 50 J=1,50
        IF(A(J)) 50,50,51
51      L=L+1
        Y=J*2
        Y=X-2.
        PRINT 52,Y,X,AQ(J)
        IF(I-25) 50,50,52
52      L=0
        PRINT 40,TT
50      CONTINUE
        GO TO 1
40      CALL TIMHOFF
41      FORMAT(F10.0)
42      FORMAT(1F1,10X3HT =F8.3,9H GM/CM2,5X4HEU =F9.4,5H MEV,5X6HDEIF =
1F7.4,6H MEV,,3X2HH(.12.2H)=E12.3,8H GM/CM2./2(1X/))
43      FORMAT(F8.3,F8.5,F8.3,A#12.3/)
44      FORMAT(2F7.2,8F12.3/)
45      FORMAT(10X,2F10.2,F13.3,F11.2,F13.3/)
46      FORMAT(1F1,10X,3HT =F8.4,9H G/CM2.////)
55      FORMAT(10X,2F10.2,F13.3/)
      END
      SUBROUTINE PROR
      COMMON T,PT,RATIO
        LDA      T
        AJP      M (1)
        STA      XX
        LAC      C2
        STA      SIGN
        LDA      XX
        ALJ      (4)
11)      LDA      C2
        STA      SIGN
        LAC      T
        STA      XX
14)      END      XX
        STA      X2
        LDA      XX
        FSH      C3
        AJP      M (2)
        LDA      C2
        FUV      X2
        STA      X22

```

	FPU	C4
	FSB	C5
	FPU	C6
	FPU	X22
	FAD	C5
	FPU	C7
	FPU	X22
	FSB	C5
	FPU	C8
	FPU	X22
	FAD	C5
	FPU	C9
	FPU	X22
	FSB	C5
	FPU	X22
	FAD	C5
	STA	ERF
	LAC	X2
	STA	X2
	FMA	X2
	FIJ	EXPF
	FIJ	ERHOK.
	FPU	C10
	FIV	XX
	FPU	ERF
	FPU	SIGN
	STA	ERF
	LDA	C2
	FAD	SIGN
	FAD	ERF
(2)	SIJ	(3)
	LAC	X2
	FIV	D1
	FAD	D2
	FPU	X2
	FIV	D3
	FSB	D4
	FPU	D5
	FPU	X2
	FAD	D6
	FPU	X2
	FPU	D7
	FSB	D8
	FPU	X2
	FAD	D9
	FPU	C2
	FPU	X2
	FSB	C5
	FPU	X2
	FIV	C9
	FAD	C5
	FPU	XX
	FPU	D10
	FPU	SIGN
	FAD	C2
(3)	FIV	RATIO

	STA	PT
	RETURN	
C2	DEC	.5
C3	DEC	1.647705
C4	DEC	11.
C5	DEC	1.
C6	DEC	9.
C7	DEC	7.
C8	DEC	5.
C9	DEC	3.
C10	DEC	-.5641896
D1	DEC	105.
D2	DEC	.07692308
D3	DEC	6.
D4	DEC	.090909091
D5	DEC	.2
D6	DEC	.11111111
D7	DEC	.25
D8	DEC	.142857143
D9	DEC	.6
D10	DEC	1.1283792
SIGN	HSS	1
XX	HSS	1
X2	HSS	1
Y22	HSS	1
FRF	HSS	1
EXPF	LIO	EXPF

END  
SUBROUTINE TIMEON

+	ENA	00000
=	EXF	7 00011R
	STA	00000
+	EXF	01000R

CLEAR ACCUMULATOR.  
TEST CHANNEL 1 FOR ACTIVE.  
CLEAR CLOCK CONTENTS TO ZERO.  
START CLOCK.

RETURN  
END

SUBROUTINE TIMEOFF

+	NDP	
=	EXF	7 00011R
	EXF	02000R
	IPA	00000
	STA	KLOCK

DUMMY STATEMENT.  
TEST CHANNEL 1 FOR ACTIVE.  
STOP THE REAL-TIME CLOCK.  
CLOCK CONTENTS TO ACCUMULATOR.  
CLOCK CONTENTS TO \*KLOCK\*.

TIME=FLOAT(KLOCK)/3600.

PRINT 1,TIME

RETURN

1	FORMAT(11H1RUN TIME =F9.2,9H MINUTES,//)
	END

END

END

T = .7500 GM/CM <sup>2</sup> .											
E <sub>0</sub> (MeV)	E <sub>L</sub> (MeV)	R Z E <sub>0</sub> (MeV)	ER Z E <sub>0</sub> (MeV)	R Z E <sub>0</sub> (MeV)	ER Z E <sub>0</sub> (MeV)	R Z E <sub>0</sub> (MeV)	ER Z E <sub>0</sub> (MeV)	R Z E <sub>0</sub> (MeV)	ER Z E <sub>0</sub> (MeV)	R Z E <sub>0</sub> (MeV)	ER Z E <sub>0</sub> (MeV)
12.20	12.20	4.574E-04	4.574E-04	7.110E-05	7.110E-05	4.203E-05	4.263E-05	4.000E-07	4.000E-07	4.000E-07	4.000E-07
12.40	12.40	4.520E-04	4.520E-04	7.113E-05	7.113E-05	4.264E-05	4.264E-05	4.120E-07	4.120E-07	4.120E-07	4.120E-07
12.60	12.60	4.408E-04	4.408E-04	7.122E-05	7.122E-05	4.267E-05	4.267E-05	4.170E-07	4.170E-07	4.170E-07	4.170E-07
12.80	12.80	4.290E-04	4.290E-04	7.399E-05	7.399E-05	4.727E-05	4.727E-05	4.475E-07	4.475E-07	4.475E-07	4.475E-07
13.00	13.00	4.164E-04	4.164E-04	8.875E-05	8.875E-05	6.556E-05	6.556E-05	5.905E-07	5.905E-07	5.905E-07	5.905E-07
13.20	13.20	4.040E-04	4.040E-04	8.903E-05	8.903E-05	6.801E-05	6.801E-05	5.604E-07	5.604E-07	5.604E-07	5.604E-07
13.40	13.40	3.914E-04	3.914E-04	9.304E-05	9.304E-05	7.076E-05	7.076E-05	6.027E-07	6.027E-07	6.027E-07	6.027E-07
13.60	13.60	3.788E-04	3.788E-04	9.535E-05	9.535E-05	7.406E-05	7.406E-05	6.161E-07	6.161E-07	6.161E-07	6.161E-07
13.80	13.80	3.662E-04	3.662E-04	9.944E-05	9.944E-05	8.097E-05	8.097E-05	6.284E-07	6.284E-07	6.284E-07	6.284E-07
14.00	14.00	3.536E-04	3.536E-04	9.574E-05	9.574E-05	8.430E-05	8.430E-05	6.547E-07	6.547E-07	6.547E-07	6.547E-07
14.20	14.20	3.410E-04	3.410E-04	9.612E-05	9.612E-05	8.745E-05	8.745E-05	6.464E-07	6.464E-07	6.464E-07	6.464E-07
14.40	14.40	3.284E-04	3.284E-04	9.653E-05	9.653E-05	9.067E-05	9.067E-05	6.592E-07	6.592E-07	6.592E-07	6.592E-07
14.60	14.60	3.158E-04	3.158E-04	9.696E-05	9.696E-05	9.397E-05	9.397E-05	6.666E-07	6.666E-07	6.666E-07	6.666E-07
14.80	14.80	3.032E-04	3.032E-04	9.740E-05	9.740E-05	9.720E-05	9.720E-05	6.775E-07	6.775E-07	6.775E-07	6.775E-07
15.00	15.00	2.906E-04	2.906E-04	9.811E-05	9.811E-05	1.010E-05	1.010E-05	6.869E-07	6.869E-07	6.869E-07	6.869E-07
15.20	15.20	2.780E-04	2.780E-04	9.898E-05	9.898E-05	1.027E-05	1.027E-05	7.010E-07	7.010E-07	7.010E-07	7.010E-07
15.40	15.40	2.654E-04	2.654E-04	9.924E-05	9.924E-05	1.026E-05	1.026E-05	7.137E-07	7.137E-07	7.137E-07	7.137E-07
15.60	15.60	2.528E-04	2.528E-04	9.995E-05	9.995E-05	1.026E-05	1.026E-05	7.271E-07	7.271E-07	7.271E-07	7.271E-07
15.80	15.80	2.402E-04	2.402E-04	1.003E-04	1.003E-04	9.933E-05	9.933E-05	7.412E-07	7.412E-07	7.412E-07	7.412E-07
16.00	16.00	2.276E-04	2.276E-04	1.013E-04	1.013E-04	9.409E-05	9.409E-05	7.561E-07	7.561E-07	7.561E-07	7.561E-07
16.20	16.20	2.150E-04	2.150E-04	1.021E-04	1.021E-04	9.469E-05	9.469E-05	7.670E-07	7.670E-07	7.670E-07	7.670E-07
16.40	16.40	2.024E-04	2.024E-04	1.029E-04	1.029E-04	9.533E-05	9.533E-05	7.802E-07	7.802E-07	7.802E-07	7.802E-07
16.60	16.60	1.898E-04	1.898E-04	1.038E-04	1.038E-04	9.601E-05	9.601E-05	8.055E-07	8.055E-07	8.055E-07	8.055E-07
16.80	16.80	1.772E-04	1.772E-04	1.047E-04	1.047E-04	9.673E-05	9.673E-05	8.237E-07	8.237E-07	8.237E-07	8.237E-07
17.00	17.00	1.646E-04	1.646E-04	1.057E-04	1.057E-04	9.750E-05	9.750E-05	8.429E-07	8.429E-07	8.429E-07	8.429E-07
17.20	17.20	1.520E-04	1.520E-04	1.067E-04	1.067E-04	9.831E-05	9.831E-05	8.632E-07	8.632E-07	8.632E-07	8.632E-07

T O .75. GP/CH2.

9.20	9.00	8.572E-004	2.197E-002	1.070E-004	2.961E-003	9.916E-005	2.293E-003	8.849E-007	1.004E-005
9.00	8.549E-004	2.203E-002	1.009E-004	2.670E-003	1.001E-004	2.393E-003	9.070E-007	1.095E-005	
9.50	9.00	8.520E-004	2.308E-002	1.101E-004	2.780E-003	1.010E-004	2.494E-003	9.306E-007	1.008E-005
9.40	9.30	8.91E-004	2.453E-002	1.114E-004	2.892E-003	1.020E-004	2.596E-003	9.596E-007	2.004E-005
9.30	9.20	8.993E-004	2.538E-002	1.127E-004	3.004E-003	1.031E-004	2.699E-003	9.820E-007	2.102E-005
9.20	9.10	8.479E-004	2.623E-002	1.141E-004	3.119E-003	1.042E-004	2.763E-003	1.010E-006	2.203E-005
9.10	9.00	8.467E-004	2.708E-002	1.155E-004	3.234E-003	1.053E-004	2.866E-003	1.039E-006	2.307E-005
9.00	8.90	8.458E-004	2.792E-002	1.170E-004	3.351E-003	1.066E-004	2.975E-003	1.070E-006	2.404E-005
8.90	8.80	8.450E-004	2.877E-002	1.186E-004	3.470E-003	1.078E-004	3.083E-003	1.103E-006	2.504E-005
8.80	8.70	8.445E-004	2.961E-002	1.203E-004	3.590E-003	1.092E-004	3.192E-003	1.136E-006	2.618E-005
8.70	8.60	8.441E-004	3.046E-002	1.220E-004	3.712E-003	1.106E-004	3.302E-003	1.174E-006	2.835E-005
8.60	8.50	8.440E-004	3.135E-002	1.236E-004	3.836E-003	1.120E-004	3.419E-003	1.213E-006	2.957E-005
8.50	8.40	8.441E-004	3.224E-002	1.257E-004	3.962E-003	1.136E-004	3.528E-003	1.254E-006	3.082E-005
8.40	8.30	8.445E-004	3.309E-002	1.277E-004	4.089E-003	1.152E-004	3.643E-003	1.297E-006	3.212E-005
8.30	8.20	8.450E-004	3.393E-002	1.296E-004	4.219E-003	1.169E-004	3.760E-003	1.342E-006	3.346E-005
8.20	8.10	8.458E-004	3.480E-002	1.320E-004	4.351E-003	1.186E-004	3.879E-003	1.390E-006	3.489E-005
8.10	8.00	8.467E-004	3.562E-002	1.342E-004	4.482E-003	1.205E-004	3.999E-003	1.441E-006	3.629E-005
8.00	7.90	8.479E-004	3.637E-002	1.366E-004	4.622E-003	1.224E-004	4.122E-003	1.495E-006	3.776E-005
7.90	7.80	8.493E-004	3.722E-002	1.391E-004	4.761E-003	1.244E-004	4.246E-003	1.553E-006	3.934E-005
7.80	7.70	8.510E-004	3.807E-002	1.417E-004	4.903E-003	1.265E-004	4.373E-003	1.614E-006	4.095E-005
7.70	7.60	8.520E-004	3.893E-002	1.444E-004	5.047E-003	1.287E-004	4.501E-003	1.679E-006	4.263E-005
7.60	7.50	8.549E-004	3.978E-002	1.472E-004	5.194E-003	1.311E-004	4.632E-003	1.749E-006	4.436E-005
7.50	7.40	8.572E-004	4.064E-002	1.502E-004	5.345E-003	1.335E-004	4.766E-003	1.823E-006	4.621E-005
7.40	7.30	8.597E-004	4.150E-002	1.534E-004	5.498E-003	1.360E-004	4.902E-003	1.903E-006	4.811E-005
7.30	7.20	8.624E-004	4.236E-002	1.566E-004	5.654E-003	1.386E-004	5.041E-003	1.988E-006	5.009E-005
7.20	7.10	8.654E-004	4.323E-002	1.601E-004	5.813E-003	1.414E-004	5.182E-003	2.079E-006	5.217E-005

T 0 .7500 8/CM2.

7.00	7.60	8.000E-006	4.409E-002	1.037E-004	5.970E-003	1.443E-004	5.320E-003	2.177E-006	5.435E-005
7.00	8.90	8.720E-004	4.407E-002	1.074E-004	6.140E-003	1.474E-004	5.474E-003	2.203E-006	5.603E-005
8.00	8.00	8.750E-004	4.904E-002	1.719E-004	6.317E-003	1.505E-004	5.624E-003	2.394E-006	5.903E-005
8.00	8.70	8.795E-004	4.672E-002	1.759E-004	6.493E-003	1.539E-004	5.770E-003	2.517E-006	6.155E-005
6.70	8.00	8.037E-004	4.708E-002	1.799E-004	6.672E-003	1.574E-004	5.939E-003	2.640E-006	6.419E-005
6.00	8.90	8.080E-004	4.809E-002	1.845E-004	6.857E-003	1.611E-004	6.097E-003	2.790E-006	6.499E-005
6.50	8.00	8.927E-004	4.939E-002	1.893E-004	7.040E-003	1.649E-004	6.261E-003	2.943E-006	6.993E-005
6.00	8.30	8.975E-004	5.128E-002	1.944E-004	7.241E-003	1.690E-004	6.430E-003	3.109E-006	7.304E-005
6.50	8.20	9.120E-004	5.119E-002	1.997E-004	7.440E-003	1.732E-004	6.604E-003	3.280E-006	7.633E-005
6.00	8.10	9.100E-004	5.209E-002	2.054E-004	7.646E-003	1.777E-004	6.781E-003	3.464E-006	7.981E-005
6.20	8.00	9.120E-004	5.318E-002	2.113E-004	7.857E-003	1.824E-004	6.964E-003	3.696E-006	8.351E-005
6.00	5.90	9.195E-004	5.393E-002	2.170E-004	8.075E-003	1.873E-004	7.151E-003	3.927E-006	8.743E-005
5.90	5.80	9.290E-004	5.489E-002	2.242E-004	8.299E-003	1.929E-004	7.343E-003	4.179E-006	9.101E-005
5.80	5.70	9.300E-004	5.578E-002	2.312E-004	8.530E-003	1.980E-004	7.541E-003	4.455E-006	9.407E-005
5.70	5.60	9.387E-004	5.672E-002	2.389E-004	8.769E-003	2.036E-004	7.745E-003	4.757E-006	9.608E-005
5.60	5.50	9.459E-004	5.767E-002	2.464E-004	9.015E-003	2.095E-004	7.959E-003	5.089E-006	9.896E-005
5.50	5.40	9.529E-004	5.862E-002	2.540E-004	9.270E-003	2.163E-004	8.171E-003	5.454E-006	1.014E-004
5.40	5.30	9.600E-004	5.958E-002	2.634E-004	9.533E-003	2.233E-004	8.394E-003	5.856E-006	1.042E-004
5.30	5.20	9.680E-004	6.059E-002	2.727E-004	9.806E-003	2.312E-004	8.629E-003	6.301E-006	1.079E-004
5.20	5.10	9.760E-004	6.153E-002	2.826E-004	1.009E-003	2.378E-004	8.862E-003	6.793E-006	1.103E-004
5.10	5.00	9.843E-004	6.251E-002	2.931E-004	1.030E-003	2.450E-004	9.100E-003	7.339E-006	1.137E-004
5.00	4.90	9.929E-004	6.353E-002	3.043E-004	1.060E-003	2.543E-004	9.363E-003	7.947E-006	1.156E-004
4.90	4.80	1.002E-003	6.456E-002	3.163E-004	1.100E-003	2.633E-004	9.620E-003	8.626E-006	1.154E-004
4.80	4.70	1.011E-003	6.552E-002	3.290E-004	1.133E-003	2.729E-004	9.899E-003	9.386E-006	1.036E-004
4.70	4.60	1.020E-003	6.650E-002	3.420E-004	1.167E-003	2.831E-004	1.010E-003	1.024E-005	1.739E-004
4.60	4.50	1.030E-003	6.757E-002	3.571E-004	1.203E-003	2.939E-004	1.040E-003	1.120E-005	1.851E-004

7 0 7500 640002.

4.30	4.40	1.00E-002	6.00E-002	3.727E-004	1.244E-002	0.954E-004	1.070E-002	1.220E-005	1.973E-004
4.40	4.30	1.050E-003	6.00E-002	3.894E-004	1.279E-002	3.174E-004	1.110E-002	1.351E-005	2.110E-004
4.30	4.20	1.00E-003	7.738E-002	4.074E-004	1.320E-002	3.307E-004	1.143E-002	1.490E-005	2.257E-004
4.20	4.10	1.73E-003	7.179E-002	4.207E-004	1.363E-002	3.440E-004	1.177E-002	1.649E-005	2.422E-004
4.10	4.00	1.81E-003	7.207E-002	4.475E-004	1.407E-002	3.595E-004	1.213E-002	1.832E-005	2.600E-004
4.00	3.90	1.03E-003	7.394E-002	4.802E-004	1.454E-002	3.754E-004	1.251E-002	2.041E-005	2.811E-004
3.90	3.80	1.15E-003	7.508E-002	4.927E-004	1.503E-002	3.924E-004	1.290E-002	2.284E-005	3.030E-004
3.80	3.70	1.10E-003	7.610E-002	5.177E-004	1.552E-002	4.100E-004	1.331E-002	2.565E-005	3.295E-004
3.70	3.60	1.12E-003	7.731E-002	5.465E-004	1.610E-002	4.301E-004	1.374E-002	2.893E-005	3.584E-004
3.60	3.50	1.339E-003	7.845E-002	5.760E-004	1.667E-002	4.510E-004	1.419E-002	3.270E-005	3.912E-004
3.50	3.40	1.25E-003	7.900E-002	6.101E-004	1.720E-002	4.734E-004	1.467E-002	3.731E-005	4.269E-004
3.40	3.30	1.01E-003	8.070E-002	6.464E-004	1.793E-002	4.975E-004	1.516E-002	4.267E-005	4.711E-004
3.30	3.20	1.72E-003	8.103E-002	6.896E-004	1.862E-002	5.233E-004	1.569E-002	4.905E-005	5.202E-004
3.20	3.10	1.04E-003	8.311E-002	7.270E-004	1.934E-002	5.510E-004	1.624E-002	5.670E-005	5.769E-004
3.10	3.00	1.04E-003	8.431E-002	7.755E-004	2.012E-002	5.807E-004	1.682E-002	6.590E-005	6.420E-004
3.00	2.90	1.03E-003	8.551E-002	8.261E-004	2.095E-002	6.125E-004	1.743E-002	7.710E-005	7.199E-004
2.90	2.80	1.212E-003	8.672E-002	8.897E-004	2.183E-002	6.464E-004	1.808E-002	9.000E-005	8.105E-004
2.80	2.70	1.220E-003	8.794E-002	9.491E-004	2.270E-002	6.826E-004	1.876E-002	1.074E-004	9.179E-004
2.70	2.60	1.220E-003	8.917E-002	1.021E-003	2.360E-002	7.209E-004	1.948E-002	1.280E-004	1.40E-003
2.60	2.50	1.231E-003	9.048E-002	1.099E-003	2.450E-002	7.614E-004	2.024E-002	1.537E-004	1.711E-003
2.50	2.40	1.233E-003	9.183E-002	1.180E-003	2.540E-002	8.037E-004	2.105E-002	1.857E-004	1.985E-003
2.40	2.30	1.222E-003	9.285E-002	1.260E-003	2.730E-002	8.447E-004	2.189E-002	2.280E-004	2.614E-003
2.30	2.20	1.410E-003	9.407E-002	1.400E-003	2.870E-002	8.887E-004	2.270E-002	2.805E-004	1.695E-003
2.20	2.10	1.410E-003	9.528E-002	1.533E-003	3.032E-002	9.324E-004	2.371E-002	3.400E-004	2.241E-003
2.10	2.00	1.09E-003	9.640E-002	1.674E-003	3.210E-002	9.750E-004	2.489E-002	4.293E-004	2.670E-003
2.00	1.90	1.03E-003	9.760E-002	1.832E-003	3.304E-002	1.015E-003	2.570E-002	5.349E-004	3.205E-003



T = .7905 gm/cm <sup>2</sup> .											
1.90	1.80	8.164E-003	9.003E-002	2.009E-003	3.904E-002	1.052E-003	2.679E-002	6.001E-004	3.073E-003		
1.80	1.70	1.143E-003	9.997E-002	2.208E-003	3.809E-002	1.089E-003	2.784E-002	8.340E-004	4.797E-003		
1.70	1.60	1.139E-003	1.138E-003	2.431E-003	4.040E-002	1.118E-003	2.894E-002	1.040E-003	5.748E-003		
1.60	1.50	1.095E-003	1.122E-003	2.008E-003	4.314E-002	1.152E-003	3.011E-002	1.201E-003	7.339E-003		
1.50	1.40	8.072E-003	1.133E-003	2.901E-003	4.612E-002	1.196E-003	3.131E-002	1.994E-003	8.633E-003		
1.40	1.30	1.040E-003	1.143E-003	3.279E-003	4.940E-002	1.259E-003	3.296E-002	1.962E-003	1.161E-002		
1.30	1.20	1.108E-003	1.153E-003	3.692E-003	5.309E-002	1.322E-003	3.388E-002	2.429E-003	1.302E-002		
1.20	1.10	9.020E-004	1.163E-003	4.091E-003	5.714E-002	1.387E-003	3.527E-002	3.045E-003	1.607E-002		
1.10	1.00	9.390E-004	1.172E-003	4.619E-003	6.170E-002	1.439E-003	3.671E-002	3.879E-003	1.997E-002		
1.00	.90	8.947E-004	1.181E-003	5.249E-003	6.700E-002	1.490E-003	3.820E-002	5.110E-003	2.496E-002		
.90	.80	8.575E-004	1.190E-003	6.011E-003	7.315E-002	1.576E-003	3.977E-002	6.952E-003	3.151E-002		
.80	.70	7.962E-004	1.198E-003	6.903E-003	7.999E-002	1.680E-003	4.149E-002	8.777E-003	4.629E-002		
.70	.60	7.280E-004	1.109E-003	8.255E-003	8.829E-002	1.747E-003	4.320E-002	1.221E-002	5.250E-002		
.60	.50	6.904E-004	1.112E-003	9.974E-003	9.422E-002	1.848E-003	4.505E-002	1.773E-002	7.233E-002		
.50	.40	5.720E-004	1.117E-003	1.240E-002	1.117E-003	1.956E-003	4.701E-002	2.749E-002	9.772E-002		
.40	.30	4.720E-004	1.122E-003	1.630E-002	1.270E-003	2.160E-003	4.907E-002	4.726E-002	1.457E-001		
.30	.20	3.911E-004	1.126E-003	2.349E-002	1.909E-003	2.609E-003	5.119E-002	9.750E-002	2.425E-001		
.20	.10	2.79E-004	1.128E-003	4.116E-002	1.916E-003	2.092E-003	5.329E-002	3.047E-001	5.472E-001		
.10	.00	8.474E-005	1.129E-003	3.74E-001	5.623E-003	1.392E-003	5.404E-002	3.409E-002	1.515E-002		

T = .7500 GM/CM2.

$E_L$ (Mev)	$E_u$ (Mev)	$S_e$ (se/ie)	$\theta_{AV}$ (deg.)	$E_{AV} S_e$ (Mev se/ie)
.00	.1	2.685E-003	71.16	1.343E-004
.10	.2	3.761E-003	56.24	5.641E-004
.20	.3	3.606E-003	54.33	9.016E-004
.30	.4	3.315E-003	50.92	1.160E-003
.40	.5	3.001E-003	49.50	1.350E-003
.50	.6	2.668E-003	47.70	1.467E-003
.60	.7	2.342E-003	46.01	1.522E-003
.70	.8	2.092E-003	44.49	1.569E-003
.80	.9	1.876E-003	42.96	1.594E-003
.90	1.0	1.664E-003	41.80	1.580E-003
1.00	1.1	1.467E-003	40.46	1.540E-003
1.10	1.2	1.356E-003	39.38	1.560E-003
1.20	1.3	1.248E-003	38.29	1.560E-003
1.30	1.4	1.121E-003	37.36	1.514E-003
1.40	1.5	1.036E-003	36.43	1.502E-003
1.50	1.6	9.203E-004	35.62	1.426E-003
1.60	1.7	8.811E-004	34.77	1.454E-003
1.70	1.8	8.008E-004	34.06	1.401E-003
1.80	1.9	7.699E-004	33.29	1.424E-003
1.90	2.0	7.014E-004	32.61	1.368E-003
2.00	2.1	6.406E-004	32.03	1.313E-003
2.10	2.2	5.996E-004	31.41	1.289E-003
2.20	2.3	5.942E-004	30.78	1.337E-003
2.30	2.4	5.711E-004	30.20	1.342E-003
2.40	2.5	5.279E-004	29.74	1.293E-003
2.50	2.6	4.812E-004	29.20	1.227E-003

T = .750 GM/CM2.

2.60	2.7	4.449E-004	28.75	1.179E-003
2.70	2.8	4.270E-004	28.27	1.174E-003
2.80	2.9	4.279E-004	27.77	1.219E-003
2.90	3.0	3.928E-004	27.37	1.159E-003
3.00	3.1	3.715E-004	26.96	1.133E-003
3.10	3.2	3.565E-004	26.56	1.123E-003
3.20	3.3	3.338E-004	26.20	1.085E-003
3.30	3.4	3.226E-004	25.81	1.081E-003
3.40	3.5	3.154E-004	25.45	1.088E-003
3.50	3.6	3.027E-004	25.10	1.075E-003
3.60	3.7	2.798E-004	24.79	1.021E-003
3.70	3.8	2.802E-004	24.43	1.051E-003
3.80	3.9	2.675E-004	24.11	1.030E-003
3.90	4.0	2.534E-004	23.81	1.001E-003
4.00	4.1	2.475E-004	23.50	1.002E-003
4.10	4.2	2.429E-004	23.21	1.008E-003
4.20	4.3	2.348E-004	22.92	9.979E-004
4.30	4.4	2.272E-004	22.64	9.882E-004
4.40	4.5	2.198E-004	22.37	9.779E-004
4.50	4.6	2.132E-004	22.11	9.702E-004
4.60	4.7	2.059E-004	21.85	9.576E-004
4.70	4.8	1.955E-004	21.62	9.288E-004
4.80	4.9	1.952E-004	21.36	9.467E-004
4.90	5.0	1.869E-004	21.13	9.253E-004
5.00	5.1	1.832E-004	20.89	9.252E-004
5.10	5.2	1.723E-004	20.69	8.875E-004

T = .7500 GM/CM2.

5.20	5.3	1.750E-004	20.44	9.187E-004
5.30	5.4	1.709E-004	20.23	9.145E-004
5.40	5.5	1.667E-004	20.01	9.087E-004
5.50	5.6	1.585E-004	19.81	8.797E-004
5.60	5.7	1.590E-004	19.60	8.985E-004
5.70	5.8	1.554E-004	19.40	8.935E-004
5.80	5.9	1.497E-004	19.21	8.760E-004
5.90	6.0	1.487E-004	19.01	8.848E-004
6.00	6.1	1.456E-004	18.82	8.807E-004
6.10	6.2	1.426E-004	18.64	8.768E-004
6.20	6.3	1.397E-004	18.45	8.732E-004
6.30	6.4	1.310E-004	18.29	8.320E-004
6.40	6.5	1.305E-004	18.11	8.417E-004
6.50	6.6	1.321E-004	17.93	8.651E-004
6.60	6.7	1.287E-004	17.76	8.561E-004
6.70	6.8	1.275E-004	17.59	8.603E-004
6.80	6.9	1.235E-004	17.43	8.461E-004
6.90	7.0	1.232E-004	17.27	8.565E-004
7.00	7.1	1.213E-004	17.11	8.549E-004
7.10	7.2	1.194E-004	16.95	8.535E-004
7.20	7.3	1.176E-004	16.80	8.523E-004
7.30	7.4	1.156E-004	16.65	8.498E-004
7.40	7.5	1.112E-004	16.51	8.288E-004
7.50	7.6	1.076E-004	16.37	8.123E-004
7.60	7.7	1.112E-004	16.21	8.507E-004
7.70	7.8	1.098E-004	16.07	8.507E-004

T = .7500 GM/CM<sup>2</sup>.

7.80	7.9	1.084E-004	15.93	8.509E-004
7.90	8.0	1.056E-004	15.79	8.396E-004
8.00	8.1	1.059E-004	15.65	8.521E-004
8.10	8.2	1.047E-004	15.52	8.530E-004
8.20	8.3	1.035E-004	15.38	8.541E-004
8.30	8.4	1.024E-004	15.25	8.554E-004
8.40	8.5	1.003E-004	15.12	8.479E-004
8.50	8.6	9.788E-005	15.00	8.369E-004
8.60	8.7	9.956E-005	14.87	8.612E-004
8.70	8.8	9.868E-005	14.75	8.635E-004
8.80	8.9	9.353E-005	14.64	8.260E-004
8.90	9.0	9.709E-005	14.50	8.690E-004
9.00	9.1	9.635E-005	14.38	8.719E-004
9.10	9.2	9.565E-005	14.26	8.752E-004
9.20	9.3	9.499E-005	14.15	8.786E-004
9.30	9.4	9.437E-005	14.03	8.824E-004
9.40	9.5	9.379E-005	13.92	8.864E-004
9.50	9.6	9.309E-005	13.80	8.890E-004
9.60	9.7	9.151E-005	13.69	8.831E-004
9.70	9.8	8.994E-005	13.59	8.770E-004
9.80	9.9	9.189E-005	13.47	9.051E-004
9.90	10.0	9.150E-005	13.36	9.104E-004
10.00	10.1	9.115E-005	13.26	9.160E-004
10.10	10.2	8.654E-005	13.16	8.784E-004
10.20	10.3	9.055E-005	13.04	9.282E-004
10.30	10.4	9.030E-005	12.94	9.346E-004

T = .7500 GM/CM2.

10.40	10.5	8.947E-005	12.84	9.350E-004
10.50	10.6	8.991E-005	12.73	9.485E-004
10.60	10.7	8.945E-005	12.63	9.527E-004
10.70	10.8	7.685E-005	12.57	8.262E-004
10.80	10.9	4.464E-005	12.55	4.843E-004
10.90	11.0	4.685E-005	12.45	5.130E-004
11.00	11.1	4.679E-005	12.35	5.171E-004
11.10	11.2	4.220E-005	12.26	4.705E-004
11.20	11.3	2.394E-005	12.21	2.693E-004
11.30	11.4	2.038E-005	12.12	2.313E-004
11.40	11.50	1.030E-005	12.05	1.180E-004
11.50	11.6	1.638E-006	12.00	1.892E-005

T = .7500 GR/CM2.

$\theta_L$ (deg/)	$\theta_u$ (deg.)	$S_e$ (se/le)
10.00	12.00	4.480E-004
12.00	14.00	1.795E-003
14.00	16.00	1.717E-003
16.00	18.00	1.745E-003
18.00	20.00	1.857E-003
20.00	22.00	1.984E-003
22.00	24.00	2.158E-003
24.00	26.00	2.317E-003
26.00	28.00	2.545E-003
28.00	30.00	2.695E-003
30.00	32.00	2.804E-003
32.00	34.00	2.737E-003
34.00	36.00	2.710E-003
36.00	38.00	2.481E-003
38.00	40.00	2.311E-003
40.00	42.00	2.171E-003
42.00	44.00	2.089E-003
44.00	46.00	1.924E-003
46.00	48.00	1.765E-003
48.00	50.00	1.700E-003
50.00	52.00	1.495E-003
52.00	54.00	1.433E-003
54.00	56.00	1.342E-003
56.00	58.00	1.223E-003
58.00	60.00	1.103E-003
60.00	62.00	1.029E-003

T = .7500 G/CM<sup>2</sup>.

62.00	64.00	8.890E-004
64.00	66.00	8.250E-004
66.00	68.00	7.161E-004
68.00	70.00	6.426E-004
70.00	72.00	5.740E-004
72.00	74.00	4.631E-004
74.00	76.00	3.708E-004
76.00	78.00	2.963E-004
78.00	80.00	2.339E-004
80.00	82.00	4.785E-005
82.00	84.00	2.347E-013
84.00	86.00	1.266E-224



TDR-63-50

## APPENDIX C

### 600-KV X-RAY PROGRAM

This appendix contains the computer program and a sample printout for 600-kv X-rays from a pulsed X-ray source. The program was written for the CDC 1604 high-speed digital computer at AFSWC.

```

COMMON T,PT,RATIO
DIMENSION O(130),W(130),C(130),AO(130)
CALL TIMEON
T=-1./5762
RATIO=1.
CALL PRON
RATIO=PT
CONST=0.30125
ACC=.5
ACC1=1.-ACC
ACC2=1.-ACC*.5
ACC3=.5/ACC2
700 READ 3,TT
IF (EOF) 44,701
701 PRINT 1,TT
RSTAR1=TT*ACC2
DELR1=TT*ACC
XP07=0.0
DO 60 I=1,125
O(I)=0.0
W(I)=0.0
AO(I)=0.
60 C(I)=0.0
K=0
IX=0
SUMF=0.0
SEL=0.0
SEOP=0.0
SUMI=0.0
SUMT=0.0
4 READ 3,F1,F2,EN
IX=IX+1
IF (EOF) 20,5
5 F=(F1+F2)*.5
SUMF=SUMF+F
A=E/.711
A11=1.0+A
A12=A11+A
A13=A12+A
A12I=LOGF(A12)
SIG=.49896*(A11/A/A+(1.0+1.0/A12-A12I/A)+A12I/(A+A)-A13/A12/A12)
SIGA=.49896*(2.*A11+A11/A/A/A12-A13/A12/A12-A11*(2.*A*(A-1.0)-1.0)
1/A/A/A12/A12-4.0*A/A/3.0/A12/A12/A12-(A11/A/A-0.5+0.5/A/A)/A*A12I)
EHAR=F*SIG/SIG
IF (EHAR-2.4) 7,6,6
6 RHAR=.391*EHAR-.0702
GO TO 8
7 RHAR=.2/A*(EHAR*(1.265-.0954*LOGF(EHAR)))
8 SF=CONST*SIG*EN
DELE=DELE+SI
N=N+1
N=NSTART
SSD=0.0
SSE=0.0

```

```

ENDP=0.0
EL=0.0
AL=F/.51(984
COSTH=11.+AL)*SQRTF(SIGA/(SIGA*AL+2.*SIG)/AL)
THETA=ACOS(COSTH)*57.2957795
ALPHA=PHAR*.5762
IF(SF) 17,17.9
9 T=(H/COSTH-RBAR)/ALPHA
T1=T
CALL PRUH
PE=PT
TIO=EXP(CONST*SIG*(P-T1))
SI=SF*PE*DELR*TIO
SD=SF*(1.-PE)*DELR*TIO
PXE=.5+PE
DELY=1.
IF(SL-1.F-20) 10,10.11
10 RSTANT=HSTANT*ACC1-
XPQ7=XPQ7+DELRST
DELR=DELRST*ACC1
GO TO 500
11 T=T+DEIX
CALL PRUP
IF(PT-PXE) 12,13,14
12 T=T-DEIX
DELY=DELY*.5
IF(1.E-6-DELY) 11,11.13
13 RLBAR=(T-T1)*ALPHA
IF(RLBAR-.77) 14,15.15
14 B=EXP((1.265-SQRTF(1.6-.3814+OGF(RLBAR,.273)))/.1988)
GO TO 16
15 B=(RLBAR+.0702)/.351
16 XQ=SL*p
J=XINTF(P*10.)+1
Q(J)=Q(J)+1.
W(J)=W(J)+THETA
C(J)=C(J)+SL
J=XINTF(THETA*.5)+1
AO(J)=AO(J)+SL
EL=EL+YQ
FDP=FDP+SE*EBAR+DELR-YQ
SSL=SSI+SL
SSD=SSD+SD
500 R=R+ACC1
DELR=DELR*ACC1
IF(R-51.F-4) 2000,2000.9
2000 GO TO (2001,17) ,N
2001 N=2
R=R+ACC3
DELR=R*2.
GO TO 9
17 SUMI=SUMI+SSL
XPQ7=XPQ7+XPQ7
SSD=SSD+XPQ
ENPD=FDP+XPQ*EBAR
SUMI=SUMI+SSD

```

```

      SEDP=SEDP+EDP
      SEL=SEL+EL
      IF (IV-24) 19,18,18
18    PRINT 1,TT
      IX=0
19    XXX=SUM1/SUME
      XXY=SUMD/SUME
      PRINT 2,F1,E2,EL,SEL,EDP,SEDP,SSL,XXY,SSD,XXY
      GO TO 4
20    CONTINUE
      PRINT 1,TT
      DO 43 J=1,130
      IF (D(J)) 43,43,39
39    K=K+1
      FJ=J-1
      X=FJ/10.
      Y=X+.1
      XX=(X+.5)*G(J)
40    Z=W(J)*H(J)
41    PRINT 500,X,Y,C(J),7,XX
      IF (XMOD(K,25)) 43,42,43
42    PRINT 1,TT
43    CONTINUE
      K=0
      PRINT 1,TT
      DO 50 J=1,50
      IF (A0(J)) 50,50,51
51    K=K+1
      X=J*2
      Y=X-2.
      PRINT 550,Y,X,A0(J)
      IF (K-25) 50,50,52
52    K=0
      PRINT 1,TT
50    CONTINUE
      GO TO 700
44    CONTINUE
      CALL TMEOFF
500  FORMAT(10X,2F10.3,E13.3,F11.2,F13.3/)
550  FORMAT(10X,2F10.2,E13.3/)
600  FORMAT(1F1)
1    FORMAT(1F1,8X3HT=F7.3//)
2    FORMAT(2F8.3,8F12.3/)
3    FORMAT(2F5.0,F10.0)
      END
      SUBROUTINE PROB
      COMMON T,PT,RATIO
      LDA T
      AJP M(1)
      STA XX
      LAC C2
      STA SIGN
      LDA XX
      SLJ (4)
11)  LDA C2
      STA SIGN

```

	LAC	T
	STA	XX
(4)	FMU	XX
	STA	X2
	LDA	XX
	FSB	C3
	AJP	M (2)
	LDA	C2
	FDV	X2
	STA	X22
	FMU	C4
	FSB	C5
	FMU	C6
	FMU	X22
	FAD	C5
	FMU	C7
	FMU	X22
	FSB	C5
	FMU	C8
	FMU	X22
	FAD	C5
	FMU	C9
	FMU	X22
	FSB	C5
	FAD	C5
	STA	ERF
	LAC	X2
	STA	X2
+	FNA	X2
	RTJ	EXPF
+	RTJ	ERROR.
+	FMU	C10
	FDV	XX
	FMU	ERF
	FAD	C5
	SLJ	(3)
(2)	LAC	X2
	FDV	D1
	FAD	D2
	FMU	X2
	FDV	D3
	FSB	D4
	FMU	D5
	FMU	X2
	FAD	D6
	FMU	X2
	FMU	D7
	FSB	D8
	FMU	X2
	FAD	D9
	FMU	C2
	FMU	X2
	FSB	C5
	FMU	X2
	FDV	C9

```

      FAD      C5
      FMU      XX
      FMU      D10
(3)   FMU      SIGN
      FAD      C2
      FDU      RATIO
      STA      PT
      RETURN
P2    DEC      .5
P3    DEC      1.647704
P4    DEC      11.
P5    DEC      1.
P6    DEC      9.
P7    DEC      7.
P8    DEC      5.
P9    DEC      3.
P10   DEC      -.5641896
B1    DEC      105.
D2    DEC      .07692308
B3    DEC      6.
D4    DEC      .090909091
D5    DEC      .2
D6    DEC      .11111111
B7    DEC      .25
D8    DEC      .142857143
D9    DEC      .6
B10   DEC      1.1283792
SIGN  RSS      1
XX     RSS      1
X2     RSS      1
X22    RSS      1
PRF     RSS      1
EXPF    LIB      EXPF
      END
      SUBROUTINE TIMEON
+      FNA      00000      CLEAR-ACCUMULATOR.
+      FYF      7 000118  TEST CHANNEL 1 FOR ACTIVE.
      STA      00000      CLEAR CLOCK CONTENTS TO ZERO.
+      FYF      010008  START CLOCK.
      RETURN
      END
      SUBROUTINE TIMEOFF
+      NOP
-      FYF      7 000118  DUMMY STATEMENT.
      FYF      020008  TEST CHANNEL 1 FOR ACTIVE.
      LDA      00000  STOP THE REAL-TIME CLOCK.
      STA      KLOCK  CLOCK CONTENTS TO ACCUMULATOR.
                        CLOCK CONTENTS TO *KLOCK*.
      TIME=FI,DATE(KLOCK)/3600.0
      PRINT *,TIME
      RETURN
1      FORMAT(11H1RUN TIME =F9.2,9H MINUTES.//)
      END
      END
      END

```

To .9.0 (Note: Headings are the same as on page 122)										
.99	.00	4.189E-05	6.109E-05	2.070E-03	2.071E-03	4.415E-04	1.700E-03	9.771E-03	3.009E-002	
.99	.55	.407E-04	2.000E-04	6.97E-03	6.107E-03	1.191E-03	1.554E-03	3.270E-02	4.053E-002	
.99	.90	1.762E-04	3.040E-04	9.399E-03	1.792E-02	1.016E-03	1.393E-03	9.819E-02	4.196E-002	
.99	.45	1.663E-04	5.911E-04	1.100E-02	2.91E-02	1.794E-03	1.107E-03	9.411E-02	4.346E-002	
.99	.40	.330E-04	6.027E-04	1.299E-02	4.150E-02	1.097E-03	1.020E-03	1.110E-01	4.509E-002	
.99	.35	6.970E-05	7.749E-04	1.220E-02	5.304E-02	1.416E-03	8.003E-04	1.340E-01	4.001E-002	
.99	.30	5.21E-05	5.247E-04	1.00E-02	6.47E-02	1.01E-03	7.042E-04	1.520E-01	4.00E-002	
.99	.25	4.210E-05	5.449E-04	8.411E-03	7.311E-02	6.002E-04	6.623E-04	1.012E-01	5.047E-002	
.99	.20	7.291E-06	6.521E-04	5.700E-03	7.091E-02	2.00E-04	5.709E-04	1.656E-01	5.244E-002	
.99	.15	.330E-05	6.539E-04	3.292E-03	6.210E-02	1.076E-04	9.171E-04	1.614E-01	5.454E-002	
.99	.10	.1E-05	6.539E-04	6.920E-04	6.209E-02	.00E-00	4.900E-04	6.203E-02	5.577E-002	
.99	.05	.00E-05	6.539E-04	.00E-00	6.209E-02	.00E-00	4.900E-04	.00E-00	5.577E-002	

(Note: Headings are the same as on page 124)

.00	.1	7.026E-003	42.51	3.513E-004
.10	.2	5.083E-003	40.39	4.625E-004
.20	.3	5.834E-005	39.07	9.586E-006



(Note: Headings are the same as on page 127)

T= .500

38.00	40.00	1.632E-003
40.00	42.00	5.102E-003
42.00	44.00	3.018E-003
44.00	46.00	3.956E-004

BIBLIOGRAPHY

Berthelot, A., Radiations and Matter, Leonard Hill (Books) Limited, London, 1958.

Bouchard, G. H., Measurement of Bremsstrahlung Dose and Spectrum from a 600 KV Pulsed X-ray Generator Using Photographic Film, SCR-524, June 1962.

Dwight, H. B., Mathematical Tables of Elementary and Some Higher Mathematical Functions, McGraw-Hill Book Co., New York, 1941.

Evans, R. D., The Atomic Nucleus, McGraw-Hill Book Co., New York, 1955.

Glasstone, S. and Edlund, E. C., The Elements of Nuclear Reactor Theory, D. Van Nostrand Co., Inc., Princeton, New Jersey, 1952.

Goldstein, H., Fundamental Aspects of Reactor Shielding, Addison-Wesley Publishing Co., Inc., Reading, Massachusetts, 1959.

Hughes, V. W. and Schultz, H. L. (ed), 1961 Methods of Experimental Physics: Atomic and Electron Physics (Vol. 4), Academic Press, New York, (Part B).

Katz, L. and Penfold, A. S., Revs. Mod. Phys. 24: 28, 1952.

Kinsman, S. (ed), Radiological Health Handbook, U. S. Department of Health, Education, and Welfare, Cincinnati, Ohio, 1957.

Lea, D. D., Actions of Radiations on Living Cells, Cambridge University Press, London, (Chap. 1), 1955.

Maienschein, F. C., et al., Gamma Rays Associated with Fission, Second Int. Conf. on the Peaceful Uses of Atomic Energy, Geneva, 1958.

Marshall, J. and Ward, A. G., Canadian Journal of Research, A15, 39, 1937.

Poll, R. A. and van Lint, V. A. J., Transient Radiation Effects in Pressure Transducers, AFSWC TDR-62-63, Air Force Special Weapons Center, Kirtland Air Force Base, New Mexico, 1962.

Rockwell, T., Reactor Shielding Design Manual, McGraw-Hill Book Co., New York, 1956.

Rossi, B., High-Energy Particles, Prentice-Hall, Inc., New York, 1952.

TDR-63-50

Segre, E., Article by Ashkin, J. and Bethe, H., Experimental Nuclear Physics, Vol 1, (Part 2), John Wiley and Sons, Inc., New York, 1953.

Semat, Henry, Introduction to Atomic and Nuclear Physics, Rinehart and Company, Inc., New York, 1958.

Siegbahn, Kai, Beta and Gamma-Ray Spectroscopy, Interscience Publishers Inc., New York, 1955.

Wu, C-S and Yuan, L. C. L. (ed), Methods of Experimental Physics: Nuclear Physics (Vol. 5, Part A, Sec. 1.1), Academic Press, New York, 1961.

DISTRIBUTION

No. cys

HEADQUARTERS USAF

1	Hq USAF (AFCOA), Wash 25, DC
1	Hq USAF (AFOCE, Lt/Col Bohannon), Wash 25, DC
1	Hq USAF (AFRDP), Wash 25, DC
1	Hq USAF (AFRNE-A, Maj Lowry), Wash 25, DC
1	Hq USAF (AFNIN), Wash 25, DC
1	USAF Directorate of Nuclear Safety (AFINS), Kirtland AFB, NM
1	AFOAR, Bldg T-D, Wash 25, DC
1	AFCRL, Hanscom Fld, Bedford, Mass
1	AFOSR, Bldg T-D, Wash 25, DC
1	ARL (RRLO), Wright-Patterson AFB, Ohio

MAJOR AIR COMMANDS

1	AFSC (SCT), Andrews AFB, Wash 25, DC
	SAC, Offutt AFB, Nebr
1	(OA)
1	(OAWS)
	ADC (Ops Anlys), Ent AFB, Colorado Springs, Colo
1	(ADLPD)
1	(ADOOA)
1	AUL, Maxwell AFB, Ala
1	USAFIT (USAF Institute of Technology), Wright-Patterson AFB, Ohio
1	USAF A, United States Air Force Academy, Colo

AFSC ORGANIZATIONS

1	FTD (Library), Wright-Patterson AFB, Ohio
2	ASD (ASAPRL), Wright-Patterson AFB, Ohio
1	RTD (RTN-W, Maj Munyon), Bolling AFB, Wash 25, DC
1	BSD (BSR6A), Norton AFB, Calif
1	SSD (SSTRS, Maj D. L. Evans), AF Unit Post Office, Los Angeles 45, Calif
1	ESD (ESAT), Hanscom Fld, Bedford, Mass

DISTRIBUTION (cont'd)

No. cys

1 AF Msl Dev Cen (RRRT), Holloman AFB, NM  
1 RADC (Document Library), Griffiss AFB, NY

KIRTLAND AFB ORGANIZATIONS

AFSWC, Kirtland AFB, NM

1 (SWEH) .

1 (SWT)

AFWL, Kirtland AFB, NM

25 (WLL)

1 (WLR)

1 (WLV)

2 (WLRPA, TSgt Sykes)

1 (WLRPT)

1 (WLRB)

OTHER AIR FORCE AGENCIES

Director, USAF Project RAND, via: Air Force Liaison Office,  
The RAND Corporation, 1700 Main Street, Santa Monica, Calif

1 (RAND Physics Div)

1 (RAND Library)

ARMY ACTIVITIES

1 Chief of Research and Development, Department of the Army  
(Special Weapons and Air Defense Division), Wash 25, DC

1 US Army Materiel Command, Harry Diamond Laboratories,  
(ORDTL 06.33, Technical Library), Wash 25, DC

1 Redstone Scientific Information Center, US Army Missile  
Command (Tech Library), Redstone Arsenal, Ala

1 Commanding Officer, US Army Signal Research & Development  
Laboratory, (SIGRA/SL-SAT-1, Weapons Effects Section), Fort  
Monmouth, NJ

1 US Army Research Office, ATTN: Richard O. Ulsh, Box CM,  
Duke Station, Durham, NC

1 Commanding General, White Sands Missile Range, ATTN: Mr.  
Glenn Elder, White Sands, NM

DISTRIBUTION (cont'd)

No. cys

NAVY ACTIVITIES

	Chief of Naval Operations, Department of the Navy, Wash 25, DC
1	(OP-36)
1	(OP-75)
	Chief of Naval Research, Department of the Navy, Wash 25, DC
1	(Code 418)
1	(Code 427)
	Chief, Bureau of Naval Weapons, Department of the Navy, Wash 25, DC
1	(RMGA-8)
1	(RRNV)
1	Chief, Bureau of Ships (Code 362B), Department of the Navy, Wash 25, DC
1	Commanding Officer, Naval Research Laboratory, Wash 25, DC
1	Commanding Officer, Naval Radiological Defense Laboratory (Technical Info Div), San Francisco 24, Calif
1	Commanding Officer and Director, Navy Electronics Laboratory (Code 4223), San Diego 52, Calif
1	Commander, Naval Ordnance Laboratory, ATTN: Dr. Rudlin, White Oak, Silver Spring, Md
1	Office of Naval Research, Wash 25, DC

OTHER DOD ACTIVITIES

1	Chief, Defense Atomic Support Agency (Document Library), Wash 25, DC
1	Commander, Field Command, Defense Atomic Support Agency (FCAG3, Special Weapons Publication Distribution), Sandia Base, NM
1	Director, Advanced Research Projects Agency, Department of Defense, ATTN: Col W. H. Innes, The Pentagon, Wash 25, DC
1	Director, Defense Research & Engineering, The Pentagon, Wash 25, DC
20	Hq Defense Documentation Center for Scientific and Technical Information (DDC), Cameron Stn, Alexandria, Va 22314

DISTRIBUTION (cont'd)

No. cys

AEC ACTIVITIES

- 1 US Atomic Energy Commission (Headquarters Library, Reports Section), Mail Station G-017, Wash 25, DC
- Sandia Corporation, Sandia Base, NM
- 1 (Dr. J. W. Easley, Dept 5300)
- 1 (Dr. Carter Broyles, Dept 5113)
- 1 (Dr. S. C. Rogers, Dept 5312)
- 1 (Dr. A. W. Snyder, Dept 5313)
- 1 Sandia Corporation (Technical Library), P. O. Box 969, Livermore, Calif
- 1 Chief, Division of Technical Information Extension, US Atomic Energy Commission, Box 62, Oak Ridge, Tenn
- 1 University of California Lawrence Radiation Laboratory (Technical Information Division), P.O. Box 808, Livermore, Calif
- 1 University of California Lawrence Radiation Laboratory, (Technical Info Div, ATTN: Dr. R. K. Wakerling), Berkeley 4, Calif
- 1 Director, Los Alamos Scientific Laboratory (Helen Redman, Report Library), P. O. Box 1663, Los Alamos, NM
- 1 Brookhaven National Laboratory, Upton, Long Island, NY
- 1 Argonne National Laboratory (Tech Library), Argonne, Ill
- 1 Oak Ridge National Laboratory (Tech Library), Oak Ridge, Tenn

OTHER

- 1 National Bureau of Standards, Radiological Equipment Section, Wash 25, DC
- 1 OTS, Department of Commerce, Wash 25, DC
- 1 Institute for Defense Analysis, Room 2B257, The Pentagon, Wash 25, DC
- THRU: ARPA
- 1 Space Technology Labs, Inc., ATTN: Lt General James H. Doolittle, One Space Park, Redondo Beach, Calif
- 1 Battelle Memorial Institute, 505 King Ave., Columbus, Ohio
- 1 Institute of the Aerospace Sciences, Inc., 2 East 64th Street, New York 21, NY
- 1 Aerospace Corporation, P.O. Box 95085, Los Angeles 45, Calif

DISTRIBUTION (cont'd)

No. cys

- 1 General Electric Company - MSD, ATTN: Dr. Sumner Stern,  
P.O. Box 8555, Philadelphia 1, Pa
- 1 General Atomic, ATTN: Dr. R. J. Jurgovan, P.O. Box 608,  
San Diego 12, Calif
- 2 General Atomic, ATTN: Dr. Victor A. J. van Lint, P.O. Box  
608, San Diego 12, Calif
- 1 IBM, Federal Systems Division, ATTN: W. A. Bohan, Owego, NY
- 3 The Boeing Co., Aero-Space Division, ATTN: Dr. G. L. Keister,  
Org. 2-5470, P. O. Box 3707, Seattle 24, Wash
- 1 General Dynamics/Fort Worth, ATTN: W. B. Rose, Fort Worth,  
Tex
- 3 Hughes Aircraft Co., Ground Systems Group, ATTN: Mr. J. E.  
Bell, P.O. Box 2097, Fullerton, Calif
- 1 Radiation Effects Information Center, ATTN: E. N. Wyler, 505  
King Avenue, Columbus 1, Ohio
- 1 DASA Data Center, General Electric TEMPO, 735 State Street,  
Santa Barbara, Calif
- 1 Director, Applied Physics Laboratory, Johns Hopkins University,  
ATTN: Mr. Robert Frieberg, 8621 Georgia Avenue, Silver Spring,  
Md
- 1 Massachusetts Institute of Technology, Lincoln Laboratory,  
ATTN: O. V. Fortier, P. O. Box 73, Lexington, Mass  
Northrop Ventura Division, Northrop Corp., 1515 Rancho Conejo  
Blvd, Newbury Park, Calif
- 1 (Dr. T. M. Hallman)
- 1 ( Don Glenn)
- 1 Lockheed Aircraft Corp., Missile & Space Division, ATTN: Mr.  
Fred Barline, Dept 5872, 1111 Lockheed Way, Sunnyvale, Calif
- 1 Space Technology Laboratories, ATTN: Dr. B. Sussholz and  
Mr. J. Maxey, 5730 Arbor Vitae St., Los Angeles, Calif
- 1 Atomics International, ATTN: W. E. Parkins, Mgr Research,  
8900 DeSoto St., Canoga Park, Calif
- 1 General Electric Company, Radiation Effects Operations,  
Defense Systems Dept., ATTN: Mr. L. Dee, 300 South Geddes  
Street, Syracuse, NY
- 1 Official Record Copy (WLRPT, Lt Sawyer)